

FINITE ELEMENT ANALYSIS OF ENAMELLED STEEL STRUCTURES



by
Mert Cevdet Günay

Submitted to Graduate School of Natural and Applied Sciences
in Partial Fulfillment of the Requirements
for the Degree of Master of Science in
Mechanical Engineering

Yeditepe University

2019

FINITE ELEMENT ANALYSIS OF ENAMELLED STEEL STRUCTURES

APPROVED BY:

Assist. Prof. Dr. Ali Fethi Okyar
(Thesis Supervisor)



Assoc. Prof. Dr. Ali Gökşenli



Assist. Prof. Dr. Onur Cem Namlı



DATE OF APPROVAL: /.... /2019

ACKNOWLEDGEMENTS

Firstly, I would like to thank my family for their belief and support throughout my M.Sc study. Also, I would like to thank my advisor, Dr. Ali Fethi Okyar for his continuous support and encouragement.

Besides my family and advisor, I would like to thank all of my colleagues in Arçelik R&D for their friendship and support.

Lastly, I would like to thank Dr. Yusuf Öztürk for his help in characterization of glass samples and Mr. Nevzat Akın from Arçelik Bolu Cooking Appliances Factory for his help in CMM measurement of oven cavities.

ABSTRACT

FINITE ELEMENT ANALYSIS OF ENAMELLED STEEL STRUCTURES

Enamelled steel components have been used widely in cooking appliances, architectural panels, chemical reactors and heat exchanger parts. Superior chemical and physical attack resistance and hygiene properties made enamelled steel a preferred material of choice for these applications. Enamelled steel is a steel-glass composite where metal acts as a substrate and a thin layer of glass powder is coated on it. By subsequent thermal processing, glass powder melts and forms a continuous layer on steel. The difference between the thermal expansion coefficients of steel and glass result in thermal deflection and warping of the structure. In order to reduce the percentage of out of tolerance products, many design alternatives are prepared through product development process. Testing every design alternative can be costly and time consuming, therefore, a simulation methodology predicting the behavior of the structure through manufacturing stage is needed. Finite element analysis is used in order to develop a methodology for the manufacturing process simulation of enamelled steel products. Viscoelastic and elastic material models are used and the results are compared. The validation of the analysis methodology is done with rectangular enamelled steel plates manufactured in Arcelik production facility. The methodology then applied to oven cavity. The oven cavities manufactured in Arcelik facility were measured dimensionally with Coordinate-Measurement Machine and the coating thicknesses were measured with elcometer. Finite element analysis results were compared with Coordinate-Measurement Machine results. Additionally, Dynamic Mechanical Analyzer was used for characterization of glass in order to obtain its temperature dependent material properties.

ÖZET

EMAYE ÇELİK YAPILARIN SONLU ELEMANLAR YÖNTEMİ İLE ANALİZİ

Emaye yapılar pişirici cihazlarda, duvar panellerinde, reaktörlerde ve ısı eşanjörlerinde yoğun olarak kullanılmaktadır. Kimyasal ve fiziksel aşınmaya karşı dirençleri ve hijyenik olmaları emaye ürünlerin bu alanlarda sıklıkla kullanılmasını sağlamıştır. Emaye çelikler, çelik ve cam katmanlarından oluşan kompozit bir yapıdır. Bu yapıda, çelik substrat görevi görür ve üstü cam tozu ile kaplanır. Termal proses ile cam tozu eritilir ve sürekli bir cam filmi oluturulur. Cam ve çelik katmanlarının termal genleşme katsayıları arasındaki fark yapıda bükülme ve çarpılmalara sebep olur. Ürün için belirlenen toleransların dışına çıkmış parçaların yüzdesini azaltmak için ürün geliştirme süreci dahilinde birçok tasarım alternatifi hazırlanır. Tüm tasarım alternatiflerinin fiziksel olarak test edilmesinin pahalı ve zaman alıcı olması sebebiyle, emaye yapının üretim sürecindeki davranışını tahmin edebilen bir simulasyon metodolojisine ihtiyaç bulunmaktadır. Üretim süreci simülasyonunu gerçekleştiren bir metodoloji geliştirmek için sonlu elemanlar yöntemi kullanılmıştır. Viskoelastik ve elastik malzeme modelleri ile analizler yapılmış ve sonuçları karşılaştırılmıştır. Analiz metodolojisinin validasyon çalışması Arçelik üretim tesisinde hazırlanmış dikdörtgen emaye çelik plakalar kullanılarak yapılmıştır. Doğrulanmış metodoloji, fırın şasi parçasının analizi için kullanılmıştır. Arçelik üretim tesisinde üretilen fırın şasileri koordinat ölçüm cihazı ile boyutsal olarak ölçülmüş, cam filmi kalınlıkları elkometre kullanılarak tayin edilmiştir. Sonlu elemanlar analizi sonuçları boyutsal ölçüm sonuçları ile karşılaştırılmıştır. Bunlara ek olarak, dinamik mekanik analiz cihazı kullanılarak cam numunelerin sıcaklığa bağlı saklama modülü hesaplanmıştır.

TABLE OF CONTENTS

ACKNOWLEDGEMENTS	iii
ABSTRACT	iv
ÖZET	v
LIST OF FIGURES	ix
LIST OF TABLES	xiv
LIST OF SYMBOLS/ABBREVIATIONS	xvi
1. INTRODUCTION	1
1.1. VITREOUS ENAMELLING.....	1
1.2. ENAMELLED STEEL.....	1
1.3. DISTORTION OF THE ENAMELLED SHEET METAL STRUCTURES	3
2. THEORY	5
2.1. ANALYTICAL CALCULATION OF THERMAL DEFLECTION BI-MATERIAL SYSTEMS	5
2.2. VISCOELASTIC BEHAVIOR	9
2.2.1. Creep, Recovery and Relaxation	10
2.2.1.1. Creep	11
2.2.1.2. Recovery.....	11
2.2.1.3. Relaxation	11
2.2.1.4. Stress Relaxation Behaviour in Enamelled Steel Systems	13
2.2.2. Continuum Viscoelasticity Formulation	14
2.2.2.1. Hereditary Integral Formulation	15
2.2.2.2. Small-Strain Viscoelasticity.....	15
2.2.2.3. Isotropic Viscoelastic Material	17
2.2.2.4. Time-Temperature Superposition.....	19
2.2.2.5. Thermo-Rheologically Simple Behavior	21
2.2.2.6. Narayanaswamy Model for Structural Relaxation.....	23
2.3. DYNAMIC MECHANICAL ANALYSIS.....	27
2.4. PREVIOUS WORKS ON FEA OF ENAMELLED STEEL	30
3. MATERIALS AND METHODS	32
3.1. GLASS.....	32

3.1.1. Properties of Glasses	32
3.1.2. Characterization of Glass.....	34
3.1.2.1. Thermal Dilatometric Analysis	35
3.1.2.2. X-Ray Fluorescence Analysis	35
3.1.3. Temperature Dependent Properties of Glass.....	37
3.1.4. Viscoelastic Characteristics of Glass.....	38
3.2. STEEL	39
3.2.1. Classification of Cold Rolled Steel Sheets for Enamelling.....	40
3.2.2. Temperature Dependent Mechanical Properties of Steel.....	40
3.3. MANUFACTURING OF ENAMELLED STEEL SAMPLES	41
3.4. MANUFACTURING OF ENAMELLED STEEL OVEN CAVITY	45
3.5. DIMENSIONAL MEASUREMENT OF OVEN CAVITIES	48
3.5.1. CMM Measurement	48
3.5.2. Coating Thickness Measurement	50
3.6. FINITE ELEMENT ANALYSIS.....	51
3.6.1. Element Type Selection.....	52
3.6.1.1. 2D Elements	54
3.6.1.2. Thin Shell Elements.....	56
3.6.1.3. Shell Elements with Composite Properties	57
3.6.2. Manufacturing Process Modelling of Enamelled Steel Sample	58
3.6.2.1. Analysis Methodology.....	59
3.6.3. Preprocessing of the Oven Cavity Finite Element Model.....	65
3.7. DYNAMIC MECHANICAL ANALYSIS.....	69
3.7.1. Fixtures and Sample Geometries in DMA	69
3.7.1.1. Axial Fixtures	69
3.7.1.2. Torsional Fixtures.....	70
3.7.2. Dynamic Mechanical Analysis of a Soda-Lime-Silicate Glass Specimen ..	71
3.7.2.1. Samples, Deformation Modes and Experiment Theory	72
4. RESULTS	74
4.1. THERMAL DEFORMATIONS IN ENAMELLED STEEL SAMPLES.....	74
4.1.1. Coating Thickness and Thermal Deformation Measurements of the Sample	74

4.1.2. Validation of Analysis Methodology: Experimental and Numerical Results	74
4.2. THERMAL DEFORMATIONS IN ENAMELLED STEEL OVEN CAVITY...	75
4.2.1. Dimensional Measurement Results of Oven Cavity	76
4.2.2. Numerical Simulation Results of Oven Cavity	77
4.3. DMA RESULTS OF SLS SPECIMENS	77
5. DISCUSSION	84
6. CONCLUSION AND FURTHER WORK	91
REFERENCES	92



LIST OF FIGURES

Figure 1.1.	Enamelled sheet metal products.....	2
Figure 1.2.	Enamelling process.	3
Figure 1.3.	Manufacturing thermograph [5].....	4
Figure 2.1.	Bonded layers with different elastic properties [10].....	5
Figure 2.2.	Bended composite system [10].....	6
Figure 2.3.	Various strain responses to a constant load [14].....	9
Figure 2.4.	Maxwell model elements: (a) Spring, (b) Dashpot [15].....	10
Figure 2.5.	Creep and recovery [14].	12
Figure 2.6.	Stress relaxation under constant strain [14].....	12
Figure 2.7.	Strain behaviour under various temperature zones [15].....	14
Figure 2.8.	The generalized Maxwell model [32].	16
Figure 2.9.	Tests at different temperatures and time-temperature shifting [37].	20

Figure 2.10. Shift of relaxation modulus at different times [32].	22
Figure 2.11. Step input for temperature and volume change [32].....	24
Figure 2.12. Volume change as a function of temperature [32].....	25
Figure 2.13. Section view of Perkin-Elmer DMA 7e [17].	28
Figure 2.14. Applied stress and material response [17].....	29
Figure 2.15. DMA relationships [17].	30
Figure 2.16. DMA of Nylon [17].....	31
Figure 3.1. Specific volume change of materials [6].	33
Figure 3.2. Viscosity change of silica glasses [6].	34
Figure 3.3. Dilatometric analysis of glass.....	35
Figure 3.4. Temperature dependent modulus of elasticity of glass.	37
Figure 3.5. Temperature dependent modulus of elasticity.....	41
Figure 3.6. Temperature dependent Poisson's ratio of steel.....	42

Figure 3.7. Temperature dependent CTE of steel.	43
Figure 3.8. Thermograph of the enamelling process.	43
Figure 3.9. Uncoated sheet metal sample on conveyor line.	44
Figure 3.10. Glass film thickness measurement points on specimen.	45
Figure 3.11. Bimaterial deflection measurement.	45
Figure 3.12. Uncoated oven cavities on production line.	46
Figure 3.13. Glass frit coated oven cavities on production line.	47
Figure 3.14. Finished oven cavities.	47
Figure 3.15. CMM measurement of uncoated oven cavity.	48
Figure 3.16. CAD models of oven cavity and its parts.	49
Figure 3.17. CMM measurement points from 1 to 17.	50
Figure 3.18. CMM measurement points from 18 to 21.	51
Figure 3.19. Two-dimensional finite element model [19].	54

Figure 3.20. Thin walled structure [21].	55
Figure 3.21. DOF in a shell element [21].	58
Figure 3.22. Finite element model of a composite structure [22].	59
Figure 3.23. Ply stacking sequence and element normal direction [22].	59
Figure 3.24. Composite property input by Hyperlaminare GUI [22].	60
Figure 3.25. CAD and finite element models of the sample.	61
Figure 3.26. Manufacturing thermograph.	61
Figure 3.27. Time-temperature graph for heating and cooling stages.	63
Figure 3.28. Displacement boundary conditions in x-direction.	64
Figure 3.29. Displacement in z-direction.	65
Figure 3.30. Manufacturing process simulation methodology flowchart.	66
Figure 3.31. User specified finite element quality criteria.	67
Figure 3.32. Finite element model of oven cavity.	68

Figure 3.33. Oven cavity and the direction of gravity.	69
Figure 3.34. Three-point bending test fixture [17].	70
Figure 3.35. TA Instruments DMA Q800.....	71
Figure 3.36. Glass specimens.	73
Figure 3.37. Glass specimen in three-point bending mode.	73
Figure 4.1. Storage modulus and $\text{Tan } \delta$ versus temperature.	82
Figure 4.2. Storage modulus change for $15 \mu\text{m}$ maximum deflection.	82
Figure 4.3. Storage modulus change for $20 \mu\text{m}$ maximum deflection.	83
Figure 5.1. Shell moment variation for elastic and viscoelastic models.....	89
Figure 5.2. Equivalent of shell moment and curvature versus temperature.....	90

LIST OF TABLES

Table 3.1.	Quantification of glass frit XRF results.	36
Table 3.2.	Deviatoric part of viscoelastic characteristics [38].	38
Table 3.3.	Volumetric part of viscoelastic characteristics [38].....	39
Table 3.4.	Structural relaxation parameters [38].....	39
Table 3.5.	Coating thicknesses of different parts.	51
Table 3.6.	Finite element types [20].	53
Table 3.7.	Element type selection [21].....	56
Table 3.8.	2D finite element types [21].	57
Table 3.9.	Thicknesses of oven chassis parts.	68
Table 3.10.	Specifications of TA Instruments DMA Q800 [21].....	72
Table 4.1.	Glass film thickness on specified points of the specimen (microns).	75
Table 4.2.	Displacements of the middle area of samples.	76
Table 4.3.	Experimental and numerical results of plate sample.	77
Table 4.4.	CMM results from uncoated oven cavities.	78

Table 4.5. CMM results from coated/enamelled oven cavities. 79

Table 4.6. Numerical simulation results with constant CTE. 80

Table 4.7. Numerical simulation results with viscoelastic behavior..... 81

Table 5.1. Deviation between experimental and numerical results. 86

Table 5.2. Numerical simulation results with viscoelastic behavior..... 88



LIST OF SYMBOLS/ABBREVIATIONS

$a(T(x,t))$	Shift function
C	Creep compliance
E^*	Complex modulus
E'	Storage modulus
E''	Loss modulus
$G(t)$	Shear modulus
G_{ijkl}	Stress relaxation function
H	Activation energy
$K(t)$	Bulk modulus
$P(t,T)$	Property function
R	Universal gas constant
t'	Instantaneous time
T_f	Fictive temperature
T_g	Glass transition temperature
T_m	Melting temperature
T_N	Neutral temperature
W_g	Weight function
X	Fraction parameter
α	Coefficient of thermal expansion
δ	Deflection
ϵ	Strain
ϵ_{th}	Thermal strain
η	Viscosity
λ^n	Relaxation time
ν	Poisson's ratio
ξ_t	Reduced time
π_d	Deviatoric component matrix

π_v	Volumetric component matrix
ρ	Curvature
σ	Stress
CTE	Coefficient of thermal expansion
DOF	Degrees of freedom
SLS-Glass	Soda-lime-silicate glass
XRF	X-Ray fluorescence



1. INTRODUCTION

1.1. VITREOUS ENAMELLING

Vitreous enamelling is a coating method where glass is fused on a substrate to obtain superior properties. Glass frit, which is powdered glass and binder, is coated on substrate, then fused to obtain a continuous glass layer.

Substrates such as sheet metal, cast iron, aluminum, stainless steel and copper can be enamelled [1].

Basic characteristics that make enamelling preferred to other coating types are:

- Aesthetic look on coated substrate
- Scratch and wear resistance
- Every desired color and tint can be applied and color wont fade with time
- Adds corrosion resistance to coated metal
- Non-Toxic
- Ease of cleaning
- High temperature resistance

Enamel coating is resistant to fire, cold and hot weather, thermal shock, acidic or basic corrosion, organic solvents and atmospheric agents. Due to properties mentioned, enamel coatings are used in general industrial applications, in communication applications and in household goods [2].

1.2. ENAMELLED STEEL

Enamelled steel is a composite structure where the metal substrate, whether it is in sheet or bulk form, is coated with a thin film of glass. Enamelling the steel substrate is done to overcome the physical and chemical attacks on the surface. Superior properties of enamelled

steel which are being hygienic, resistance to corrosion, scratch and other chemical and physical attacks make it an ideal application for household appliances such as cooking ware, sanitary ware, bath tubs and hot water boilers. Also, enamelled steel has many other applications in industry due to its superior properties. Silos, chemical reactors, cisterns, water purification reservoirs and some parts of heat exchangers are made out of enamelled steel [3]. In Figure 1.1, enamelled steel components used in different applications can be seen.



Figure 1.1. Enamelled sheet metal products.

Sheet metal parts are formed and welded before the enamelling process. Sheet metal acts as a substrate for enamel application. The enamelling process starts with the preparation of a wet slurry of glass frit and colouring ingredients. The slurry is applied on degreased and prepared sheet metal surface manually or automatically by specialized robotic systems with nozzles. After this stage, firing cycle is applied to obtain a continuous glass layer. Firing cycle starts from room temperature and increases up to 830-850°C, where glass frit particles fuse and form a single layer. From this temperature, enamelled part is cooled down to room temperature. After firing step, enamelled steel part is naturally cooled down to

room temperature. There can be more than one layers of coating. For some applications, a primary layer(Ground coating) of coating is applied in order to coat the outer layers(cover coating) or to improve the new layers adhesion. There can be more than one firing stage for a multilayered enamelled sheet metal part. Figure 1.2 represents the enamelling process steps.

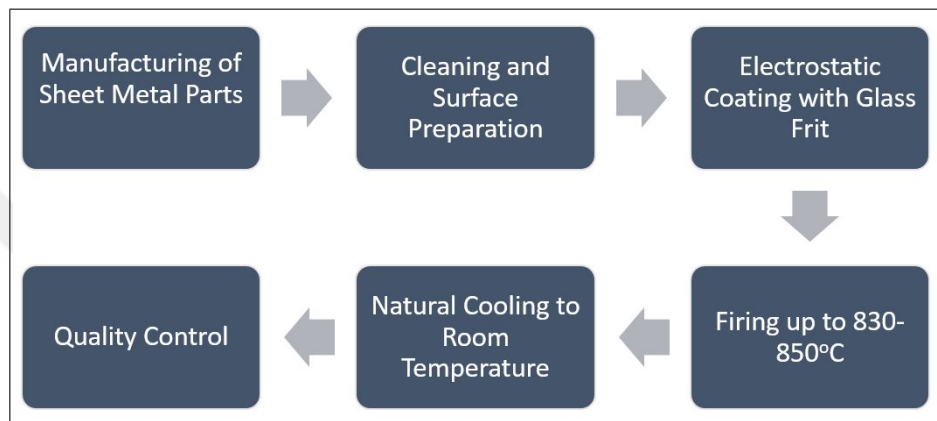


Figure 1.2. Enamelling process.

1.3. DISTORTION OF THE ENAMELLED SHEET METAL STRUCTURES

Although its superior properties on hygiene, corrosion and scratch resistance, enamelled sheet metal parts show up significant distortion problems during manufacturing stage. The enamel-steel system is a bi-material system where layers of different materials comes up with different modulus of elasticity and thermal expansion coefficients. Glass layer has a lower thermal expansion coefficient than steel below glass transition temperature. Because of the difference, residual stresses are developed during cooling stage. Figure 1.3 shows the thermograph of enamelled steel manufacturing. Since the enamelled part is deviated from the primary design, further assembly onto this part can end with spalling and chipping of the enamel coating.

Glass frit is applied on sheet metal which form a layer of glass powder. Since there are no bond between the glass powders, it can not develop any stress. At cooling stage, generally

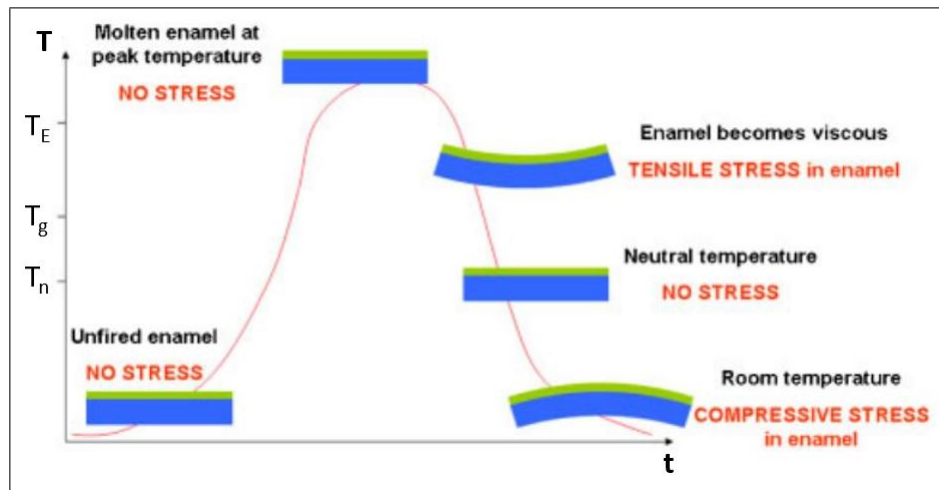


Figure 1.3. Manufacturing thermograph [5].

below softening temperature of the glass [5], glass layer start to develop stress. Above glass transition temperature, glass layer has a higher thermal expansion coefficient than steel. Glass layer has tensile stress and steel layer has compressive stress at this stage. Glass transition temperature of glasses used in enamelling are around 510°C and 530°C [29]. Below glass transition temperature, glass has a lower thermal expansion coefficient than steel. From glass transition temperature to room temperature, residual stresses developed distort the enamel-steel system. At room temperature, glass layer is under compressive and steel layer is under tensile stress. Distortion of the enamelled sheet metal parts results with out-of-tolerance products. These distorted products are usually fail during quality control stage.

Losses due to faulty enamelled steel products affect the industry in serious manner. Design for manufacturing should be applied in order to reduce the faulty product ratio. Product design for enamelled steel parts needs to be designed with support of analysis. Physical testing of every design change applied by the designers will be costly. To shorten the duration of the design stage and increase the number of design variations in order to produce the best possible component, virtual testing of the design becomes crucial. A thermo-mechanical finite element model that take the temperature dependent mechanical properties of glass and metal layers can predict the distortions after manufacturing.

2. THEORY

2.1. ANALYTICAL CALCULATION OF THERMAL DEFLECTION BI-MATERIAL SYSTEMS

Formulations are developed with the analogy of bending of two bonded layers with no slip at the interface [10]. By using these formulations, one can calculate the thermal deflections and thermal stresses developed during cooling from neutral temperature to room temperature. Enamel layer behaves as an elastic material below T_N so enamel/steel composite system can be taken as two bonded layers with different elastic properties. Figure 2.1 represents two bonded layers. E , t and α are Young's modulus, thickness and coefficient of thermal expansion.

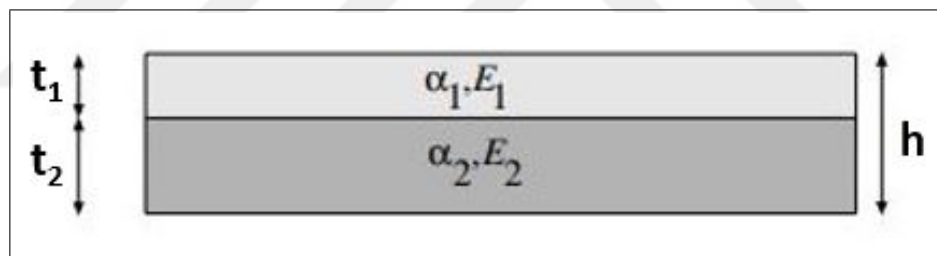


Figure 2.1. Bonded layers with different elastic properties [10].

Two different materials have different thermal expansion coefficients. If $\alpha_2 > \alpha_1$, with decreasing temperature the layer with higher thermal expansion coefficient will shrink more than the other layer. Both layers are bonded so they can't move with respect to each other. Because of this, the composite system will bend because of the bending moment as shown in Figure 2.2.

The forces in each layer are equal to obtain equilibrium.

$$P = P_1 = P_2 \quad (2.1)$$

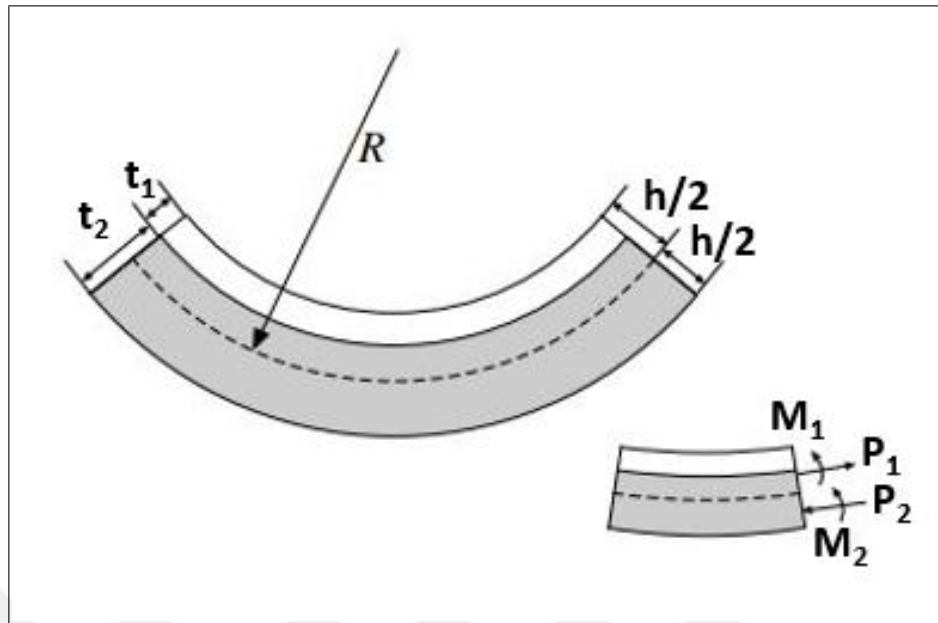


Figure 2.2. Bended composite system [10].

The equilibrium of moments

$$P \frac{h}{2} = M_e + M_s \quad (2.2)$$

Bending moments are;

$$M_s = \frac{E_s I_s}{\rho} \quad (2.3)$$

$$M_e = \frac{E_e I_e}{\rho} \quad (2.4)$$

Moment of Inertia of two layers are;

$$I_e = \frac{b h_e^3}{12} \quad (2.5)$$

$$I_s = \frac{b h_s^3}{12} \quad (2.6)$$

Substituting the bending moments in (2.2)

$$P\frac{h}{2} = M_e + M_s = \frac{E_e I_e + E_s I_s}{\rho} \quad (2.7)$$

Thermal expansion of the layers develops tensile, compressive forces and bending. Strain in each layer are;

$$\epsilon_s = \alpha_s \Delta T + \frac{P}{bh_s E_s} + \frac{h_s}{2\rho} \quad (2.8)$$

$$\epsilon_e = \alpha_e \Delta T + \frac{P}{bh_e E_e} + \frac{h_e}{2\rho} \quad (2.9)$$

Since there is no slip at the enamel/steel interface, strains are equal;

$$\epsilon_s = \epsilon_e \quad (2.10)$$

$$\alpha_s \Delta T + \frac{P}{bh_s E_s} + \frac{h_s}{2\rho} = \alpha_e \Delta T - \frac{P}{bh_e E_e} + \frac{h_e}{2\rho} \quad (2.11)$$

Letting m be enamel/steel thickness ratio;

$$m = \frac{h_e}{h_s} \quad (2.12)$$

where n is the enamel to steel Young's modulus ratio;

$$n = \frac{E_e}{E_s} \quad (2.13)$$

General equation for thermally induced curvature of composite beam[11];

$$\frac{1}{\rho} = \frac{6(\alpha_e - \alpha_s)\Delta T(1+m)^2}{h(3((1+m)^2) + (1+mn)(m^2 + \frac{1}{mn}))} \quad (2.14)$$

To simplify the formulation, we need a parameter, K [9],

$$K = \frac{3(1+m)^2}{(3((1+m)^2) + (1+mn)(m^2 + \frac{1}{mn}))} \quad (2.15)$$

The equation becomes

$$\frac{1}{\rho} = K(2\Delta T \frac{\alpha_e - \alpha_s}{h}) \quad (2.16)$$

Thermally induced deflection at the tip of the composite beam is;

$$\delta = \frac{Kb^2}{h}(\alpha_e - \alpha_s)\Delta T \quad (2.17)$$

Maximum stress in enamel layer

$$\sigma_{max}(e) = -\frac{P}{bh_e} - h_e E_e \frac{1}{2\rho} \quad (2.18)$$

Maximum stress in steel layer

$$\sigma_{max}(s) = -\frac{P}{bh_s} + h_s E_s \frac{1}{2\rho} \quad (2.19)$$

Stress in enamel layer at a given point in z-direction

$$\sigma_e(z) = \sigma_{max}(e) - \frac{\delta}{b^2} E_e z \quad (2.20)$$

Stress in steel layer at a given point in z-direction

$$\sigma_s(z) = \sigma_{max}(s) - \frac{\delta}{b^2} E_s z \quad (2.21)$$

2.2. VISCOELASTIC BEHAVIOR

When some materials get under rapid elastic action and then held at that condition, they undergo a slow and continuous increase of strain. When the stressing condition is removed, material exhibit an initial elastic recovery and continuous strain decrease with a decreasing rate. These materials are sensitive to the rate of stressing and straining. Such materials are considered as viscoelastic [14]. Figure 2.3 shows the different strain responses to a constant load.

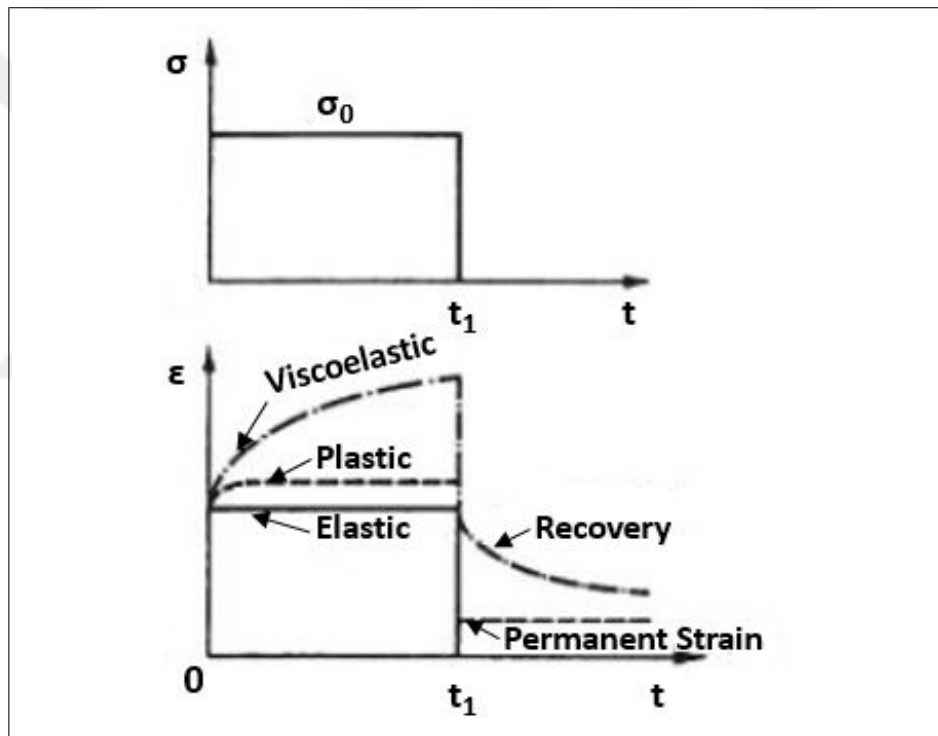


Figure 2.3. Various strain responses to a constant load [14].

Viscoelastic materials show elastic and viscous behaviour during deformation. Such materials can be mathematically modelled by using elements that simulate these two characteristics. They can be modelled with combination of dashpot and spring elements shown in Figure 2.4.

Spring element demonstrates Hookean behaviour and dashpot element demonstrates

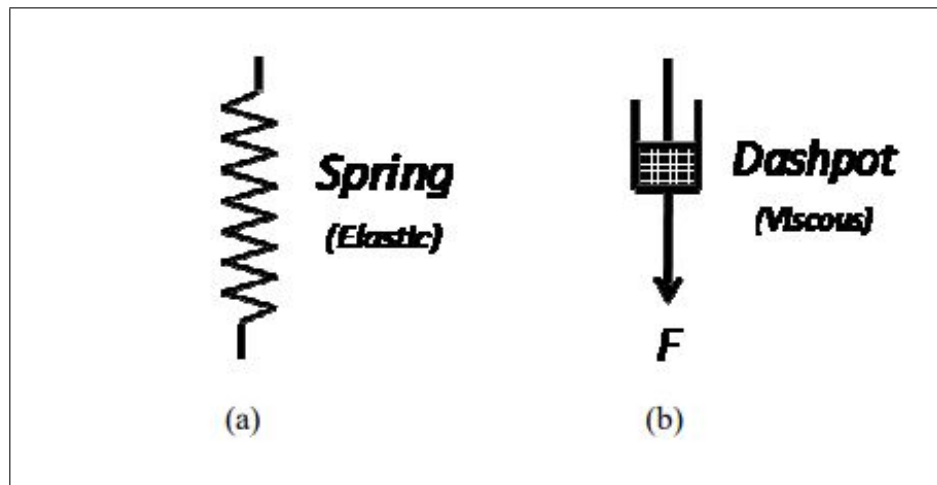


Figure 2.4. Maxwell model elements: (a) Spring, (b) Dashpot [15].

Newtonian behaviour for liquids. Hooke's law for solids,

$$\epsilon = \frac{\sigma}{E} \quad (2.22)$$

In the equation, σ is the stress, ϵ is the strain and E is the Young's modulus.

The viscous behaviour shows non-Hookean behaviour and has resemblance with Newtonian materials. In these materials, stress is proportional to first derivative of strain[16].

Newtonian law for liquids,

$$\frac{d\gamma}{dt} = \frac{\sigma}{\eta} \quad (2.23)$$

In the equation, σ is the stress, η is the viscosity of the fluid in the dashpot and γ is the strain.

2.2.1. Creep, Recovery and Relaxation

Viscoelastic response of materials under different loading and unloading conditions are defined as creep, recovery and relaxation.

2.2.1.1. Creep

Creep is the time-dependent and permanent deformation of materials under constant load. It is observed in all kinds of materials [6]. Creep phenomenon is generally explained in three stages. First stage is the primary stage where creep occurs with a decreasing rate. The second step is called the secondary stage. In this step, creep deformation continues with a constant rate. The third stage is named as tertiary stage. In this stage, creep deformation occurs at an increasing rate which ends up in fracture [14].

Total strain of the material at any time is represented as sum of elastic strain ϵ^e and creep strain ϵ^c ,

$$\epsilon = \epsilon^e + \epsilon^c \quad (2.24)$$

2.2.1.2. Recovery

When the load on the material is removed, elastic strain of the material is reversed. Also, some part of the creep strain recovers with a decreasing rate.

For metals, only a small portion of time-dependent creep is recovered. On the other hand, for plastics, large portion of the time-dependent creep can be recovered. Some plastics may fully recover the creep strain if the enough time is allowed [14].

2.2.1.3. Relaxation

If a viscoelastic material is subjected to constant strain, developed stress will decrease with time in a decreasing rate as shown in Figure 2.5 and 2.6.

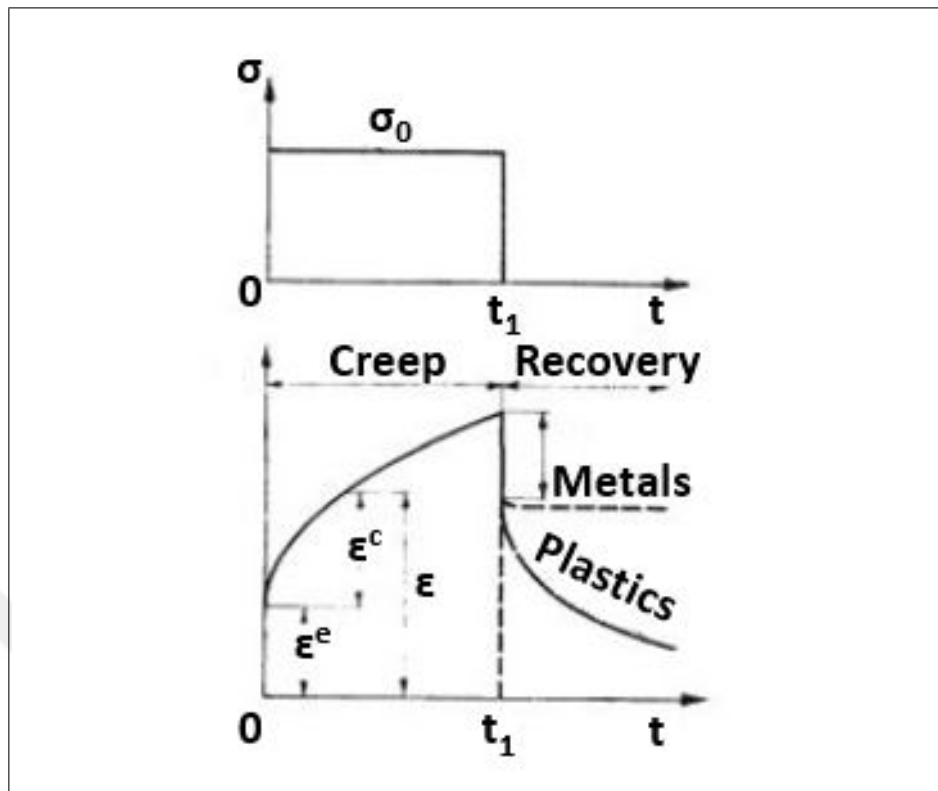


Figure 2.5. Creep and recovery [14].

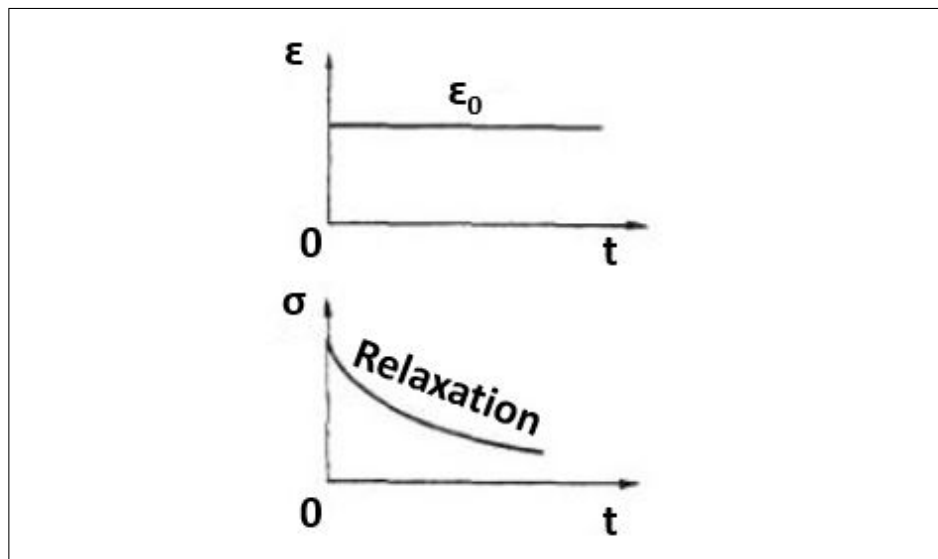


Figure 2.6. Stress relaxation under constant strain [14].

2.2.1.4. Stress Relaxation Behaviour in Enamelled Steel Systems

Stress relaxation is mostly known as a behaviour related to metallic and polymeric materials but glasses also show this behaviour. At elevated temperatures, glasses show time dependent relaxation and stresses developed during cooling stage recovers with time. Stress relaxation is associated with viscoelastic behaviour.

Stress relaxation behaviour of glass is strictly dependent to temperature. This behaviour can be considered into three separate temperature regions.

Constant stress σ_0 was applied on the glass sample at time t_0 and removed at time t_1 . The time-dependent strain responses to the applied constant stress are illustrated in Figure 2.7 with respect to three different temperature regions.

- Case (i): Below T_g (Glass transition temperature): At this temperature range, glass acts as an elastic material. Strain due to constant stress σ_0 is fully recovered as expected from an elastic body. Theoretically, path $A_2 - B_2$ is equal to $C_2 - D_2$.
- Case (ii): In the transition region (Near to T_g), response of the glass to constant stress σ_0 is both elastic and viscous. Line $A_3 - B_3 - C_3 - D_3 - E_3$ shows the elastic and viscous properties on the same segment. In segment $A_3 - B_3$, instantaneous loading at t_0 results in elastic response. From B_3 to C_3 , under constant stress σ_0 , strain is both elastic and viscous. When the load is removed at t_1 , an instantaneous recovery occurs, which is shown in segment $C_3 - D_3$ and the amount of recovery at this instant is equal to $A_3 - B_3$. In segment $D_3 - E_3$, time dependent recovery continues. The non-recoverable strain is equal to the segment $E_3 - F_3$.
- Case (iii): Above glass transition region: In segment $A_4 - B_4 - C_4 - D_4$, strain response of the glass to constant stress σ_0 can be seen. Glass behaves as a viscous material in this temperature region. When instantaneous load is applied at t_0 , there are no instantaneous elastic strain. Material shows time dependent strain in segment $A_4 - B_4$. As stress is removed at t_1 , material does not show recovery as expected in elastic bodies. Segment $C_4 - D_4$ is the non-recoverable strain, the material has permanent viscous strain after t_1 .

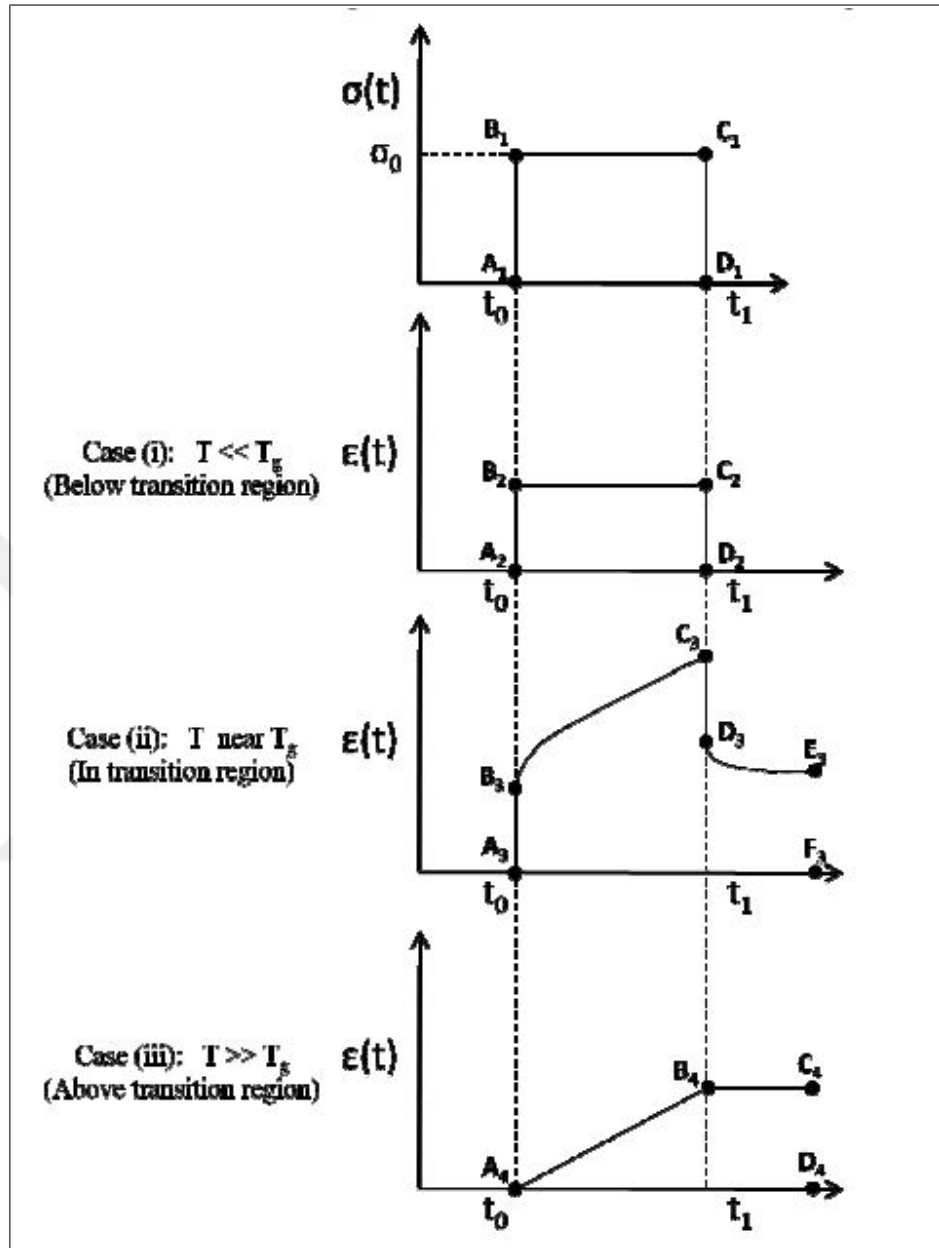


Figure 2.7. Strain behaviour under various temperature zones [15].

2.2.2. Continuum Viscoelasticity Formulation

Glass behaves as a viscoelastic material for temperatures around its glass transition range. Unstable and temperature influenced mechanical behavior in this region makes the use of viscoelastic material model necessary in order to predict the deformation of the enamelled

product correctly. In this section, small-strain viscoelasticity, mathematical models for viscoelastic material response, time-temperature superposition principle, thermorheologically simple behaviour and Narayanaswamy model are discussed.

2.2.2.1. Hereditary Integral Formulation

The constitutive equations used for viscoelastic materials are dependent on entire history of stress and strain state. This behavior can be indicated by hereditary integrals which are derived by taking stress and strain development during successive timesteps into account.

2.2.2.2. Small-Strain Viscoelasticity

A constitutive relation taking stress relaxation into account can be developed in hereditary integral formulation.

$$\sigma_{ij}(t) = \int_0^t G_{ijkl}(t - \tau) \frac{d\epsilon_{kl}(\tau)}{d\tau} d\tau + G_{ijkl}(t) \epsilon_{kl}(0) \quad (2.25)$$

$t - \tau$ is the time interval, G_{ijkl} are the stress relaxation functions. Stress relaxation functions represent the stress relaxation response of the material to an applied strain. The relaxation functions can be indicated by using Prony series. [32]

$$G_{ijkl}(t) = G_{ijkl}^\infty + \sum_{n=1}^N G_{ijkl}^n \exp \frac{-t}{\lambda^n} \quad (2.26)$$

where λ^n is relaxation time, G_{ijkl}^∞ is the long term modulus. The short term or instantaneous modulus can be described by,

$$G_{ijkl}^0 = G_{ijkl}(0) = G_{ijkl}^\infty + \sum_{n=1}^N G_{ijkl}^n \quad (2.27)$$

Using this formulation, stress can be considered as summation of the stresses in a generalized maxwell model. Generalized Maxwell or Wiechert model is a mathematical model to indicate the stress relaxation behavior of a material. Elastic behavior of the material

is modeled with a spring and viscous behavior is modeled with a dashpot analogy[33]. The stress is therefore,

$$\sigma_{ij}(t) = \sigma_{ij}^{\infty}(t) + \sum_{n=1}^N \sigma_{ij}^n(t) \quad (2.28)$$

where

$$\sigma_{ij}^{\infty} = G_{ijkl}^{\infty} \epsilon(t) \quad (2.29)$$

$$\sigma_{ij}^n = \int_0^t G_{ijkl}^n \exp -(t - \tau) / \lambda^n \frac{d\epsilon_{kl}(\tau)}{d\tau} \quad (2.30)$$

Generalized maxwell model is represented in Figure 2.8. In order to discretize the

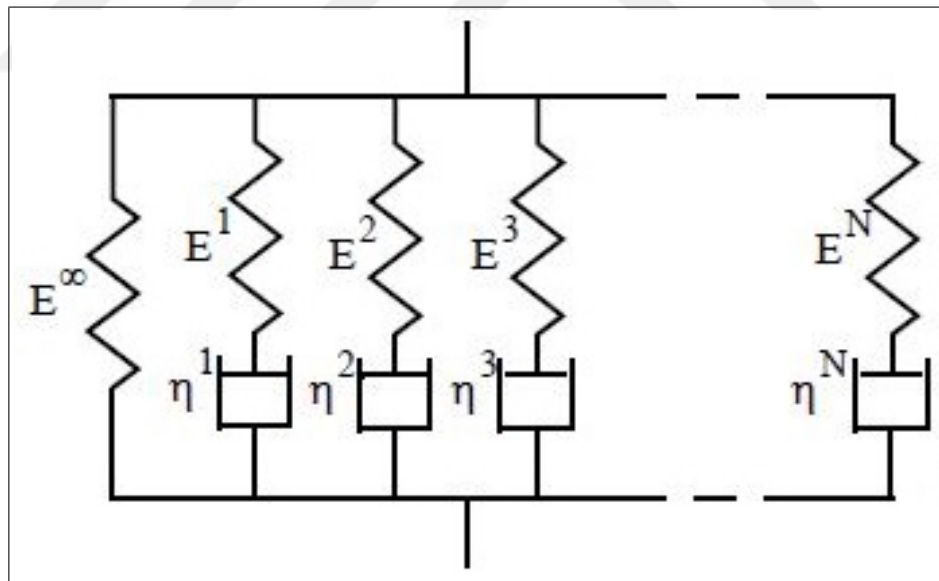


Figure 2.8. The generalized Maxwell model [32].

constitutive equation, incremental approach is used. The total time is divided into timesteps

$\Delta t = t_m - t_{m-1}$. Incremental equation for total stress is formulated as,

$$\Delta\sigma_{ij}(t_m) = [G_{ijkl}^0 - \sum_{n=1}^N 1 - \beta^n G_{ijkl}^n] \Delta\epsilon_{kl}(t_m) - \sum_{n=1}^N \alpha^n(\Delta t) \sigma_{ij}^n(t_m - \Delta t) \quad (2.31)$$

where

$$\alpha^n(\Delta t) = 1 - \exp\left(-\frac{\Delta t}{\lambda^n}\right) \quad (2.32)$$

and

$$\beta^n(\Delta t) = \alpha^n(\Delta t) \frac{\lambda^n}{\Delta t} \quad (2.33)$$

2.2.2.3. Isotropic Viscoelastic Material

Glass is an isotropic material due to lack of orientations in its microstructure. Therefore, it fits the isotropic viscoelastic material definition around its transition temperature. For an isotropic viscoelastic material, volumetric and deviatoric behavior are time dependent and described by bulk and shear modules. These two behavior are decoupled.

The shear and bulk modules are indicated in a Prony series [32],

$$G(t) = G^\infty + \sum_{n=1}^N G^n \exp\left(-\frac{t}{\lambda_d^n}\right) \quad (2.34)$$

$$K(t) = K^\infty + \sum_{n=1}^N K^n \exp\left(-\frac{t}{\lambda_v^n}\right) \quad (2.35)$$

Deviatoric and volumetric component matrices are expressed as,

$$[\pi_d] = \begin{bmatrix} 4/3 & 2/3 & 2/3 & 0 & 0 & 0 \\ 2/3 & 4/3 & 2/3 & 0 & 0 & 0 \\ 2/3 & 2/3 & 4/3 & 0 & 0 & 0 \\ 0 & 0 & 0 & 1 & 0 & 0 \\ 0 & 0 & 0 & 0 & 1 & 0 \\ 0 & 0 & 0 & 0 & 0 & 1 \end{bmatrix}$$

$$[\pi_v] = \begin{bmatrix} 1 & 1 & 1 & 0 & 0 & 0 \\ 1 & 1 & 1 & 0 & 0 & 0 \\ 1 & 1 & 1 & 0 & 0 & 0 \\ 0 & 0 & 0 & 0 & 0 & 0 \\ 0 & 0 & 0 & 0 & 0 & 0 \\ 0 & 0 & 0 & 0 & 0 & 0 \end{bmatrix}$$

Incremental equation for total stress is then expressed as,

$$\begin{aligned} \Delta\sigma(t_m) &= [G^0 - \sum_{n=1}^{N_d} [1 - \beta_d^n(\Delta t)G^n]]\pi_d\Delta\epsilon(t_m) \\ &\quad [K^0 - \sum_{n=1}^{N_v} [1 - \beta_v^n(\Delta t)K^n]]\pi_v\Delta\epsilon(t_m) \\ &\quad - \sum_{n=1}^{N_d} (\alpha_d^n(\Delta_d^n(t_m - \Delta t))) - \sum_{n=1}^{N_v} (\alpha_v^n(\Delta_v^n(t_m - \Delta t))) \end{aligned} \quad (2.36)$$

where

$$\Delta\sigma_d^n(t_m) = \beta_d^n(\Delta t)G^n\pi_d\Delta\epsilon(t_m) - \alpha_d^n\sigma_d^n(t_m - \Delta t) \quad (2.37)$$

$$\Delta\sigma_v^n(t_m) = \beta_v^n(\Delta t)K^n\pi_v\Delta\epsilon(t_m) - \alpha_v^n\sigma_v^n(t_m - \Delta t) \quad (2.38)$$

2.2.2.4. Time-Temperature Superposition

Time-temperature characterization of polymeric materials and glass-forming liquids require a large number of tests in their expected working temperature range. These tests to measure relaxation modulus or creep compliance of a material are done for constant temperatures and can take long periods of laboratory work. This kind of discrete tests for different temperatures are both expensive and time consuming. Some properties of the viscoelastic materials can be measured at different temperatures for shorter time intervals and by shifting the resulting curves on to a reference curve of arbitrary temperature, a composite curve that represent the material property for all temperatures and times can be constructed. This composite curves are called as master curves. In figure 2.9(a), three short time interval tests are done for different temperatures, T_1, T_r, T_2 where $T_2 > T_r > T_1$. Also there is a long duration test result for T_r . In figure 2.9(b), short duration curves are shifted on to curve of the reference temperature, T_r . By this method, a master curve that represent material property for T_1, T_r and T_2 in a larger time duration is obtained. Time-temperature shift

enables us to obtain the property, P , for time t and temperature, T , from the data obtained for temperature T_r . The transformation from $t|_T$ to $t|_{T_r}$ is done by the shift $a_T(T, T_r)$ [37]:

$$\log(t|_{T_r}) \equiv \log\left(\frac{t|_T}{a_T(T, T_r)}\right) \quad (2.39)$$

Master curve is determined for a reference temperature and time. The property function calculated from master curve is,

$$P(t, T) = P\left(\frac{t}{a_T(T, T_r)}, T_r\right) \quad (2.40)$$

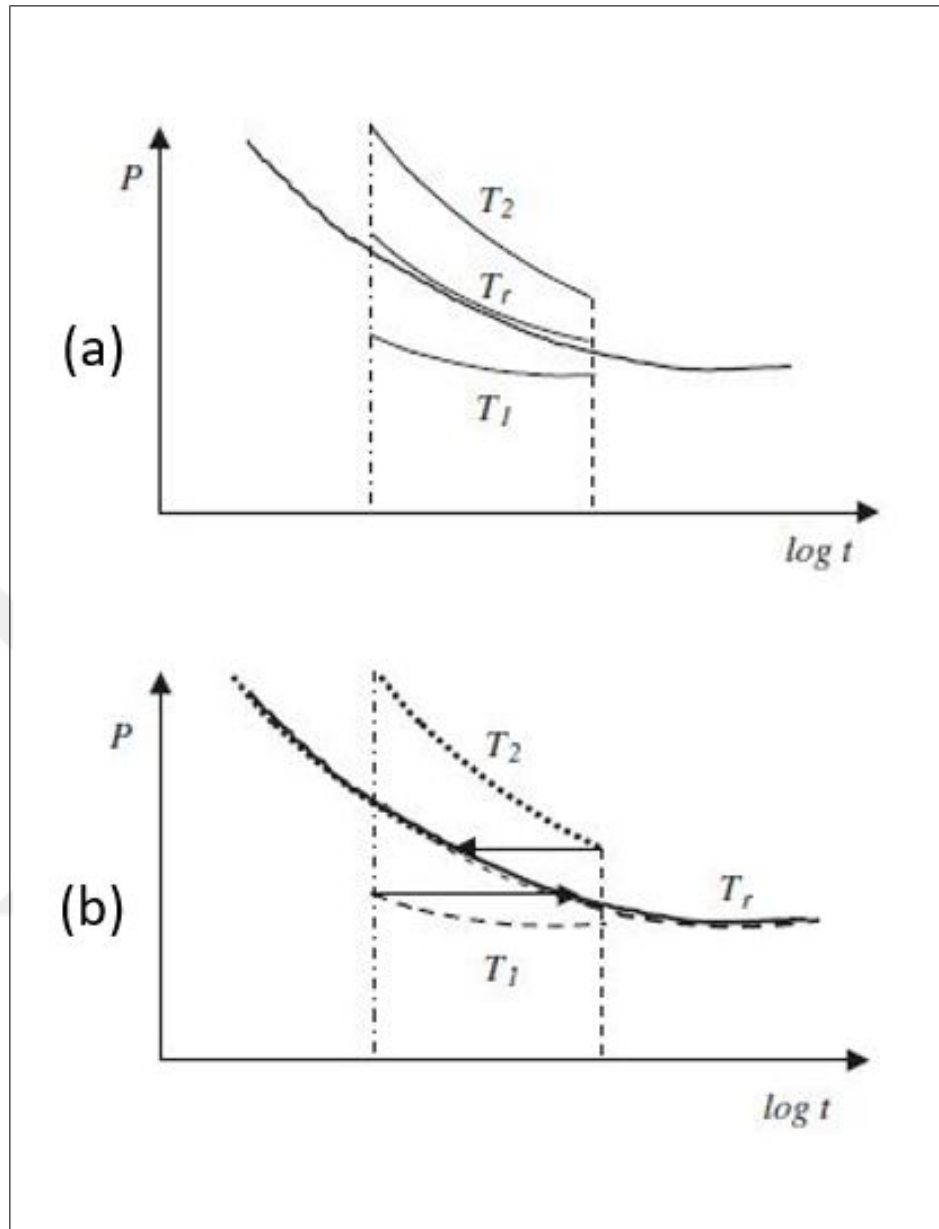


Figure 2.9. Tests at different temperatures and time-temperature shifting [37].

Applying time-temperature superposition into relaxation modulus can be stated as,

$$M(t, T) = M\left(\frac{t}{a_T(T, T_r)}, T_r\right) \quad (2.41)$$

Materials which time-temperature superposition principle is viable are named as thermo-rheologically simple materials. These material behavior is discussed in section 2.2. Time-temperature superposition principle can be used for derivation of their constitutive

equations. The relaxation modulus and creep compliance of these materials are $M(t)$ and $C(t)$, so the constitutive equations for all constant temperature are,

$$\sigma(t) = M\left(\frac{t}{a_T(T, T_r)}\right)\epsilon(0) + \int_0^t M\left(\frac{t-s}{a_T(T, T_r)}\right)\frac{d}{ds}\epsilon(s)ds \quad (2.42)$$

$$\epsilon(t) = C\left(\frac{t}{a_T(T, T_r)}\right)\sigma(0) + \int_0^t C\left(\frac{t-s}{a_T(T, T_r)}\right)\frac{d}{ds}\sigma(s)ds \quad (2.43)$$

Time-temperature superposition principle up to this point is derived for constant temperature. To use the principle for nonconstant/variable temperature states, a shift function which is dependent on position and time is needed. For this purpose, a shifted or reduced time argument is derived [37].

$$\xi_t = \int_0^t \frac{d\tau}{a_T(T(x, \tau), T_r)} \quad (2.44)$$

By using reduced time, constitutive equations applicable for varying temperatures can be derived.

$$\sigma(t) = M(\xi_t)\epsilon(0) + \int_{0+}^t M(\xi_t - \xi_s)\frac{d}{ds}\epsilon(s)ds \quad (2.45)$$

$$\epsilon(t) = C(\xi_t)\sigma(0) + \int_{0+}^t C(\xi_t - \xi_s)\frac{d}{ds}\sigma(s)ds \quad (2.46)$$

2.2.2.5. *Thermo-Rheologically Simple Behavior*

The rate of processes in viscoelastic materials are highly dependent on temperature variation. These rate changes cannot be ignored when there is a noticeable temperature change. The response functions shift translationally with respect to change of temperature along a logarithmic axis. When this shift occurs without changing the shape of function, it is called simple. The materials exhibit this behavior are characterized as thermo-rheologically

simple materials.

A reduced time for a given temperature can be defined for Thermo-Rheologically Simple materials according to temperature field. Viscoelastic equilibrium and compatibility equations are not equal to the elastic equations when the shifted time is used.

In case of Thermo-Rheologically Simple materials, all characteristic functions obey the same property. The shape of the shift function stays the same in any temperature but shifts with respect to temperature variation. This behavior can be seen in figure 2.10 where relaxation modulus shifts parallel to time axis [32]. $E_T(\ln t)$ is the relaxation modulus as a

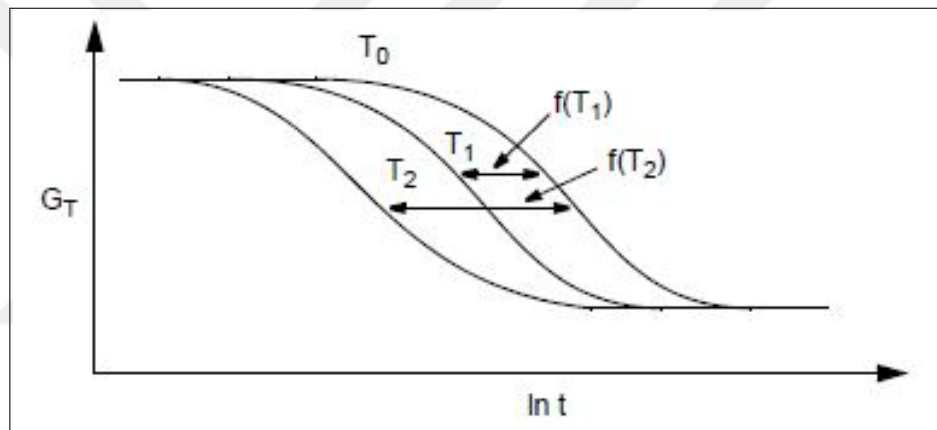


Figure 2.10. Shift of relaxation modulus at different times [32].

function of $\ln t$ at uniform temperature, T .

$$E_T(\ln t) = E_{T_0}[\ln t + f(T)] \left(\frac{\rho T}{\rho_0 T_0} \right) \quad (2.47)$$

With increasing temperatures, modulus curve increases towards shorter times and shifts left. $f(T)$ is a positive increasing function for $T > T_0$. Relaxation modulus as a function of time at a constant temperature is,

$$G_T(t) = E_T(\ln t) \quad (2.48)$$

Therefore,

$$G_T(t) = G_{T_0}(\xi) \quad (2.49)$$

When the temperature is not constant, the shift function is $a(T(x, t))$, the rate of change of reduced time is,

$$d\xi = a_T[T(x, t)]dt \quad (2.50)$$

Shift function can be specified with respect to Arrhenius equation[32].

$$\ln A_t = \left(\frac{H}{R}\right) \left(\frac{1}{T} - \frac{1}{T_g}\right) \quad (2.51)$$

where A_t is a time based shift factor. H is activation energy, R is universal gas constant. T is the temperature and T_g is the glass transition temperature.

An Arrhenius type relation for the appropriate definition of the temperature dependency of relaxation times is developed [34][36].

$$\xi(t, T) = \int_0^t \exp\left(-\frac{H}{R} \left(\frac{1}{T_{ref}} - \frac{1}{T(t')}\right)\right) dt' \quad (2.52)$$

2.2.2.6. Narayanaswamy Model for Structural Relaxation

Narayanaswamy developed a structural relaxation model for design of heat treated processes where glass exposed to temperature change. In this model, time dependence of physical properties(volume) are taken into account [35][34]. In glass transition region, molecular rearrangement rate is fast and occur in scale of minutes and hours. Below glass transition temperature, viscous properties of the material is dominant and a solidus state is present. Above glass transition temperature, material get into equilibrium state easily and a liquidus state exists. With respect to these informations, glass transition phenomenon can be

explained as a variation of temperature dependence of properties of a liquid while cooling. When the liquid is exposed to a stress while it is in transition temperature, time dependent change in dimensions occur because of viscoelasticity of the material. If a liquid in its transition region is subjected to an instantaneous temperature variation, time-dependent change in volume occurs as indicated in figure 2.11(a). This process is called structural relaxation [32]. Suppose that a glass is at T_1 , then instantaneously cooled down to T_2 at t_0 . Sudden change in volume is $\alpha_g(T_2 - T_1)$ continuing with relaxation towards $V(\infty, T_2)$. Total volume change with at t_1 is $\alpha_l(T_2 - T_1)$ as shown in figure 2.11(b). Rate of volume change is controlled by a characteristic time labeled as relaxation time [32]. Parameter α_g is thermal expansion coefficient of glass in solid state and α_l is thermal expansion coefficient of glass in liquid state.

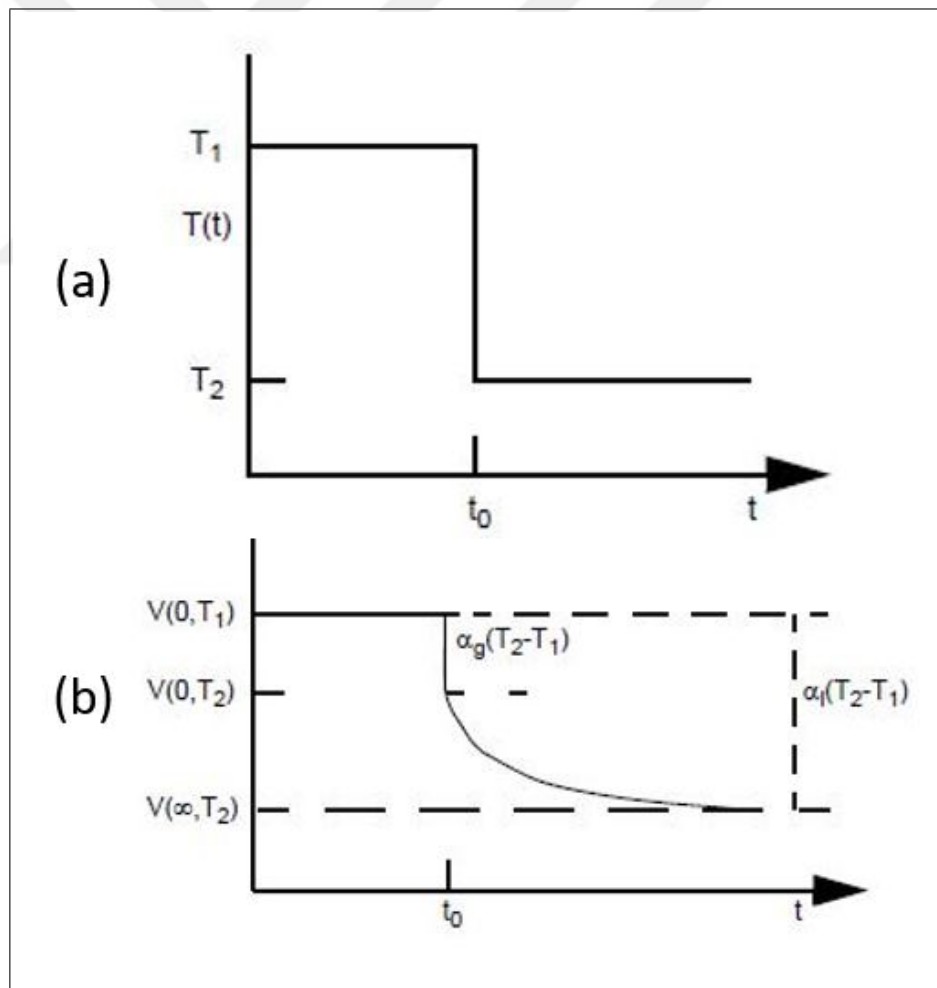


Figure 2.11. Step input for temperature and volume change [32].

The slope dV/dT in figure 2.12 changes with respect to α_l at higher temperatures and α_g for lower temperatures. Glass transition temperature T_g lies in the middle of the transition region. At lower temperatures, atoms vibrate but cannot make relatively large displacements. On the other hand, at higher temperatures, atoms can make larger displacements because of liquid-like state of the glass. Because of this fact, volume changes in higher temperatures are larger than lower temperatures, so α_g is smaller than α_l .

During heating-cooling cycle, property of the material stays in a nonequilibrium temperature that lags behind the applied process temperature. This nonequilibrium temperature that the material resides is called as fictive temperature, T_f . If the applied temperature is T_1 but the material shows nonequilibrium behavior of fictive temperature, this temperature can be indicated by $T_f(T_1)$. Fictive temperature can be determined by drawing a line from $V(T_0)$ with slope of α_l and another line starting from $V(T_1)$ with slope of α_g . The temperature at the intersection of these two lines gives the fictive temperature. Below glass transition region, fictive temperature reaches a temperature where it can no longer change, this temperature is called glass transition temperature T_g . The volume change can be

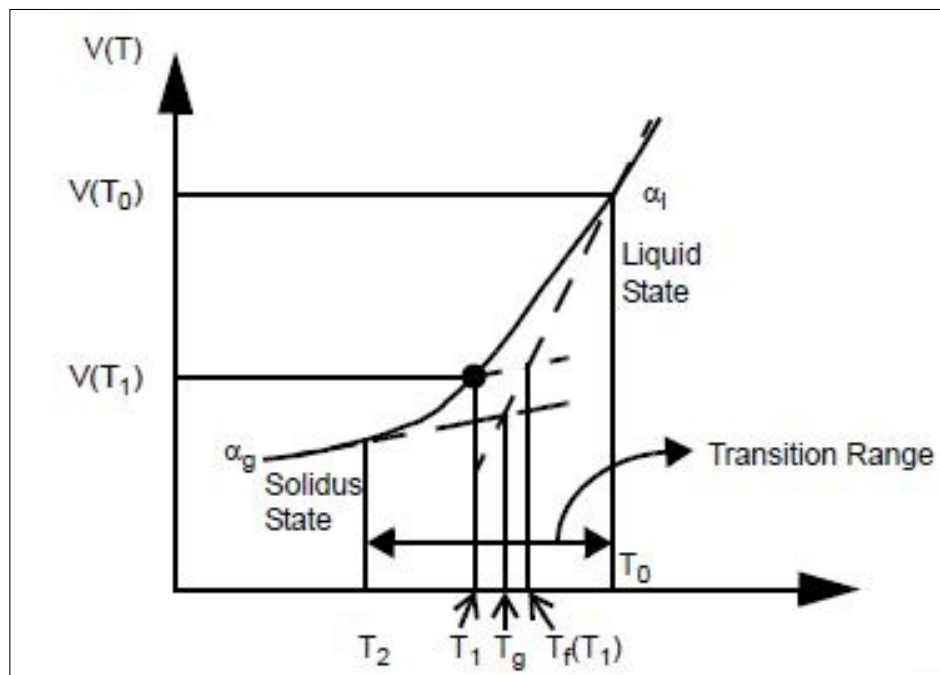


Figure 2.12. Volume change as a function of temperature [32].

described as,

$$V(T_2, t) = V(T_1, \infty) + \alpha_g(T_2 - T_1) + (\alpha_l - \alpha_g)(T_f(t) - T_2) \quad (2.53)$$

where $T_f(T)$ is instant value of the fictive temperature. The response function, M_V , controls the value of T_f and material property. It is assumed to be linear.

$$\frac{V(t) - V(\infty)}{V(0) - V(\infty)} = M_V(\xi(t)) = \frac{T(t) - T(\infty)}{T(0) - T(\infty)} \quad (2.54)$$

By time-temperature superposition of Boltzmann, fictive temperature at any time can be calculated.

$$T_f(t) = T(t) - \int_{-\infty}^t M_V(\xi(t)) - \xi(t') \frac{d}{dt'}(T(t'))(dt') \quad (2.55)$$

Reduced time, $\xi(t)$, is used to unite different response curves into a single master curve. The reduced time in MSC Marc follows the equation:

$$\xi(t) = \int_{-\infty}^t \frac{\tau_{ref}}{\tau(T(t'))} dt' \quad (2.56)$$

τ_{ref} is reference relaxation temperature at reference temperature T_{ref} . The relaxation time τ at a particular time and temperature can be indicated as,

$$\tau = \tau_{ref} \exp\left(-\frac{H}{R}\right) \left(\frac{1}{T_{ref}} - \frac{x}{T} - \frac{(1-x)}{T_f}\right) \quad (2.57)$$

The parameter x controls how many percent of the fictive temperature participates to relaxation time. It is also called as fraction parameter and ranges between 0 to 1. H is the activation energy and R is the universal gas constant. A response function is,

$$M_V(\xi) = \exp\left(-\frac{\xi}{\tau}\right) \quad (2.58)$$

Multiple response functions cannot exist but multiple response functions can be summed

with respect to their weights.

$$M_V(\xi) = \sum_{i=1}^n (W_g)_i \exp\left(-\frac{\xi}{\tau}\right) \quad (2.59)$$

where $\sum (W_g)_i \simeq 1$.

In Daudeville and Carre's work[39], the effect of structural relaxation on the thermal strain is shown as,

$$\epsilon_{th} = \alpha_g(T(t) - T_f(t)) + \alpha_l(T_f(t) - T_0) \quad (2.60)$$

2.3. DYNAMIC MECHANICAL ANALYSIS

DMA (Dynamic Mechanical Analysis) can be described as application of an oscillating force to a sample and analyzing the response of the sample material to that applied force [17]. Researchers can calculate properties like viscosity from phase lag between the applied force and material's response. Also, modulus of the sample material can be learned from the recovery. These properties are associated with material's damping property, which is the ability to lose energy as heat.

DMA is widely used in polymeric materials in order to determine T_g , curing temperature and so on. In same manner, glasses can be analyzed by DMA in order to determine time-dependent modulus, creep, recovery and stress relaxation properties. As we know, these properties are traditionally calculated by tensile or compressive testing. The difference of DMA with traditional methods is that the analysis is not static, rather dynamic. Also, results are obtained from material's damping properties and they can be obtained in short time intervals.

Fig 2.13 shows the section view of a Perkin-Elmer DMA 7e. There are many sample shapes and interchangeable measuring systems for these shapes. Temperature that the experiment

is held can be changed because measuring system and sample are in a furnace.

DMA applies an oscillatory force which causes a stress pattern changing sinusoidally with time. Fig 2.14 shows the sinusoidal patterns of applied stress and material's response. By calculating the amplitude of deformation and the phase lag between two waves, viscosity and damping can be determined. F_d is the oscillatory force and F_s is the static force [17].

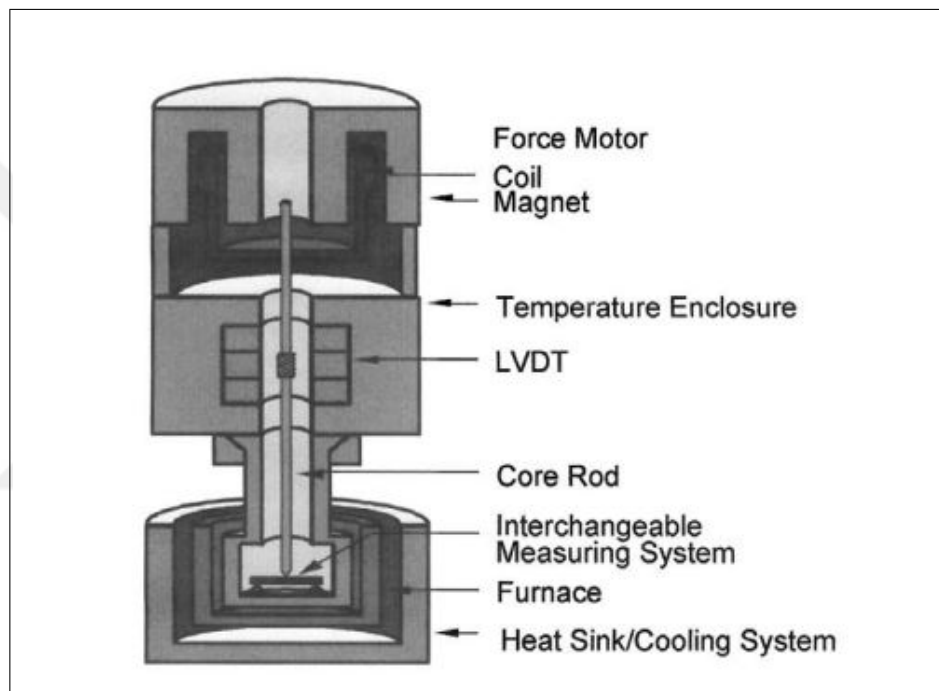


Figure 2.13. Section view of Perkin-Elmer DMA 7e [17].

The modulus calculated by DMA is not exactly the same as Young's modulus. Young's modulus is the slope of the stress-strain curve in elastic region. However, in DMA, complex modulus E^* , storage modulus E' and loss modulus E'' are determined. These three different moduli enables us to determine the material's ability to recover and store energy E' , ability to lose energy E'' and also the ratio of these two parameters $\tan\delta$, which is known as damping [17].

$$E^* = E' + iE'' \quad (2.61)$$

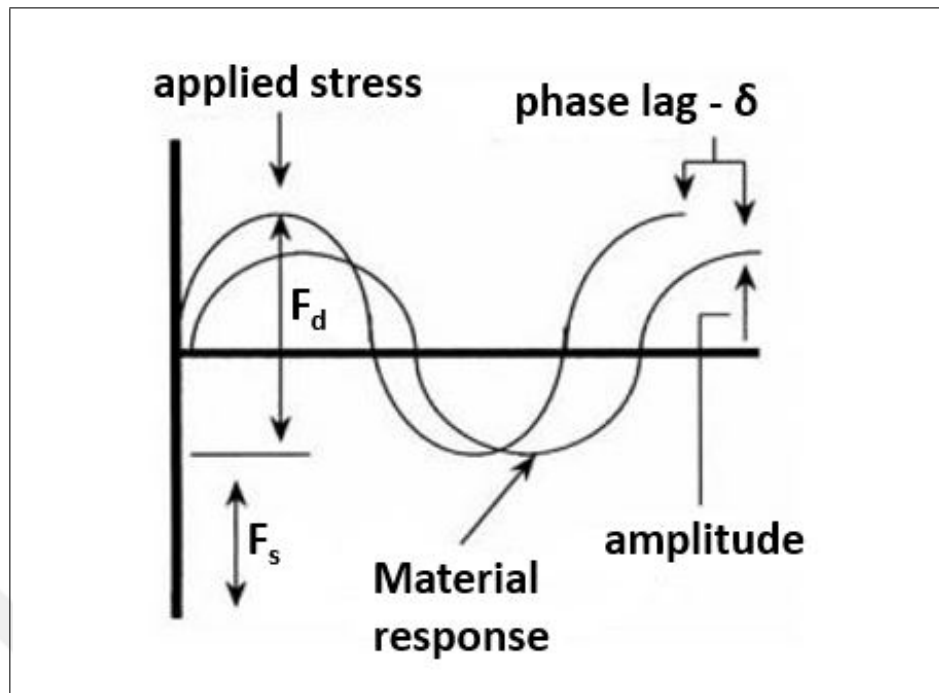


Figure 2.14. Applied stress and material response [17].

$$\tan\delta = \frac{E''}{E'} \quad (2.62)$$

$$\eta^* = \frac{E''}{\omega} \quad (2.63)$$

In Fig 2.15, relationship between storage and loss modulus can be seen. As material becomes more elastic, δ angle gets smaller. For a perfectly rigid material, δ would be zero and E^* and E' would be equal. Tendency to flow is calculated as viscosity and shown as η^* .

In Fig 2.16, DMA of nylon can be seen. Change of storage modulus and $\tan\delta$ with temperature should be noted. Upper line represents storage modulus and lower line is the $\tan\delta$.

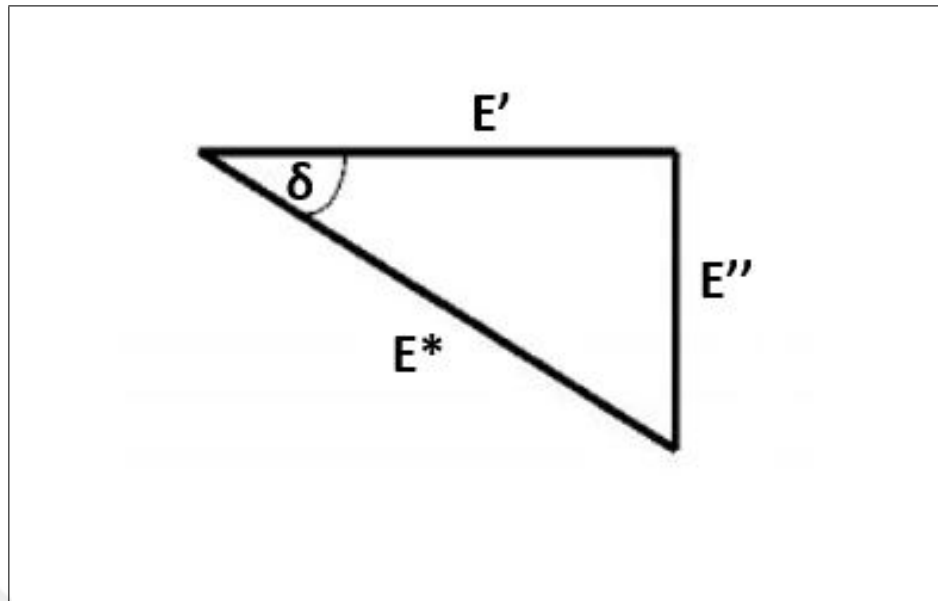


Figure 2.15. DMA relationships [17].

2.4. PREVIOUS WORKS ON FEA OF ENAMELLED STEEL

Enamelled steel structures have been studied on subjects such as microstructure [23] [24], cleanability [27], scratch resistance [23], chemical attack resistance [28], aesthetics [26] and mechanical response during manufacturing [9][5][29].

Van Abeele et al. [9] studied enamelled cantilever beam by first using the Timoshenko thermostat theory. Deflection and stress results for cantilever beam layers are calculated by analytical formulation. In addition, finite element analysis of enamelled cantilever plate is done and validated with Klotz test. In Klotz test procedure, an enamelled steel sample is heated by electric current thermal deflection of the sample is measured by an inductive displacement sensor. In the same time, temperature is measured with an infrared pyrometer. By this method, thermal deflection at stated any temperature can be observed. Van Abeele et al. have done finite element simulations of the enamelled steel sample and validated with the Klotz test. After the validation of the model, several enamelled steel parts line baking tray, hob top and architectural panels are done.

Cooreman et al. [5] searched thermal warping and sagging of enamelled steel parts using

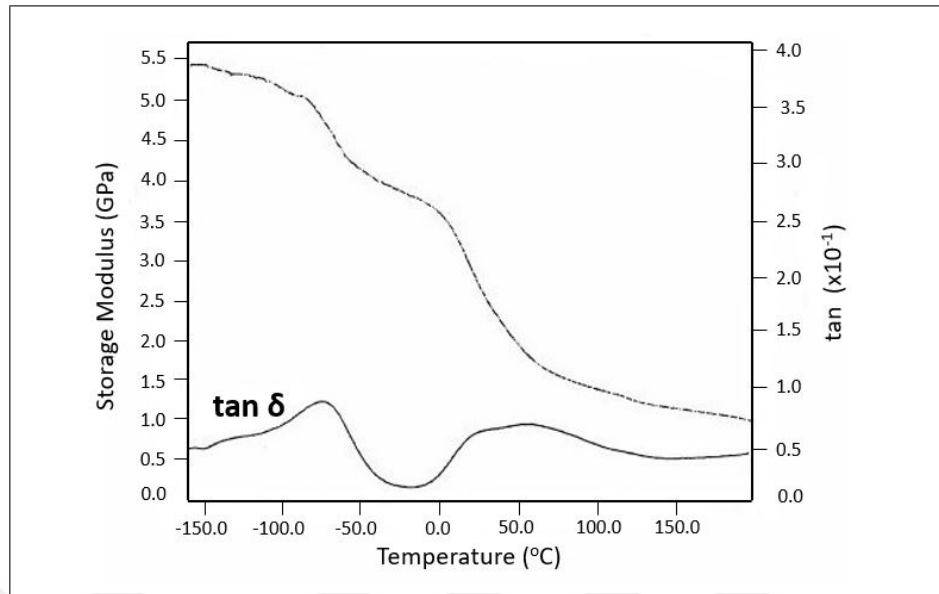


Figure 2.16. DMA of Nylon [17].

integrated finite element simulations. User subroutines which allow stress and structural relaxation effects are implemented in Abaqus are used to predict the mechanical behavior of enamelled steel parts. Stress relaxation can be explained in terms of constant strain and constant stress. Under constant strain, stress will decrease exponentially. Under constant stress, strain will increase gradually. Structural relaxation implies that thermal expansion is not only depend on temperature but also thermal history of the material. T_g can change with different thermal history and this effect is related with structural relaxation.

Son et al. [29] developed a finite element analysis methodology to predict mechanical behavior of enamelled steels. The study is done with u-bending model. The technique involves sheet metal forming analysis and thermal analysis. Thermal analysis is done in order to simulate the manufacturing process. Analysis and experiments are done for different enamel layer configurations. After the simulations, deformations of specimens are measured. Validation study is done with springback comparison between the FE analysis and experiments. In order to model the glass transition effect in enamel layer, the elastic modulus of glass is given as approaching to zero above 450°C.

3. MATERIALS AND METHODS

Enamelled sheet metal is a composite system composed of glass and metal layers. Metal layer acts as substrate for the glass layer. To perform manufacturing analysis of a enamelled sheet steel component, temperature dependent material models should be used. In this chapter, material properties are given and analysis methodology is discussed.

3.1. GLASS

In the production temperature range of enamelled sheet steel, glass material undergoes a transition range called the glass transition range. Many properties like thermal expansion coefficient, modulus of elasticity and viscosity change in accordance to if the temperature is below or above glass transition temperature, T_g .

3.1.1. Properties of Glasses

By definition, “Glass is an amorphous solid completely lacking in long range, periodic atomic structure, and exhibiting a region of glass transformation behaviour.” [4]. A material, rather it is organic, inorganic or metallic, which exhibits glass transformation behaviour is a glass.

Non-crystalline materials such as glass solidify differently than crystalline materials. As the glass cools down, its viscosity increases continuously with decreasing temperature. There is no unique liquid to solid transformation temperature for glasses. One of the differences between crystalline and non-crystalline materials is that, glasses exhibit a dependence of their specific volume (volume per unit mass) on temperature. Figure 3.1 represents the change of specific volume over temperature. Crystalline materials exhibit a discontinuous decrease of specific volume at the melting temperature, T_m . Non-Crystalline materials show a continuous decrease of specific volume with decreasing temperature. Upon this temperature reduction, slope of the curve slightly decreases at a particular point what is defined as glass transition temperature, or fictive temperature, T_g . Below the glass transition

temperature, material is considered as glass. Above this temperature, material is considered as supercooled liquid and at elevated temperatures as liquid [6].

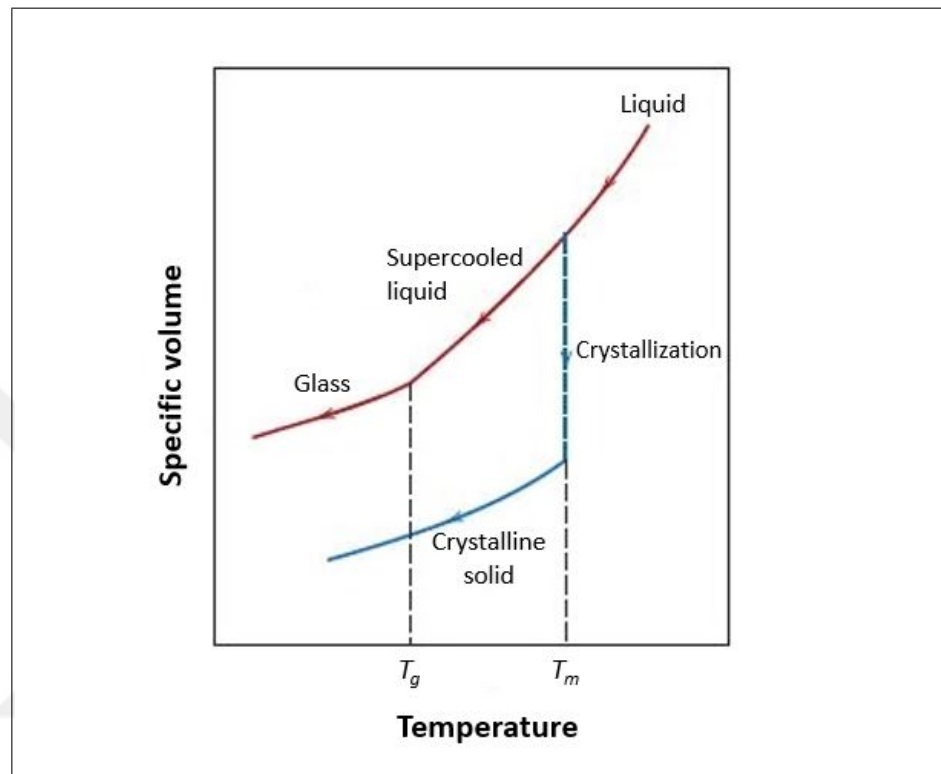


Figure 3.1. Specific volume change of materials [6].

Change of viscosity with changing temperature is another important characteristic of glass-manufacturing operations. Fig.3.2 shows the viscosity versus temperature (Logarithmic) for several types of glasses. Several viscosity values are important in glass forming processes.

- Melting Point: Temperature that the viscosity is $10\text{Pa}\cdot\text{s}$. At this temperature, glass is fluid enough to be considered liquid.
- Working Point: Corresponds to the temperature at which the viscosity is $10^3\text{Pa}\cdot\text{s}$. At this temperature, the glass can be deformed easily.
- Softening Point: The ultimate temperature at which the glass piece can be handled without causing significant deformation. The viscosity is $4 \cdot 10^6\text{Pa}\cdot\text{s}$.
- Annealing Point: Temperature that the viscosity is $10^{12}\text{Pa}\cdot\text{s}$. At this temperature,

atomic diffusion is rapid enough to remove all the residual stresses in 15 minutes.

- Strain Point: Below this temperature, fracture will occur without any plastic deformation. Viscosity is 3×10^{13} Pa·s at this temperature[6].

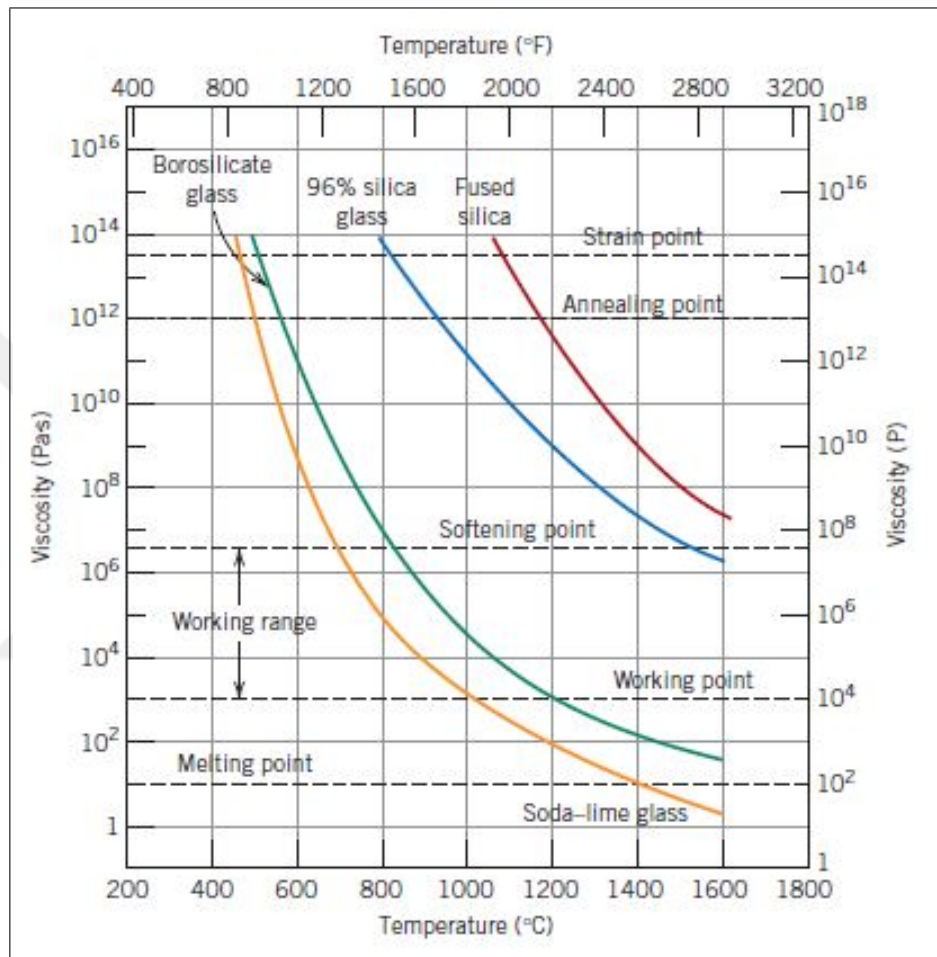


Figure 3.2. Viscosity change of silica glasses [6].

3.1.2. Characterization of Glass

Identification of material properties like glass transition temperature and thermal expansion coefficient require material characterization tests. For identification of these properties, thermal dilatometric analysis is used. Also, for identifying the chemical composition of the glass frit, XRF(X-Ray Fluorescence) analysis is done.

3.1.2.1. Thermal Dilatometric Analysis

Changes in dimension of a specimen through the thermal changes in its environment can be precisely measured with dilatometer. Measurements that can be done with dilatometer are determination of thermal expansion, phase transformations, kinetics studies, softening points, phase diagram construction and sintering temperatures and rates. Dimensional changes of the specimen can be used in order to determine the process parameters by using the thermal cycles which is used in exact process [12].

Dilatometric analysis of the glass frit sample is done by using Netzsch 402c dilatometric analysis device. Temperature range of the analysis is from 20 C° to 650 C°. The heating rate is 10 C°/minute. The glass frit is annealed at 1250 C° for three hours, then poured in a mold to obtain a sample suitable for dilatometric analysis. The analysis result is presented in Figure 3.3.

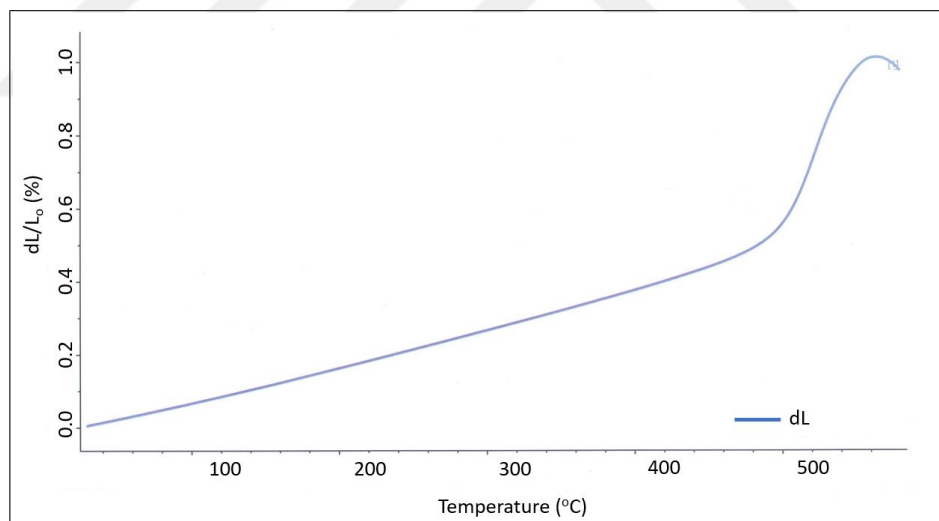


Figure 3.3. Dilatometric analysis of glass.

3.1.2.2. X-Ray Fluorescence Analysis

Composition of the glass frit is determined by XRF analysis. X-ray fluorescence is an analytical technique to determine the elemental composition of materials. This was done by measuring the secondary x-ray emitted after the material is excited by a primary x-ray

source. Every element has its unique secondary x-ray which can be seen as a fingerprint of that element. Semi-quantitative XRF analysis is done by Panalytical PW 2404 X-ray fluorescence spectrometer. The compounds in glass frit and their percentages are presented in Table 3.1.

Table 3.1. Quantification of glass frit XRF results.

Oxides	Concentration(%)
Na ₂ O	12.945
F	0.826
MgO	0.136
Al ₂ O ₃	1.374
SiO ₂	57.274
P ₂ O ₅	0.029
SO ₃	0.672
K ₂ O	5.571
Cl	0.031
CaO	2.466
TiO ₂	4.072
Cr ₂ O ₃	0.920
MnO	2.954
Fe ₂ O ₃	5.442
Co ₃ O ₄	1.584
NiO	0.245
CuO	0.515
ZnO	0.010
SrO	1.264
ZrO ₂	0.334
MoO ₃	0.032
BaO	1.301

3.1.3. Temperature Dependent Properties of Glass

As mentioned in section 3.1.1, mechanical properties of glasses change with respect to viscosity and temperature. Viscosity decreases as temperature increases. There are two approaches about the change of modulus of elasticity through manufacturing stage. As indicated in section 1.3, modulus of elasticity curve can be given as an input up to T_N in order to predict the deformations below neutral stress point which is about 350-380°. The second approach is to define the temperature dependent modulus of elasticity up to 600-650C° as indicated in Figure 3.4. According to Cooreman, there is a temperature where glass becomes capable of stress development. At temperatures higher than this point, glass is viscous enough to relax sufficiently without causing a deformation in glass-steel system.

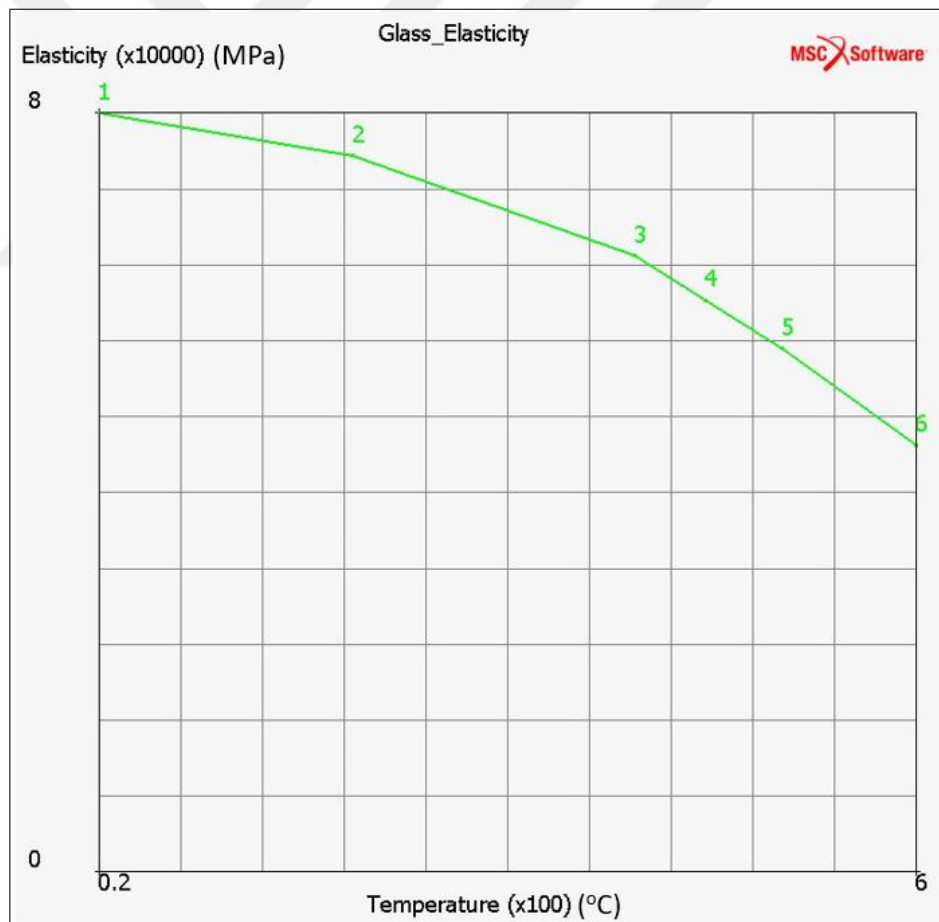


Figure 3.4. Temperature dependent modulus of elasticity of glass.

Glass frit has a similar chemical composition to window(Soda-Lime-Silicate) glass.

Poisson's ratio for window glass does not change significantly with respect to increasing temperature, therefore taken as 0.22 throughout whole analysis [31].

Dilatometric analysis graph is shown in Figure 3.3. Glass transition temperature, T_G is determined as 500°C. Thermal expansion coefficient, α is determined by the slope of the curve as $1.03 \cdot 10^{-5} \frac{1}{^\circ\text{C}}$. Carre et al. [38] mentioned that the thermal expansion coefficient of glass in liquid state is three times the solid state. In this study, thermal expansion coefficient of glass layer in liquid state is taken as $3.09 \cdot 10^{-5} \frac{1}{^\circ\text{C}}$.

3.1.4. Viscoelastic Characteristics of Glass

Glasses can be accepted as viscoelastic material in its glass transition region as mentioned in section 2.2. In this study, viscoelastic material properties of soda-lime-silica glass is used. Study of Carre et al. [38] is taken as a reference for viscoelastic material modelling. The deviatoric, volumetric and structural relaxation parameters are presented in Tables 3.2, 3.3 and 3.4. Reference temperature is, $T_{ref} = 596^\circ\text{C}$:

Table 3.2. Deviatoric part of viscoelastic characteristics [38].

\mathbf{w}_{1i}	$\mathbf{\tau}_{1i}$
0.09256167	0.0002219596
0.1021670	0.001672941
0.1387652	0.02163904
0.1990315	0.2103019
0.2605422	0.9835313
0.2069324	3.376455

The characteristics used in reduced time calculations are, $x=0.5$ and $\frac{H}{R} = 76200\text{K}$

Table 3.3. Volumetric part of viscoelastic characteristics [38].

w_{2i}	τ_{2i}
0.02223075	0.000030801
0.02240328	0.00061147
0.02871376	0.0012435
0.2136628	0.011836
0.3940633	0.073738
0.3189240	0.125040

Table 3.4. Structural relaxation parameters [38].

C_i	λ_i
0.0561	51.67
0.5074	231.55
0.2163	629.36
0.1320	1710.9
0.0408	4650.0
0.0421	20845

3.2. STEEL

In enamel-steel system, steel acts as a substrate for glass layer. Temperature range of manufacturing is between 830-850°C to room temperature. Mechanical properties of steel change with temperature. Temperature dependent modulus of elasticity, Poisson's ratio and thermal expansion coefficient graphs must be used in order to model the material behavior correctly.

For enamelling process, there are specialized steels that are suitable for enamelling. Adhesion, formability and surface properties of these differ from other type of steels. Steel sheets for enamelling are low carbon and cold rolled. There are distinctive

characteristics that distinguish enamel-quality steel sheets from other low carbon sheets. These characteristics are mainly due to differences in sheet metal production processes. In this respect, enamel quality sheets are separated from other low carbon but not enamel quality sheets.

3.2.1. Classification of Cold Rolled Steel Sheets for Enamelling

It is possible to classify the steel sheets for enamelling under three groups. These are: Decarburized (Type 1), normal (Type 2) and interstitial-free (Type 3) [7].

- Type 1: By application of sheet decarburization, extremely low carbon content is achieved. This steel sheet is sufficient for direct cover coat enamelling. Also, this material is applicable for ground and cover coat enamelling. It shows sag resistance and good formability.
- Type 2: This steel is applicable for ground and cover coat enamelling applications. The composition of Type 2 steels are obtained through melting operations.
- Type 3: This steel is an interstitial-free steel and applicable for ground and cover coat enamelling. Composition of the Type 3 steels are obtained through melting operations. It has excellent formability and good sag resistance[8].

These three different sheet metal grades can be classified according to their mechanical properties or their ability to be used directly in enamelling processes.

The tempered sheet metal has different standards according to TS EN 10209, ASTM A 424, ISO 5001, EN 10209 coded standards. Although the basic sheet characteristics specified in these standards are the same, there are minor differences in classification patterns.

3.2.2. Temperature Dependent Mechanical Properties of Steel

Increasing temperature affects the mechanical properties such as modulus of elasticity, Poisson's ratio and thermal expansion coefficient. With increasing temperature, stretching of the atomic bonds becomes easier therefore mechanical properties dependent on these bond

stretching resistance decreases. DC04EK is used in oven cavity component. Temperature dependent mechanical properties of DC04EK steel is shown in Figures 3.5, 3.6 and 3.7.

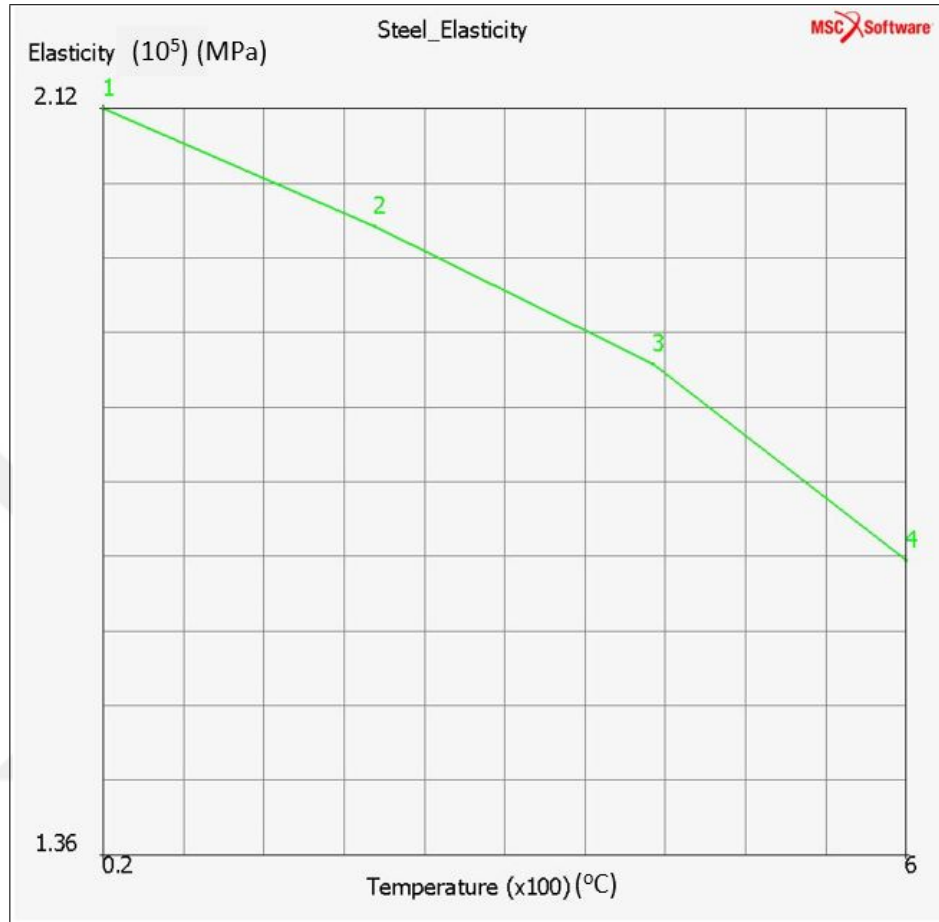


Figure 3.5. Temperature dependent modulus of elasticity.

3.3. MANUFACTURING OF ENAMELLED STEEL SAMPLES

For validation of the enamelled steel manufacturing finite element simulation, rectangular enamelled steel plates of DC04 grade are manufactured. Experiment was held at Arcelik Cooking Appliances Facility at Bolu, Turkey.

Manufacturing process starts with laser cutting of sheet metal specimens from sheet metal roll. Specimens are 200 mm in length, 50 mm in width and has 1 mm thickness. In order to attach the specimens on to conveyor line, two circular holes of 7 mm diameter are opened. Oil and dirt coming from both roll and cutting process must be cleaned before enamelling



Figure 3.6. Temperature dependent Poisson's ratio of steel.

process starts. Cleaning process is done by putting the steel specimens in a cleaning solution for one hour. After the cleaning process, the specimens are dried and get into coating stage. Specimens are hung on conveyor line which gets them into coating chamber as shown in Figure 3.9. Glass frit is sprayed from specialized nozzles. Two sides of the rectangular specimens are coated with frit. In order to measure the bimaterial deflection effect correctly, one side of the specimen is cleaned out of frit. This cleaning stage is done by hand. After this stage, conveyor carries the specimens into furnace where the glass frit is melted and form a continuous film on sheet metal. The temperature-time graph of the furnace stage can be seen in Figure 3.8. Total process time in the furnace is 19 minutes and it starts from 20°C up to 840°C and then cool down to 20°C again.

The glass film thickness was measured using an elcometer from the five specified points on each sample. Measurement points are shown in Figure 3.10.

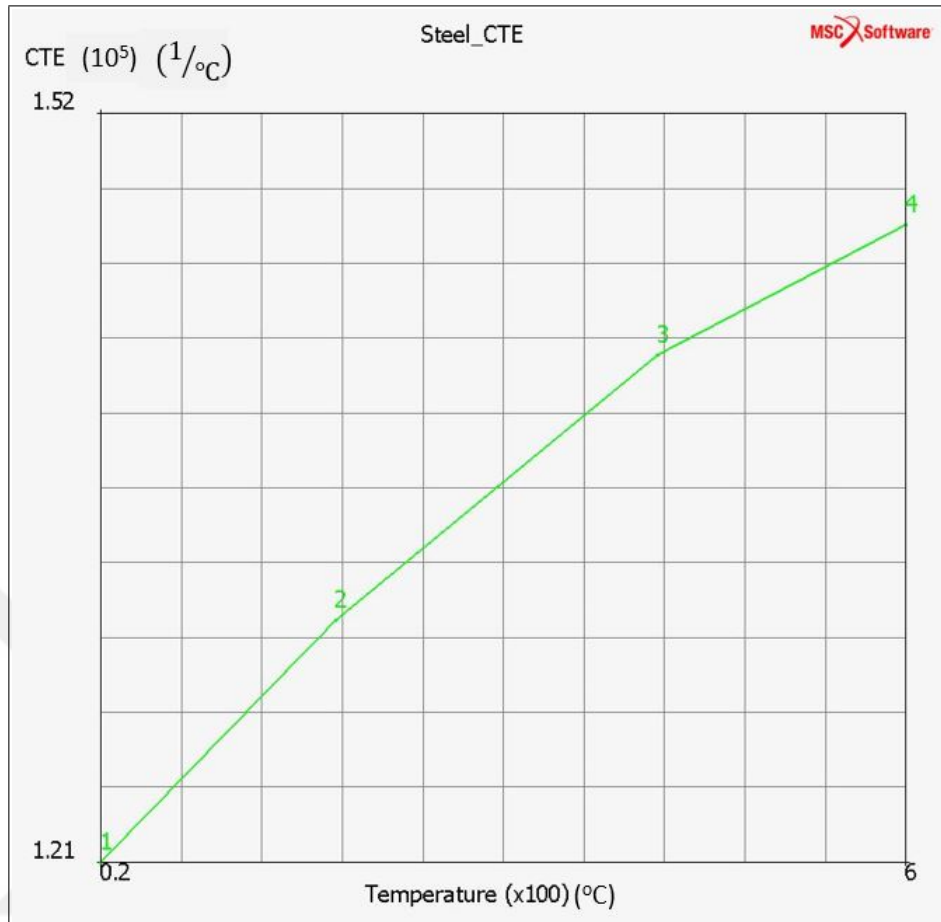


Figure 3.7. Temperature dependent CTE of steel.

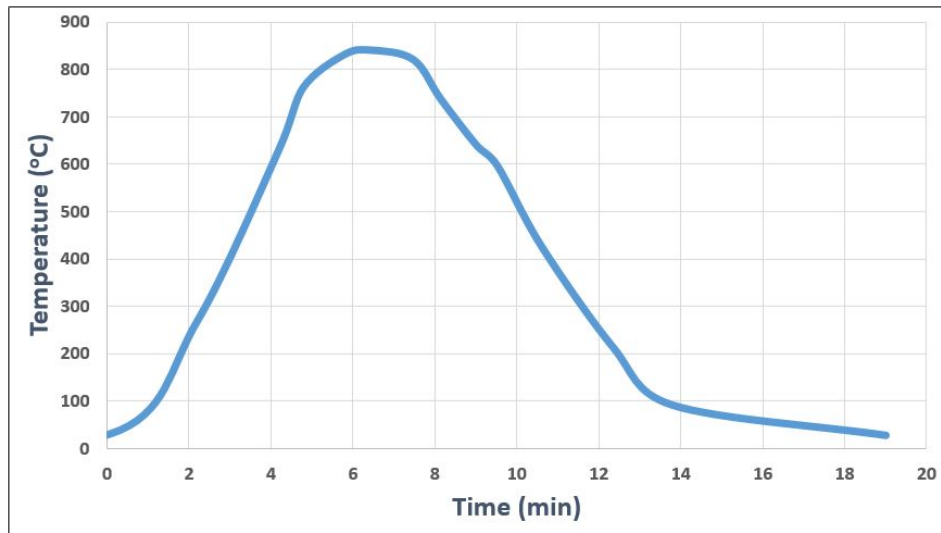


Figure 3.8. Thermograph of the enamelling process.

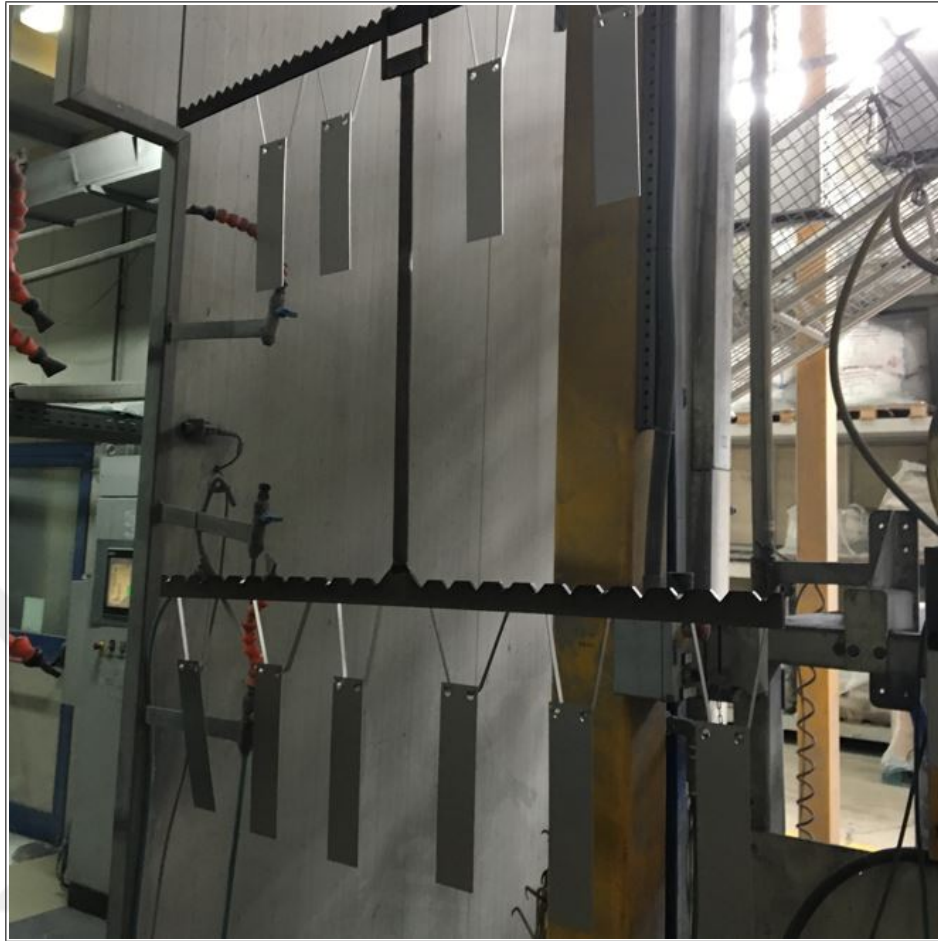


Figure 3.9. Uncoated sheet metal sample on conveyor line.

19 samples were prepared and measurements were taken from the specified points. Table 4.1 shows the thickness values of each specimen on each specified point in micrometers.

The arithmetic mean of the glass thickness values are 121.9 micrometers. Therefore, the thickness of glass layer in enamel-steel system will be taken as 0.122 mm.

To measure the deformation caused by the bimaterial effect, samples are positioned in such a way that two ends are touching the surface. The deflection in the middle part is measured with a caliper. All the samples are measured as indicated in Figure 3.11. Table 4.2 indicates the deflection of each sample in +z direction.



Figure 3.10. Glass film thickness measurement points on specimen.

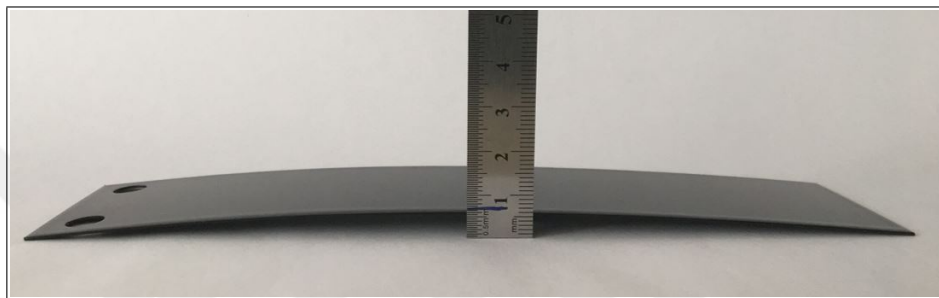


Figure 3.11. Bimaterial deflection measurement.

3.4. MANUFACTURING OF ENAMELLED STEEL OVEN CAVITY

Oven cavity is an enamelled steel product act as a chassis component for ovens. All the systems and components are mounted on oven cavity. The deformations on this component directly affects the further performance of the oven. An improperly mounted system or component will bring quality and functionality problems. To design better oven cavities, engineers should try different designs and end up with a robust design. The manufacturing process of oven cavity involves sheet metal forming, joining and enamelling stages. Producing a prototype for every design idea can be costly. Therefore, a valid finite element model that predicts the deformations after manufacturing stage has great importance.

Manufacturing of oven cavities involve three stages. Forming of sheet metal parts of oven cavity, joining of these parts and enamelling the joined sheet metal component. In this study, forming and joining stages of oven cavity are not covered.

Enamelling stage is performed as similar to enamelled steel sample manufacturing stage as mentioned in section 3.3. Formed sheet metal parts are joined to produce a sheet metal oven cavity body. After this step, the grease and dirt cleaned with an acidic solution in industry scale baths. Cleaned oven cavities are dried out-of this solution and get into coating stage where a nozzle spray glass frit and the interior of the oven cavity is coated with this powder electrostatically. It is impossible to be only coating the interior of the oven cavities. The exterior surface is coated either. But the thickness of the coating on exterior surface is relatively small comparing to interior, which will be mentioned in the following chapter. Then the oven cavities go into heating stage where the glass powder melt and form a continuous glass layer which is known as enamel. Figures 3.12, 3.13 and 3.14 shows the uncoated, glass frit coated and finished oven cavities on production line.



Figure 3.12. Uncoated oven cavities on production line.



Figure 3.13. Glass frit coated oven cavities on production line.



Figure 3.14. Finished oven cavities.

3.5. DIMENSIONAL MEASUREMENT OF OVEN CAVITIES

3.5.1. CMM Measurement

Oven cavities are measured by Zeiss Contura CMM (Coordinate Measurement Machine) in Arcelik Bolu Cooking Appliances Factory. There are two measurement stages, uncoated and enamelled. The components are measured with respect to CAD models and their deviation is calculated. 19 separate oven cavities with same design and manufactured by the same production process are measured and the arithmetic mean of the deviations are presented. By using coordinates of points on the oven cavity, 21 separate dimensions on each oven cavity are measured. In Figure 3.15, CMM measurement of uncoated oven cavities can be seen.

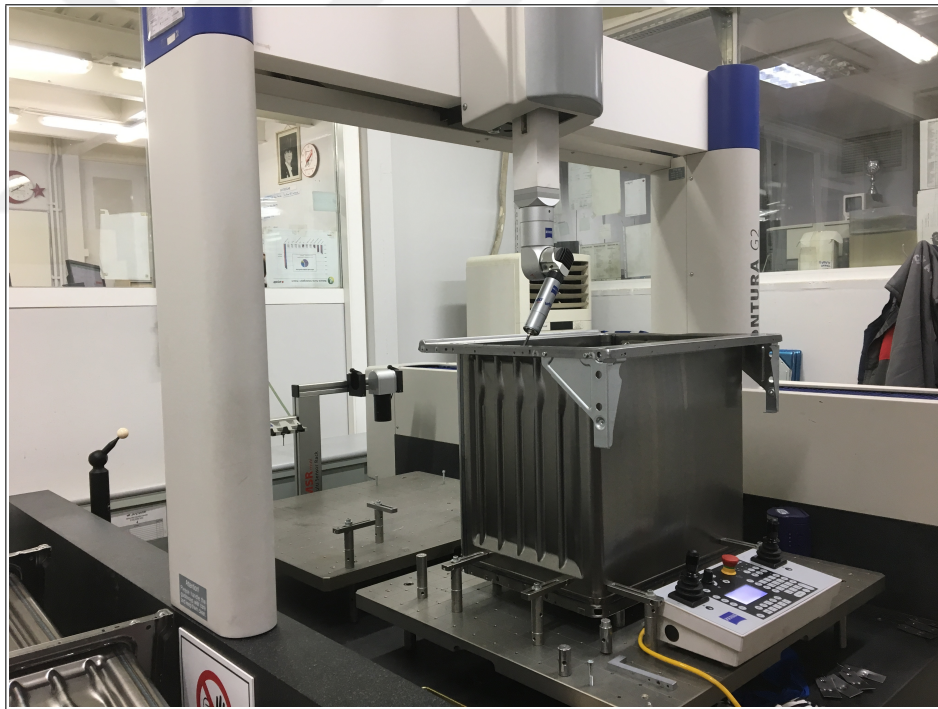


Figure 3.15. CMM measurement of uncoated oven cavity.

Table 4.4 indicates the arithmetic mean of measurements taken from 41 points on 19 separate oven cavities. Location of the measured area, direction, CMM measurement, measurement same point or distance between two points from CAD model and deviation between samples and CAD model are presented. All the measurements are in millimeters. CAD model of the

oven cavity and its parts can be seen in Figure 3.16.

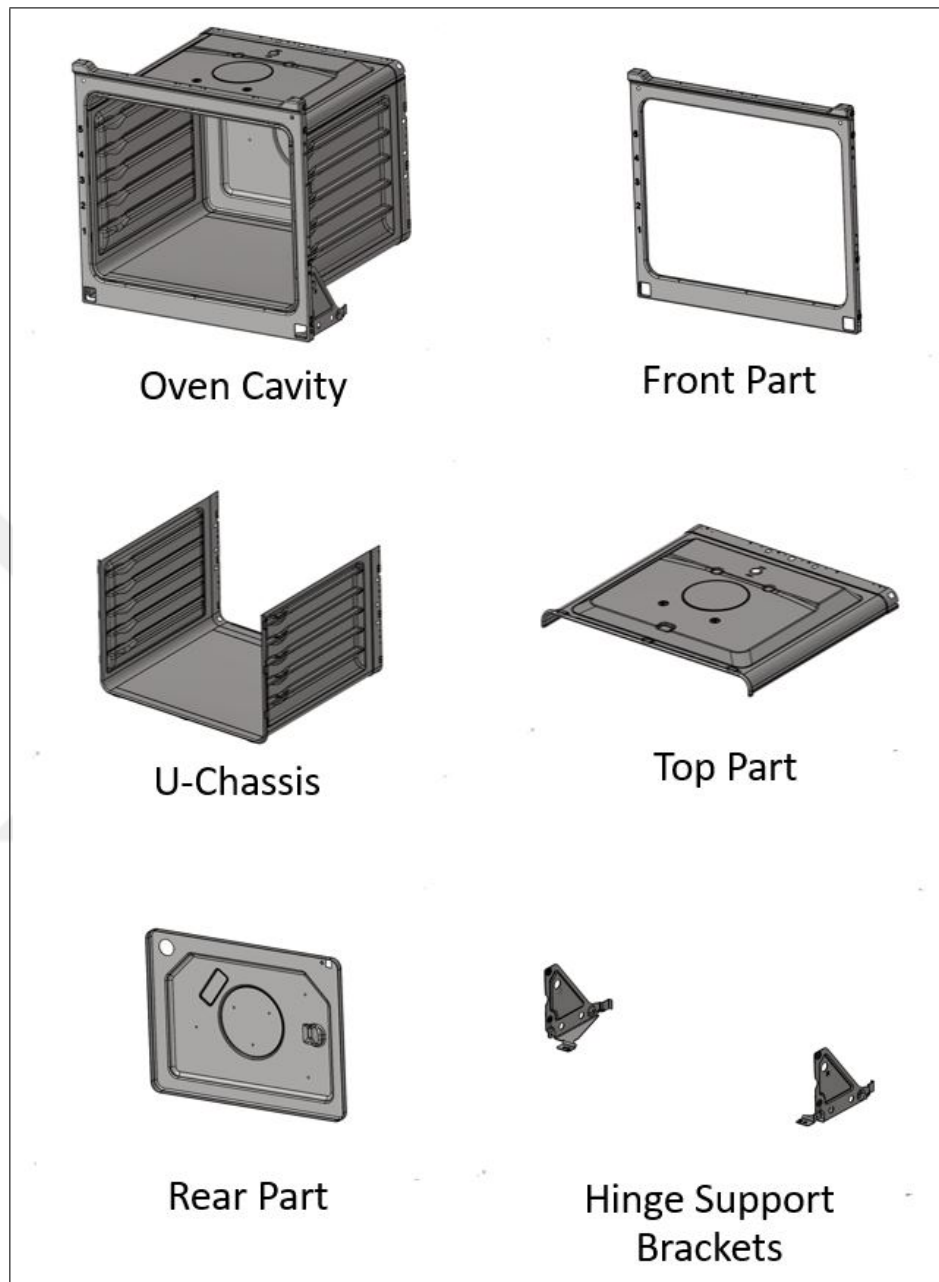


Figure 3.16. CAD models of oven cavity and its parts.

Figures 3.17 and 3.18 show the locations of the points measured. From measurement 1 to 17, distances between opposing shelves are given. From 18 to 21, distance between the flat surface of the front part and rear part are given.

After CMM measurement, uncoated oven cavities are put into enamelling process. After

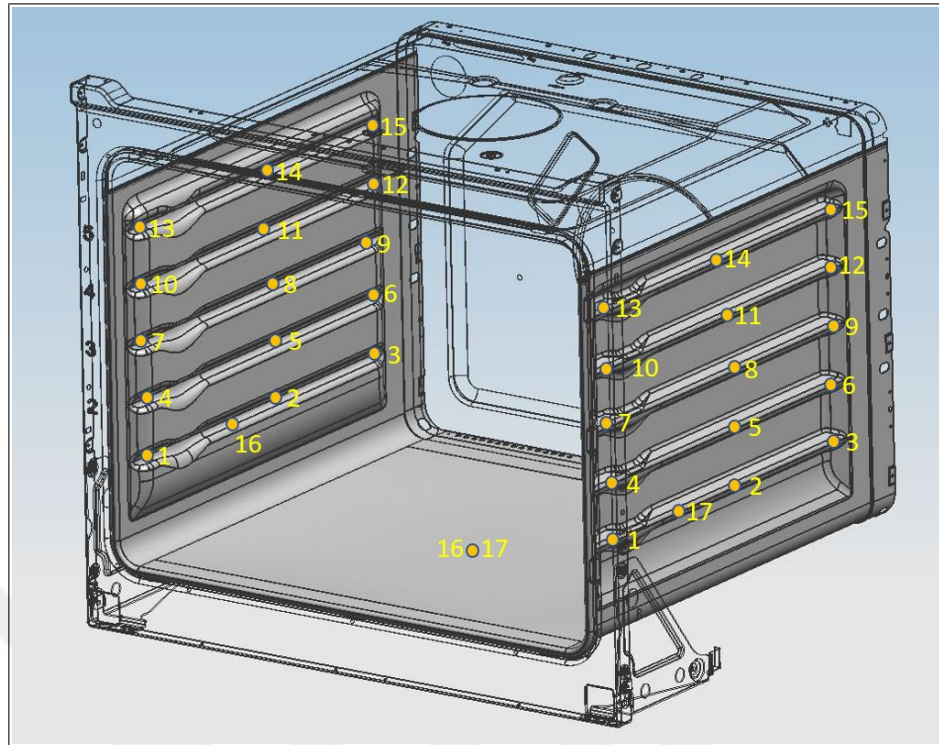


Figure 3.17. CMM measurement points from 1 to 17.

this process, the same oven cavities are taken into CMM measurement and the same points indicated in Table 4.4 are measured again and the results are shown in Table 4.5. The deviation between uncoated and coated (Enamelled) oven cavities are also presented. All the measurements are in millimeters. In Table 4.5, measurements taken from coated oven cavities can be seen.

3.5.2. Coating Thickness Measurement

Thermal deformation of enamelled steel components are directly related to thickness of the glass coating thickness on steel substrate. Since the glass frit is sprayed from a nozzle while the oven cavities are attached to production line, coating thickness of glass can vary on different parts on the component. The glass coating thickness of 19 separate oven cavity samples are measured with Dr. Nix QNix 4500 coating thickness measurement device. Arithmetic mean of the thickness values are given in micrometers. Table 3.5 indicates the mean thickness values for the parts.

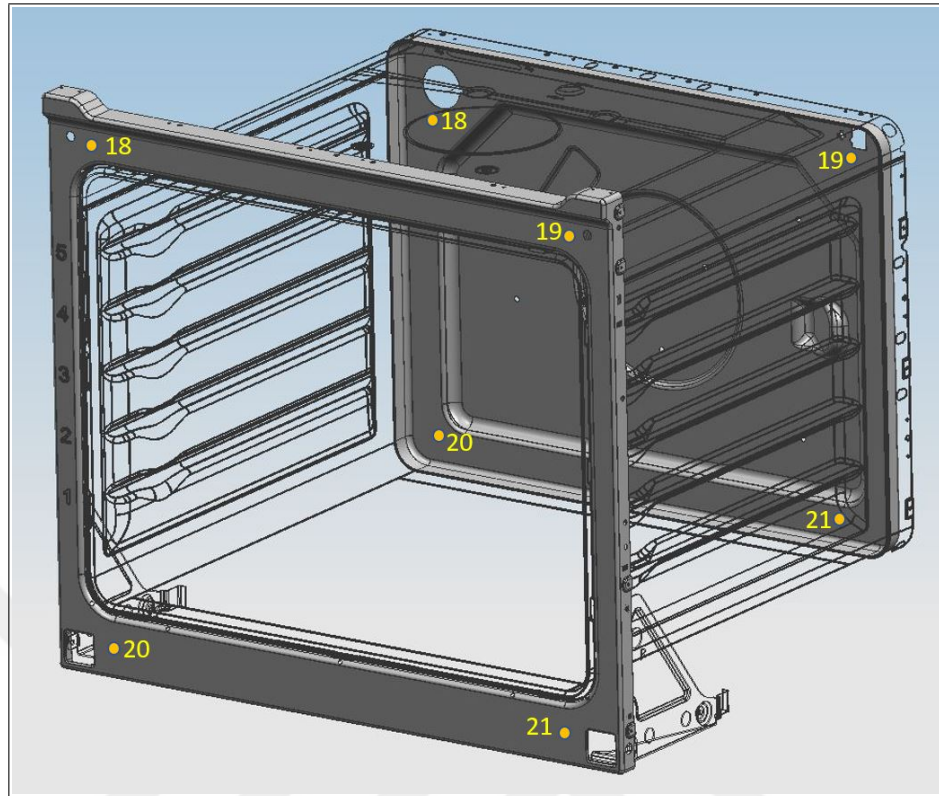


Figure 3.18. CMM measurement points from 18 to 21.

Table 3.5. Coating thicknesses of different parts.

Part	Mean Coating Thickness (μm)
Front Part	108.0395
Top Part	139.4105
U-Chassis	137.2196
Rear Part	127.2737
Hinge Support Brackets	50

3.6. FINITE ELEMENT ANALYSIS

Deformation prediction of enamel-steel systems require implementation of computational methods into account. Analytical and numerical methods are used in order to compute the deformations occur after manufacturing due to bimaterial effect.

Finite element analysis (FEA) is a method used for numerical solution of a wide range of engineering and physics problems. These problems can be heat transfer, structural analysis, electromagnetic potential or mass transport problems. Analytical solution of these problems can be time consuming or even be impossible. In addition, complex geometries used in many engineering applications complicate the computability of an exact solution. In order to have a good approximation and solving engineering and design problems, numerical methods such as finite element analysis are used.

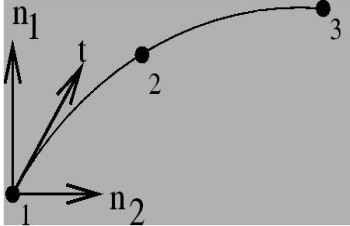
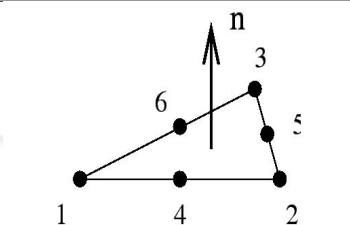
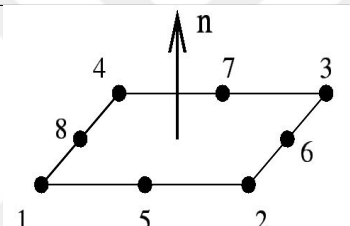
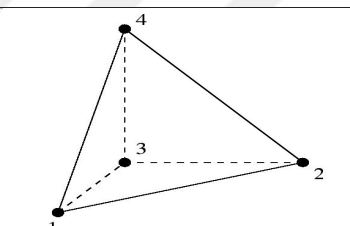
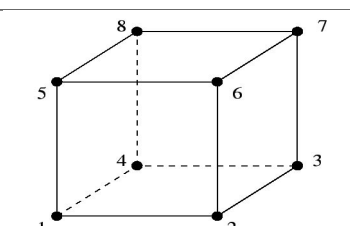
In finite element analysis, rather than dealing with a continuous problem, the structure is divided into finite number of well-defined components which are called *finite elements*. By using finite elements, continuum problems can be discretized. Discrete problems with a large number of finite elements can be solved by modern digital computers.

A finite element can be visualized as a small piece of a structure with well-defined morphology [19]. Modeling a structure with finite elements arise the question of representation of the actual geometry. By using finite elements, the model will be an approximation of the structure. In order to model the structure more accurately, different types of elements are developed. There are one, two and three-dimensional elements. Elements are connected to each other from points which are called nodes. Table 3.6 shows some element types. It should be noted that nodes are not always on the tips, but also can be on the edges of the elements. These type of elements are referred as *quadratic* and their element formulation is different than linear elements. Dividing the structure into elements and nodes is the main strategy in finite element method. Divided model, which is an assemblage of elements and nodes, is called *finite element mesh*. Figure 3.19 shows finite element mesh of a gear tooth. 6 node triangular elements are used to model the geometry.

3.6.1. Element Type Selection

In finite element analysis, good representation of the geometry will enable the analyst to get the nearest approximate result to the actual values. Modeling different geometries require different element types in order to achieve a good representation. As mentioned before, there are one, two and three-dimensional elements. There are also elements that represent

Table 3.6. Finite element types [20].

	Type
	1D Beam Element (Quadratic)
	2D Triangular Quadratic Element
	2D Quadrilateral Quadratic Element
	3D Tetrahedral Element
	3D Brick Element

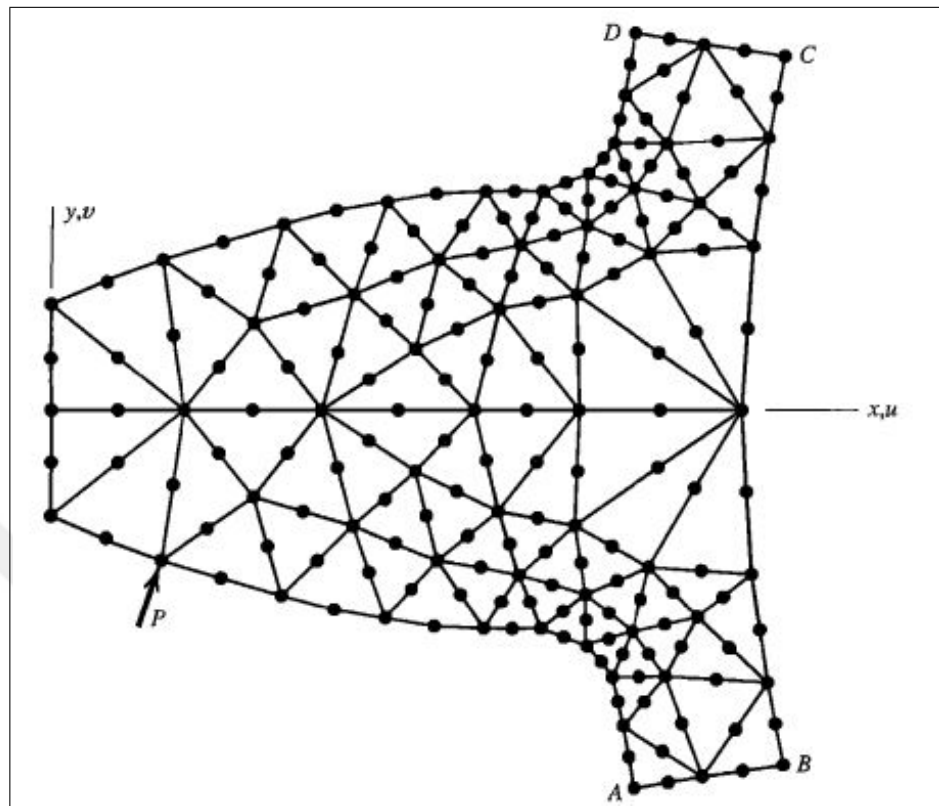


Figure 3.19. Two-dimensional finite element model [19].

welds, springs, dampers or gaps. In Table 3.7 element types, shapes, additional input data and their practical applications can be seen. Beams, rods, bars, pipes can be modeled with 1D elements with a predefined cross-section. Structures where the size at one dimension is quite smaller than the other two dimensions (Sheet metal parts, plastic parts etc.), these materials can be modeled with 2D elements, on other words, *shell elements*. When all three dimensions are comparable with each other, three-dimensional elements are used.

3.6.1.1. 2D Elements

Structures which has two dimensions much larger than the third-dimension can be discretized with 2D elements. Shell elements are planar and they can be visualized like paper [21]. Size of the third-dimension or thickness can be assigned with additional input data by the analyst. For better representation, middle surfaces of the thin walled structure

are extracted. Figure 3.20 shows the middle surface of a thin plate. Since middle surfaces are two dimensional, half of the thickness is assigned to top and bottom.

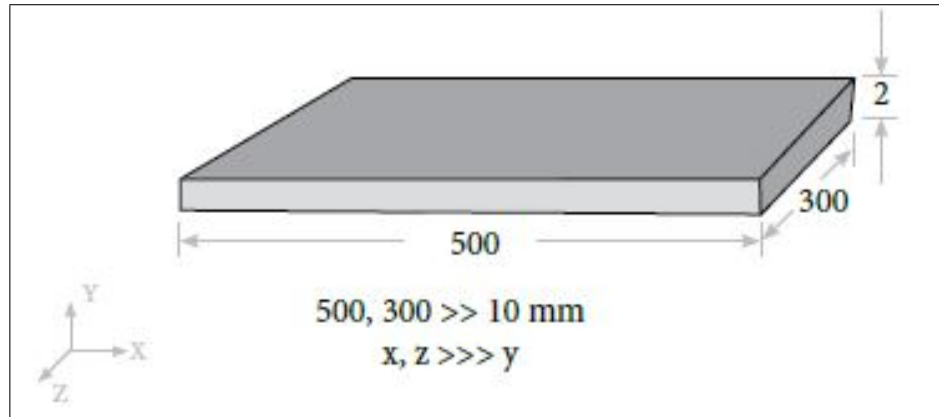
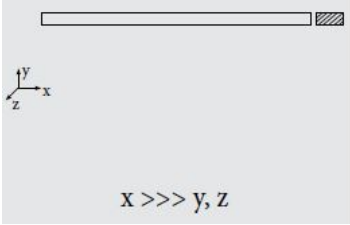
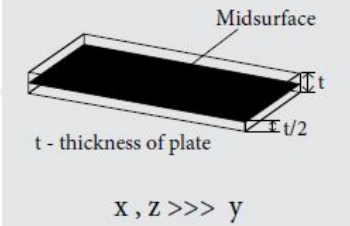
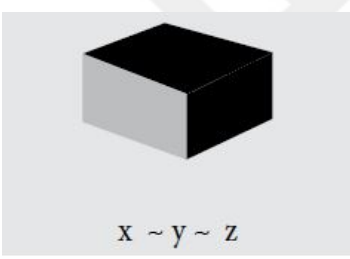
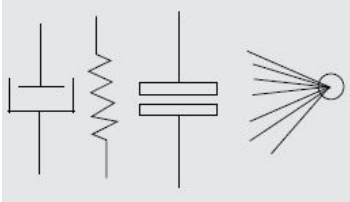


Figure 3.20. Thin walled structure [21].

Problems that can be represented in two dimensions arrive with the need for different 2D element formulations. Plane stress, plane strain, plate, membrane, thin shell and axisymmetric solid are some of these element types. Each element has its own application area which is shown in Table 3.8.

Table 3.7. Element type selection [21].

	Type and Shape	Data	Application
 <p>$x \gg y, z$</p>	1D Element, Line	Area of Cross-Section	Rod, bar, beam, pipe, axisymmetric, Longshafts, beams, pin joint, connection elements, etc.
 <p>Midsurface t - thickness of plate $x, z \gg y$</p>	2D Element, Quad, Tria	Thickness	Thin shell, plate, membrane, plane stress, plane strain, axisymmetric solid, etc.
 <p>$x \sim y \sim z$</p>	3D Element, Solid, Tetra, penta, hex, pyramid	None	Transmission casing, engine block, crankshaft, etc.
	Other Elements		Mass, Spring, Damper, Gap, Rigid and Weld Elements

3.6.1.2. Thin Shell Elements

Thin shell elements is the most general type of 2D elements. Unlike the other members of 2D element family, every node in a shell element has 6 degrees of freedom. In figure 3.21, degrees of freedom in a shell element are represented. U_x, U_y, U_z are translational and $\theta_x, \theta_y, \theta_z$ are rotational degrees of freedom.

Table 3.8. 2D finite element types [21].

Element Type	Total # of DOF	Application
Plane Stress	8	Thin sheet metal parts like aircraft skin, narrow beams
Plane Strain	8	Underground pipes, wide beams, dams
Plate	12	Bending load application
Membrane	12	Balloon, Baffles
Thin Shell	24	Most general type of 2D elements, used in many applications
Axisymmetric Solid	8	Pressure vessels, objects of revolution

3.6.1.3. Shell Elements with Composite Properties

Composite material is the combination of two or more dissimilar materials. These constituent materials are physically and chemically different from each other. When they combined into a composite, the resulting material has superior properties from its constituents. Finite element analysis of composite structures require specification of the layers according to material properties, thickness and orientation. There are many finite element analysis packages which can carry out composite analysis like MSC Nastran, MSC Marc, Altair Optistruct, Abaqus etc. A finite element preprocessor with composite modeling capacities should be used for correct modeling the structure.

Altair HyperMesh is a finite element preprocessor which is capable of generating large-scale finite element models. Preprocessing starts with importing CAD file into HyperMesh to exporting the finite element model into solver. Programme has developed shell element composite modeling capabilities and a specialized GUI in order to define the laminate properties is available.

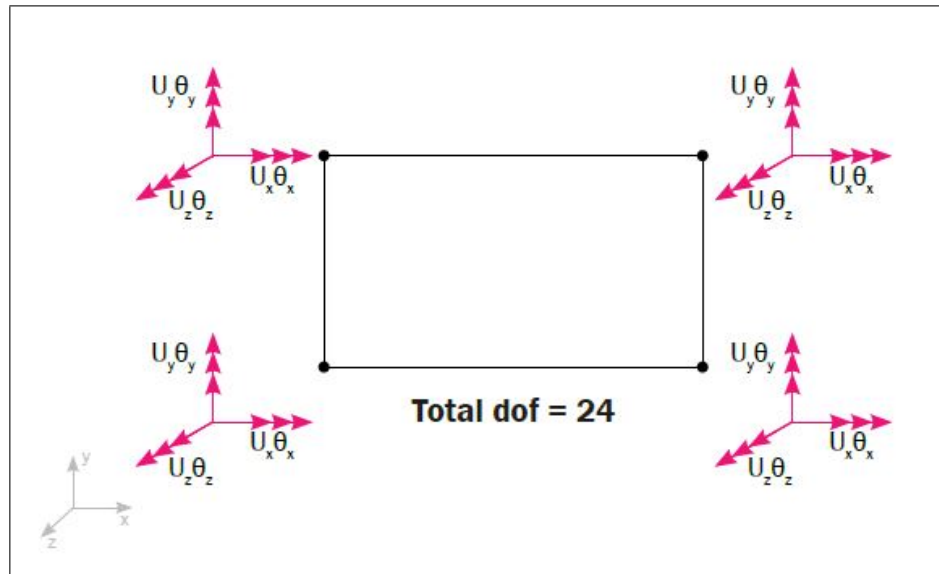


Figure 3.21. DOF in a shell element [21].

Composite structure is modeled with shell elements. An example of a shell meshed composite structure is shown in Figure 3.22. Different colors on model points to different ply stacking sequences. Ply stacking is set from Hyperlaminated GUI. As shown in Figure 3.23, ply stacking sequence is regulated with respect to element normal.

By using Hyperlaminated GUI, as shown in Figure 3.24, material, thickness and orientation of plies can be entered as input. Also, failure mechanism of the composite material can be defined.

In this study, composite properties are defined in MSC Marc. Rather than using property cards as in HyperMesh, composite material properties are defined by using composite material card in MSC Marc.

3.6.2. Manufacturing Process Modelling of Enamelled Steel Sample

In order to validate the finite element model of the enamelled steel manufacturing, samples with simple geometry are produced in Arcelik Bolu Cooking Appliances Factory. The displacements are measured from the samples as indicated in Section 3.3.

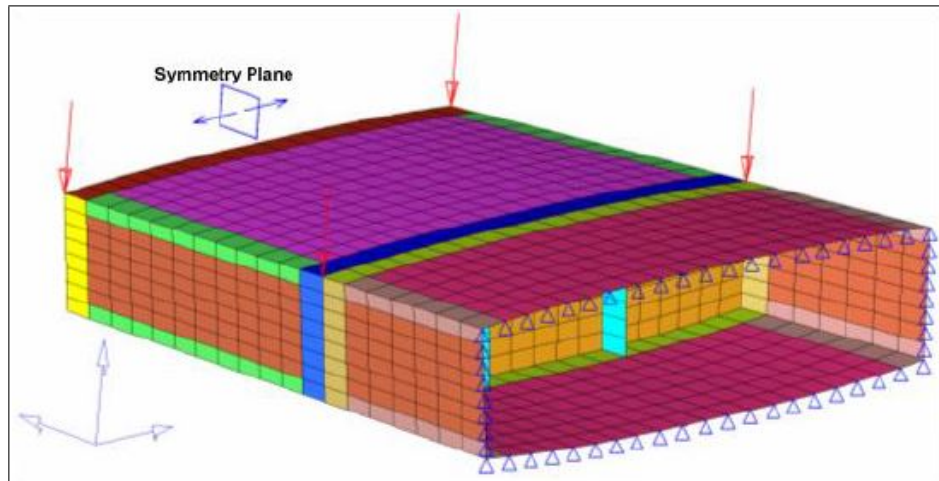


Figure 3.22. Finite element model of a composite structure [22].

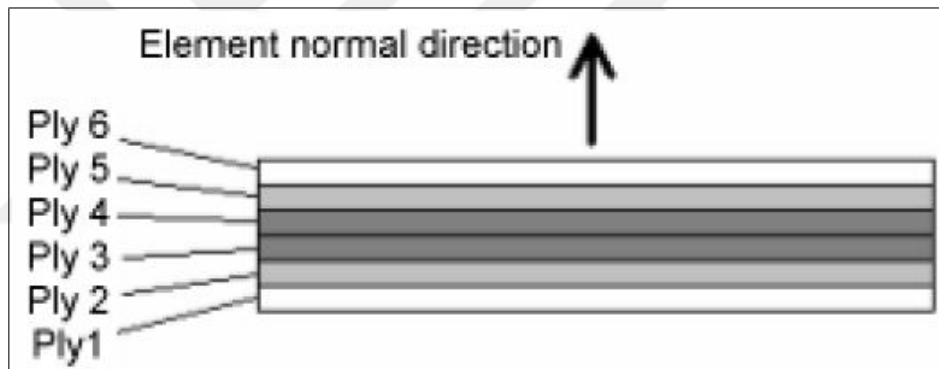


Figure 3.23. Ply stacking sequence and element normal direction [22].

3.6.2.1. Analysis Methodology

A methodology to perform manufacturing simulation of enamelling process is developed. Since the sample is a sheet metal plate with glass layer, a surface model is designed. The surface is meshed with 2D finite elements with quad and tria elements. Desired element size is 5.00 and the minimum element size is 2.49 mm which is close to the holes on the sample. For modelling and meshing steps, Altair Hypermesh is used. Figure 3.25 represents the surface and finite element models of the sample.

Preprocessing step is performed with Hypermesh and the finite element mesh is exported

Laminate definition

Name: Color: Optimization

Stress and failure theory output:

Output ply stress results: Failure Theory:

Interlaminar shear allowable:

Stacking sequence convention:

Convention: Ply thickness:

Repetitions: Common thickness:

Ply lay-up order:

	Material	Thickness T1	Orientation ^o	SQUOT	No. of Repetitions	Integration Points
1	carbon_fiber	1.2	45.0	YES	1	1
2	matrix	0.2	90.0	YES	1	1
3	carbon_fiber	1.2	-45.0	YES	1	1
4	matrix	0.2	-90.0	YES	1	1
5	carbon_fiber	1.2	90.0	YES	1	1

Add/Update plies:

	Material	Thickness T1	Orientation ^o	SQUOT	No. of Repetitions	Integration Points
			0	NO	1	1

Above Selected
 Below Selected

Figure 3.24. Composite property input by Hyperlaminat GUI [22].

into MSC Marc. In version 2017.2 of Altair Optistruct, shell elements with composite property are not compatible with temperature dependent material models. Due to this, analysis continues with MSC Marc.

Temperature dependent material models of steel and glass are introduced with mechanical property versus temperature tables. Also, temperature versus time tables are inputted in analysis to solve the problem with structural dynamic transient method. Time-temperature graph of the enamelling process is shown in Figure 3.26. At point (a), sheet steel sample is coated with glass frit. At this point, the temperature is 20°C and the frit cannot develop any stress since it is in powder form. At point (b), where temperature is 840°C, glass frit fuses and forms a viscous layer, due to low viscosity, stress relaxation process is rapid enough to prevent any stress development until point (c). At point (c), temperature is 600°C and viscosity becomes high enough to allow stress development in enamel layer. From (c) to (d), where it becomes 20°C again, the thermal deformation occurs due to different thermal

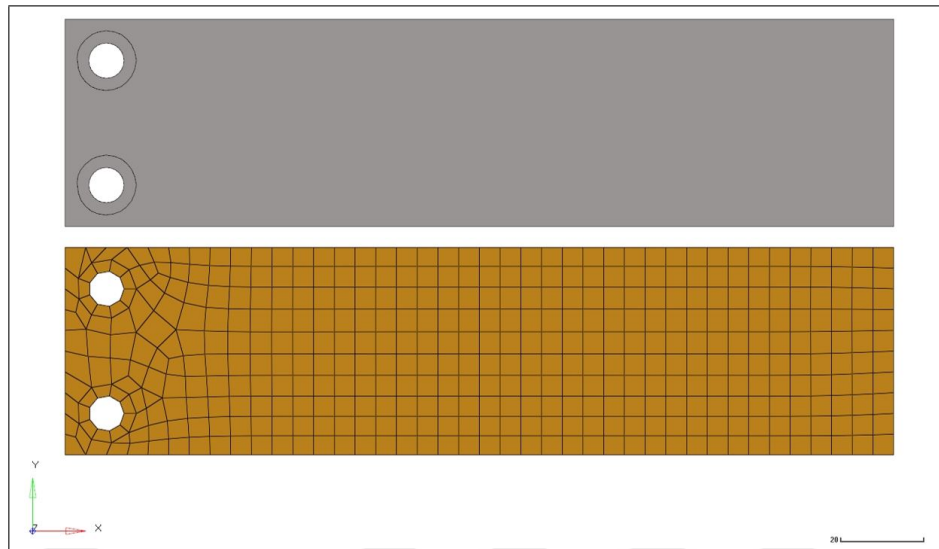


Figure 3.25. CAD and finite element models of the sample.

expansion factors of steel and glass layers.

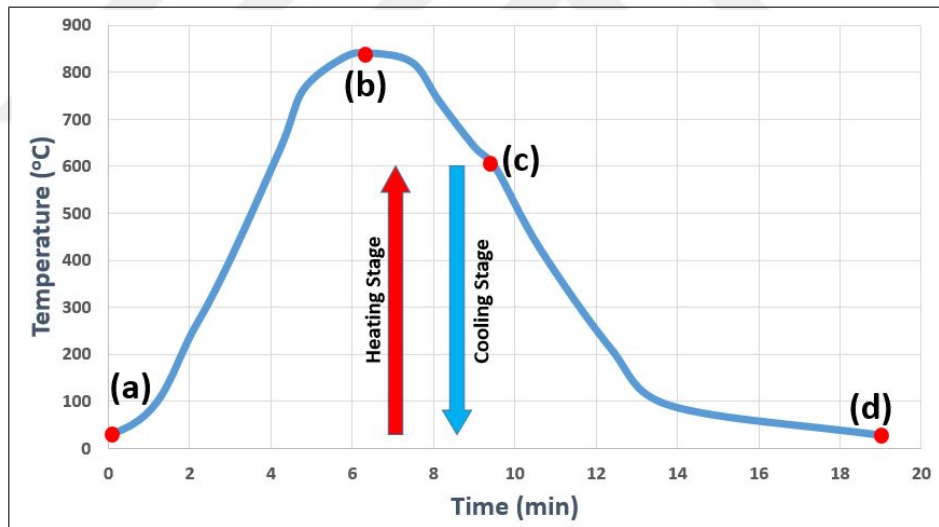


Figure 3.26. Manufacturing thermograph.

Rather than modelling whole 19 minutes of enamelling process, analysis is divided into two stages, heating and cooling. In the heating stage, which covers from point (a) to (c), sample is heated only with steel property from 20°C to 600°C. There is no stress development and no bending effect from point (a) to (c), it is reasonable to take the sample as if it is only steel. The expanded finite element mesh is then imported into second stage, cooling. At this point, (c), it is 600°C and composite material properties are applied. The cooling stage,

which is from 600°C to 20°C, is done with composite material properties where steel and glass layers are present.

Temperature-time graph of heating stage can be seen in Figure 3.27(a). Since there is only steel property and there are no heating rate effect in the material model, this stage is set as heating from 20°C to 600°C in 1 seconds where analysis time is divided into 50 timesteps. Each timestep covers 0.02 seconds in heating stage. The cooling stage, however, is highly dependent on cooling rate where stress and structural relaxation parameters are present in material model. Therefore, whole temperature-time graph from point (c) to (d) is set. The cooling stage takes 585 seconds. The cooling stage is divided into 2340 timesteps where every timestep covers 0.25 seconds. The temperature-time graph of cooling stage is shown in Figure 3.27(b).

Geometric properties of the shell elements are set as 3D Shell. Thickness is inputted as 0.82 mm (0.7 mm steel and 0.12 mm for glass layers).

For steel layer, elastic-plastic isotropic material model is used. Temperature dependent modulus of elasticity, Poisson's ratio and thermal expansion coefficients are given. For glass layer however, three different material model scenarios are applied. These are; single thermal expansion coefficient, two thermal expansion coefficients (solid and liquid) and two thermal expansion coefficients with viscoelastic properties.

Initial and boundary conditions for heating are specified as state variable nodal temperature. Initial condition for heating stage is 20°C and boundary condition is given as increasing nodal temperature according to time-temperature table shown in Figure 3.27(a). Also, gravity is defined in x-direction and in order to avoid rigid body motion, zero-displacement in x-direction boundary condition is applied for two nodes at the very end of the sample as indicated in Figure 3.28. For cooling stage, initial condition is 600°C. The thermal boundary condition for this stage defined with respect to Figure 3.27(a). Similar gravity and zero-displacement boundary conditions applied in the heating stage were also applied in the cooling stage.

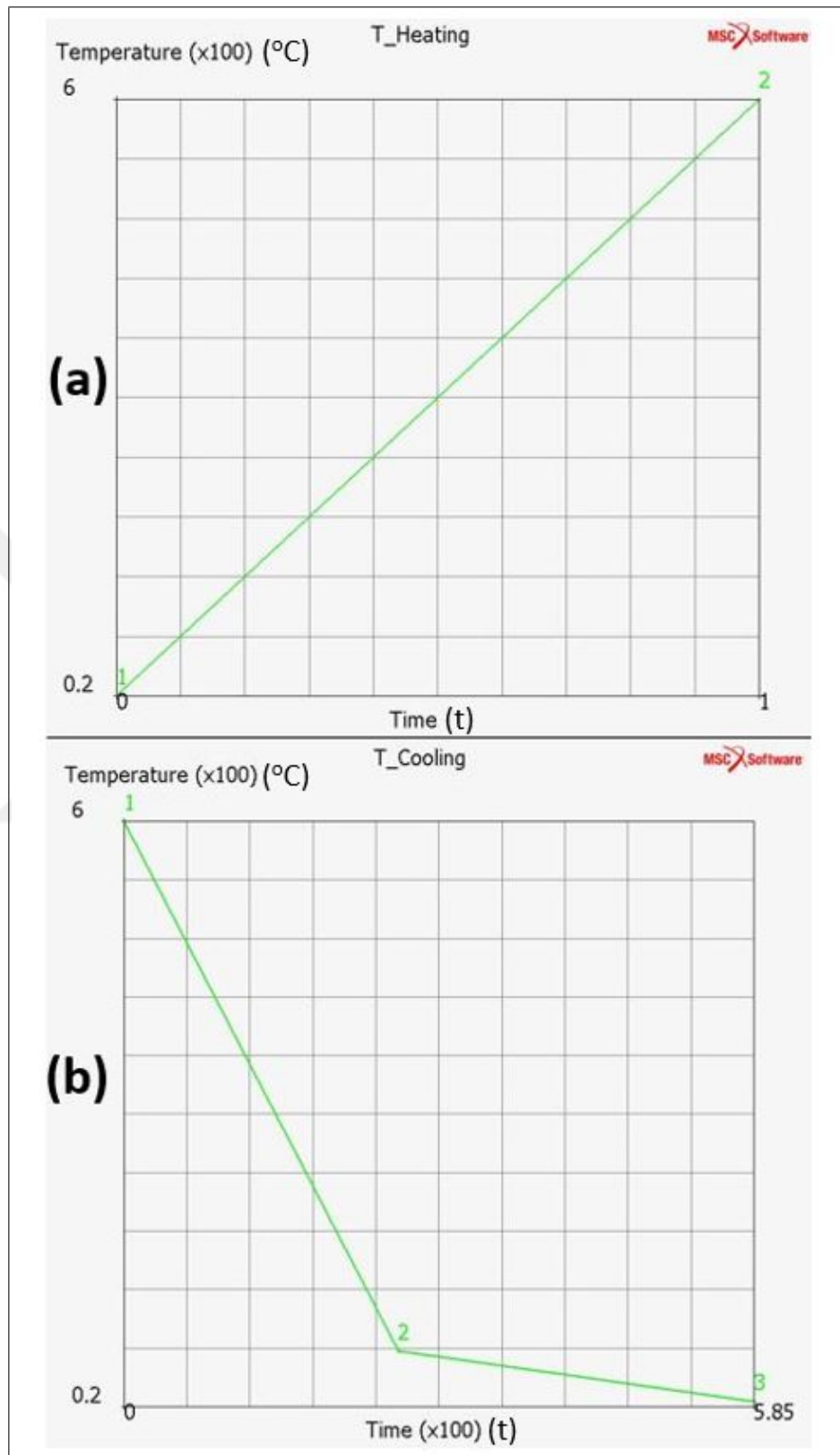


Figure 3.27. Time-temperature graph for heating and cooling stages.

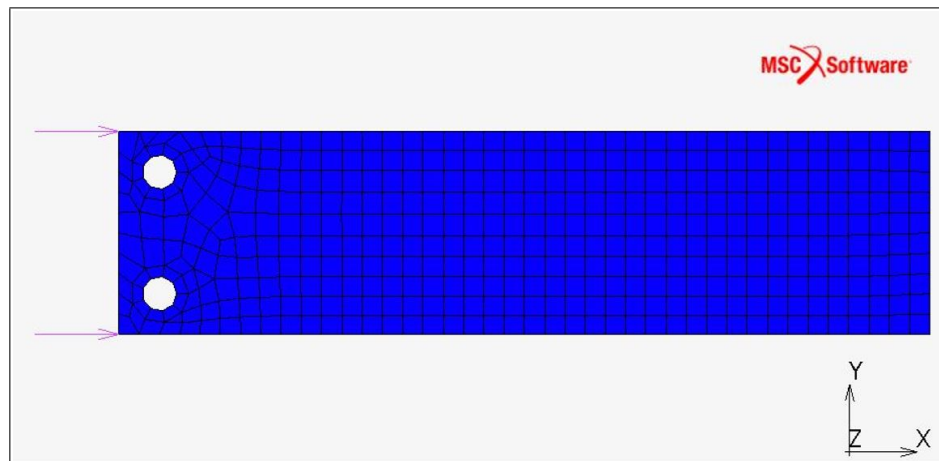


Figure 3.28. Displacement boundary conditions in x-direction.

Due to time-dependent temperature variation of the analysis, structural dynamic transient loadcase is used. Total analysis time and respective timesteps for heating and cooling stages are defined in two different loadcases.

The second part of the methodology is cooling stage. As a result of the heating analysis, we obtained an expanded finite element model. This finite element model is imported into cooling analysis. Importing the expanded finite element model is done by first opening the result file(.t16) in Hyperview, a postprocessor program developed by Altair, and the expanded model is exported in Nastran format(.bdf). The expanded finite element model is then imported into MSC. Marc and prepared for cooling analysis.

As mentioned above, the sample is cooled down from 600°C to 200°C with 0.25 second timesteps. In this stage, material model is selected as composite. The layer thicknesses are specified in this part. At the end of the cooling analysis, the deformed finite element mesh is obtained. The deformed mesh is imported into Altair Hypermesh to measure the deformation in the middle-area of the sample, just like the measurement of the real sample as indicated in Section 3.3. Figure 3.29(a) shows the displacement in z-direction. In order to measure the displacement of the deformed finite element mesh correctly, two nodes are selected from both ends and a line is created by these nodes. The middle point of this line is marked with a node. Then the distance from this node to the middle area of the deformed mesh is measured. The results are nearly similar with the arithmetic mean of the

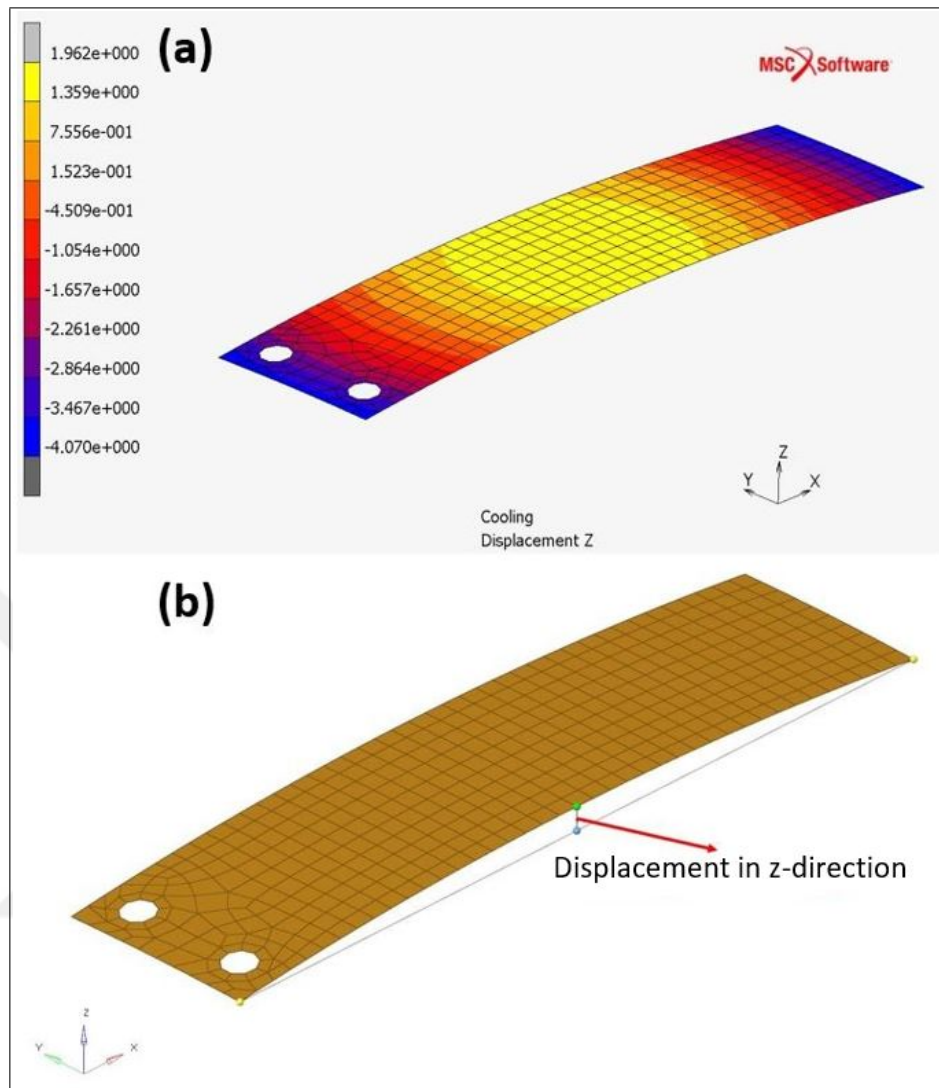


Figure 3.29. Displacement in z-direction.

sample deformation in z-direction. In Figure 3.29(b), the measurement system can be seen. Manufacturing simulation flowchart is indicated in Figure 3.30.

3.6.3. Preprocessing of the Oven Cavity Finite Element Model

Preprocessing of oven chassis is done with Altair Hypermesh. Since shell elements will be used, middle surfaces of 3D parts are created. The finite element mesh is created with BatchMesher GUI in Hypermesh. BatchMesher is an automatic mesher which works with the element quality criteria inputted by the user. Figure 3.31 shows the element criterias specified by the user. Targeted element size is 3 mm with minimum element size of 0.5 mm.

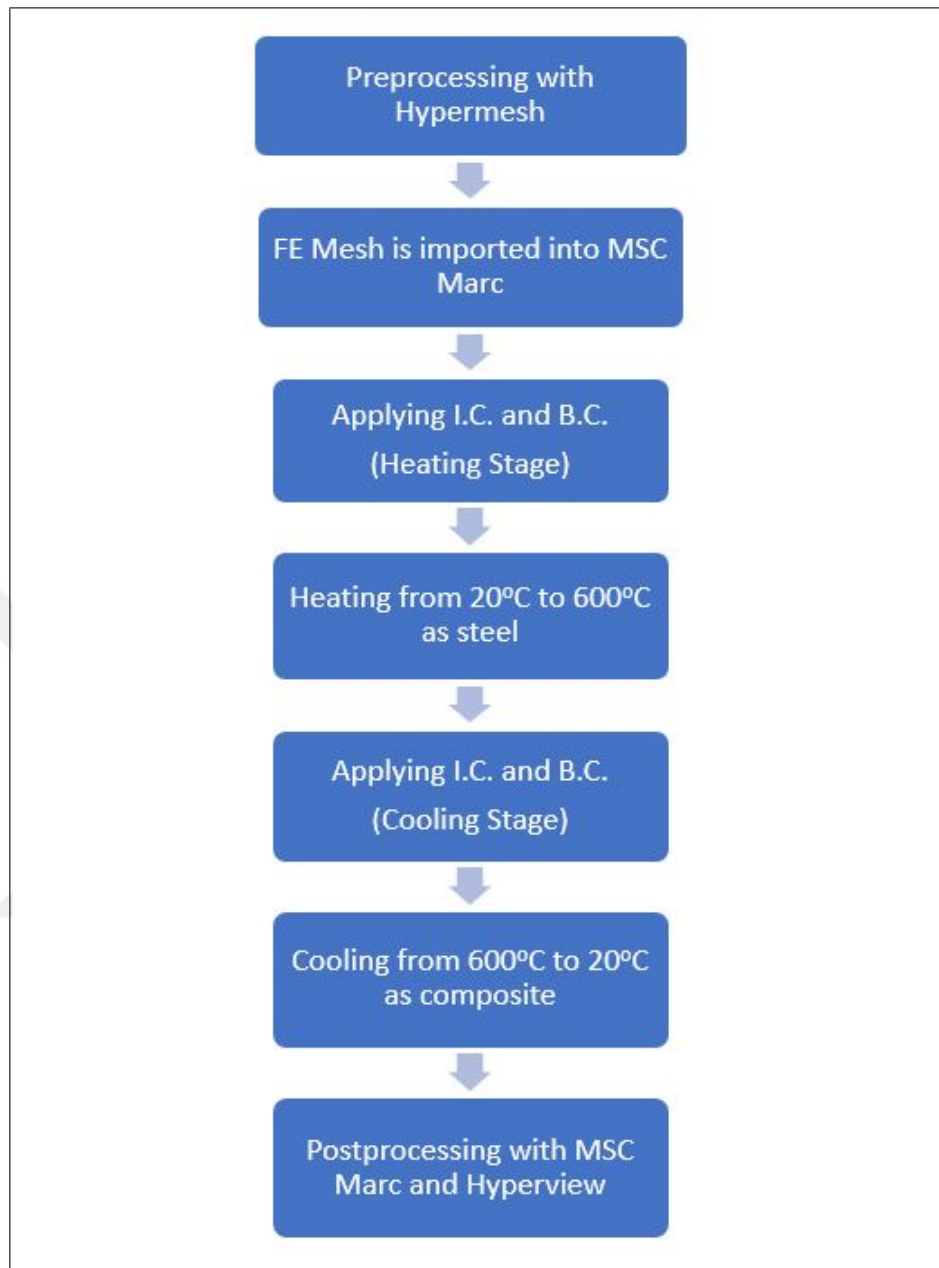


Figure 3.30. Manufacturing process simulation methodology flowchart.

The resulting finite element model has minimum element size of 0.5 mm and total number of elements are 141700.

Criteria Parameters

Target element size: Advanced Criteria Table

Checks	On	Fail	Individual Methods
Min Size	<input checked="" type="checkbox"/>	0.50	Minimal height
Max Size	<input checked="" type="checkbox"/>	15.00	
Aspect Ratio	<input checked="" type="checkbox"/>	10.00	HyperMesh
Warpage	<input checked="" type="checkbox"/>	20.00	HyperMesh
Max Interior Angle Quad	<input checked="" type="checkbox"/>	150.00	
Min Interior Angle Quad	<input checked="" type="checkbox"/>	30.00	
Max Interior Angle Tria	<input checked="" type="checkbox"/>	130.00	
Min Interior Angle Tria	<input checked="" type="checkbox"/>	20.00	
Skew	<input checked="" type="checkbox"/>	60.00	HyperMesh
Jacobian	<input checked="" type="checkbox"/>	0.50	At integration points
Taper	<input type="checkbox"/>	0.60	HyperMesh
% of Trias	<input checked="" type="checkbox"/>	6.00	

Use min length from timestep calculator

Min Size	On	Fail
User input	<input checked="" type="checkbox"/>	0.50
Based on time step	<input checked="" type="checkbox"/>	4.511

Figure 3.31. User specified finite element quality criteria.

In order to reduce CPU time and eliminate convergence problems, welded areas between the parts are not modelled and these parts (U-Chassis, rear and top parts) are united into a single body. The front part is linked to the rest of the oven chassis and hinge support brackets by rigid body elements. Figure 3.32 shows the finite element model of the oven cavity. Different element colors indicate different parts of oven cavity.

As mentioned in Section 3.3, glass layer thickness of different parts of the oven cavity has different values. In Table 3.9, glass and steel layer thicknesses of oven cavity parts are indicated.

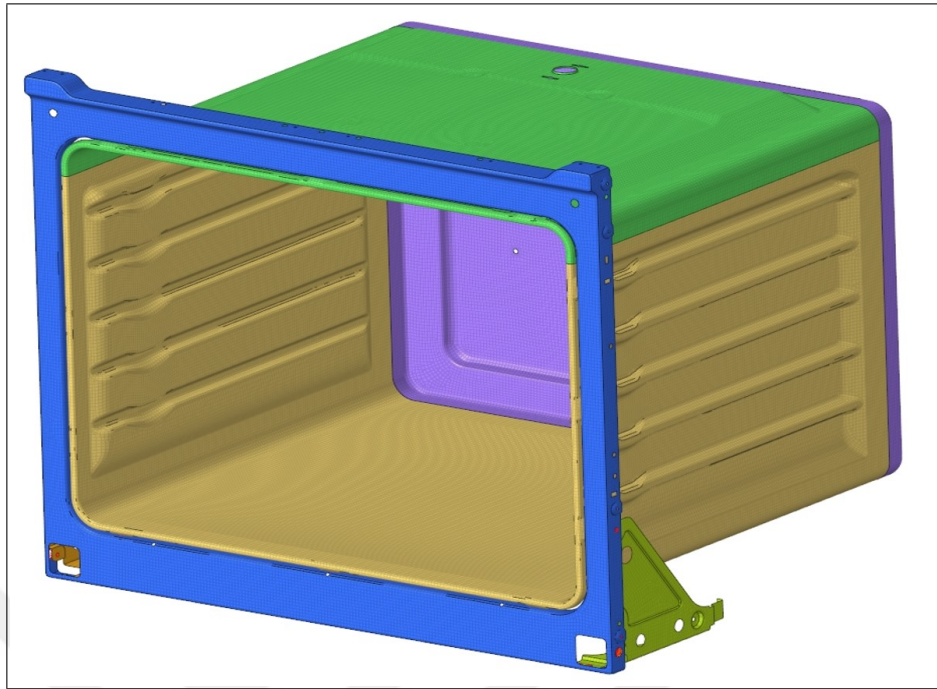


Figure 3.32. Finite element model of oven cavity.

Table 3.9. Thicknesses of oven chassis parts.

Part	Steel(mm)	Glass(mm)	Composite(mm)
Front	0.8	0.108	0.908
Top	0.6	0.139	0.739
U-Chassis	0.6	0.137	0.737
Rear	0.8	0.127	0.927
Brackets	1.25	0.05	1.3

The analysis methodology is the same with enamelled sample mentioned in Section 3.6.2. The enamelling simulation of the oven cavity has two parts, heating and cooling.

Boundary conditions are applied to three nodes on the rear part as displacement and rotation on x-axis are inhibited. Since the gravity is applied in negative x-axis direction, the boundary conditions simulate as if the oven cavity is hanged and the front gap is oriented to the ground. In Figure 3.33, direction of gravity is indicated. At the end of the analysis, MSC. Marc result

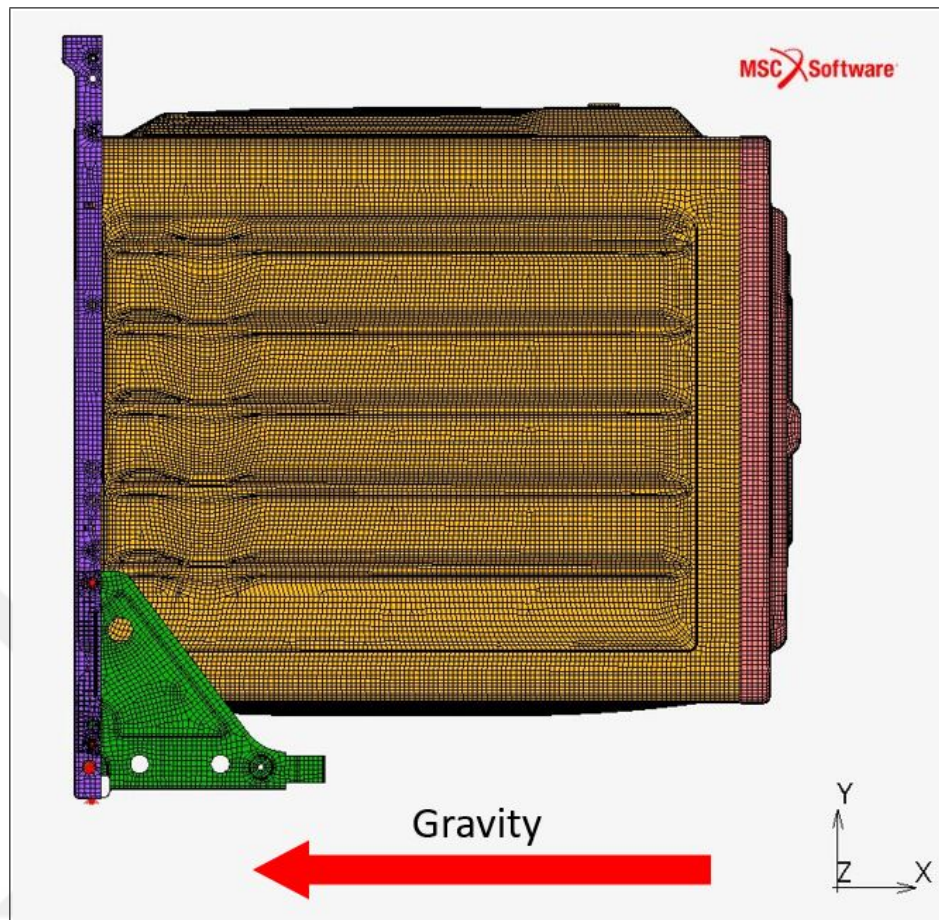


Figure 3.33. Oven cavity and the direction of gravity.

file(.t16) is opened in Hyperview and exported in Nastran format(.bdf). This file is opened in Hypermesh and the dimensions mentioned in Section 3.4 is measured on nodal basis.

3.7. DYNAMIC MECHANICAL ANALYSIS

3.7.1. Fixtures and Sample Geometries in DMA

Fixtures can be get into two groups with respect to the type of applied load.

3.7.1.1. Axial Fixtures

- Three-Point and Four-Point Bending
- Dual and Single Cantilever

- Parallel Plate and Variants
- Bulk
- Extension/Tensile
- Shear Plates and Sandwiches

3.7.1.2. Torsional Fixtures

- Parallel Plate
- Cone and Plate
- Couette
- Torsional Beam and Braid

In order to measure storage modulus of glass, the most suitable testing method is three-point bending. Unlike polymers, glasses are more sensitive to tensile stresses than compressive stresses. Constraints on the sample should not produce extra tensile stresses in order to avoid premature fracture. Because of this fact, cantilever fixtures are eliminated.

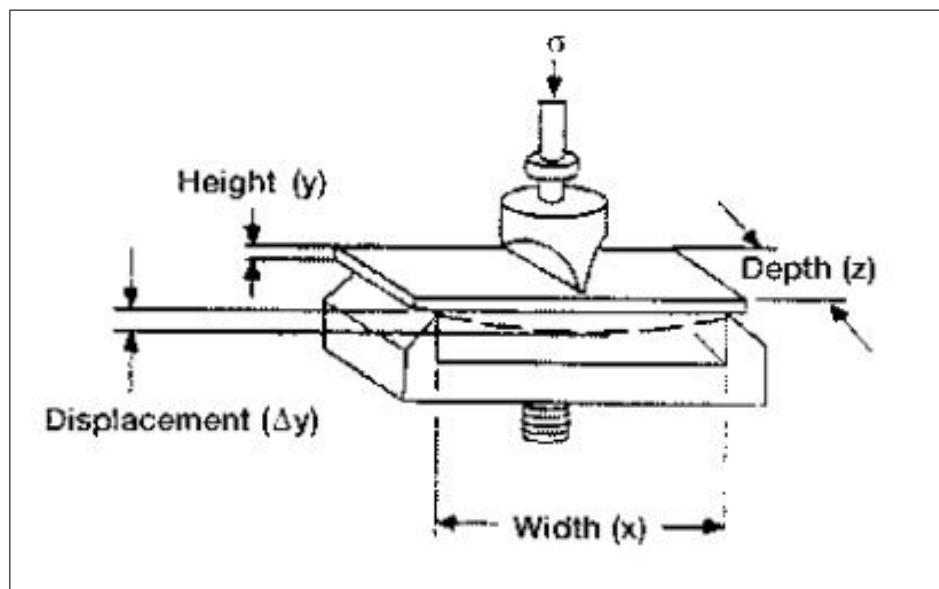


Figure 3.34. Three-point bending test fixture [17].

3.7.2. Dynamic Mechanical Analysis of a Soda-Lime-Silicate Glass Specimen

Young's modulus of glass layer in enamelled structures has a great importance in order to successfully predict the mechanical behaviour of the structure during manufacturing and application stages. Dynamic mechanical analysis of a SLS(Soda-Lime-Silicate) glass is done to measure the storage modulus and $\tan \delta$ with respect to temperature and frequency.

TA Instruments DMA Q800 dynamic mechanical analyzer is used in these experiments. The specifications of the device is listed in Table 3.10 . Its working temperature range is enough to spot the glass transition temperature of SLS glass, which is around 500°C. The output values of the TA Q800 DMA are storage modulus, loss modulus, compliance, $\tan \delta$, complex modulus, complex/dynamic viscosity, creep compliance, relaxation modulus, temperature, static/dynamic force, time, stress/strain, frequency, sample stiffness and displacement. Figure 3.35 is the device used in tests.

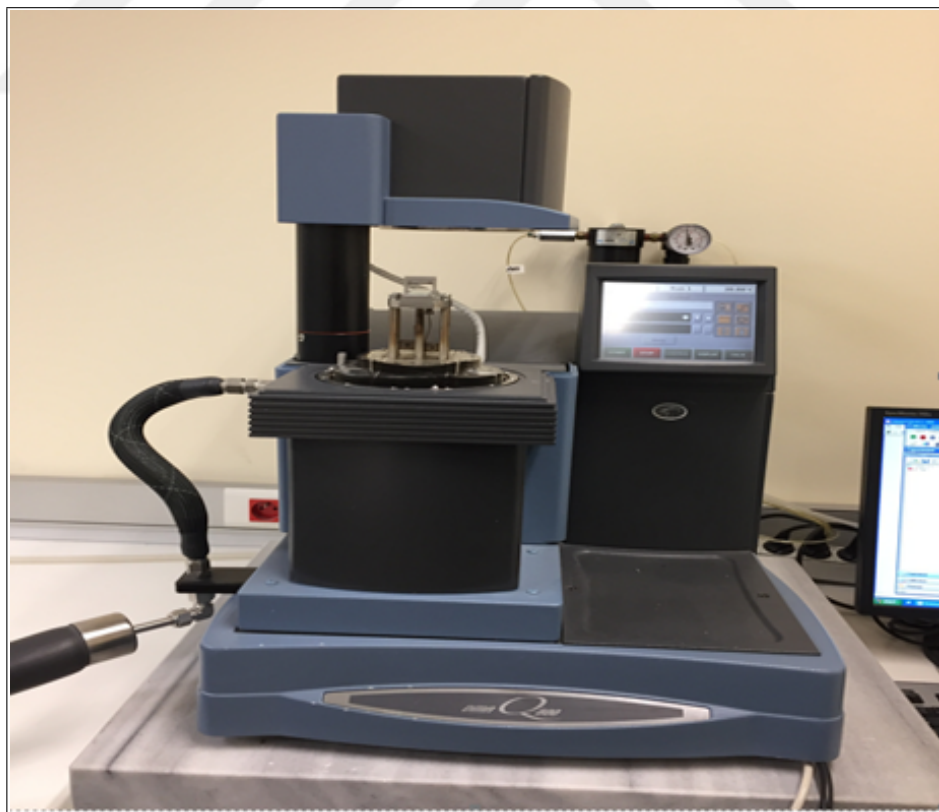


Figure 3.35. TA Instruments DMA Q800.

Table 3.10. Specifications of TA Instruments DMA Q800 [21].

Maximum Force	18 N
Minimum Force	0.0001 N
Force Resolution	0.00001 N
Strain Resolution	1 nanometer
Modulus Range	10^3 to 3×10^{12} Pa
Modulus Precision	$\pm 1\%$
Tan δ Sensitivity	0.0001
Tan δ Resolution	0.00001
Frequency Range	0.01 to 200 Hz
Dynamic Sample Deformation Range	± 0.5 to $10000 \mu\text{m}$
Temperature Range	-150 to 600°C
Heating Rate	0.1 to $20^\circ\text{C}/\text{min}$
Cooling Rate	0.1 to $10^\circ\text{C}/\text{min}$

3.7.2.1. Samples, Deformation Modes and Experiment Theory

Three-point bending test is widely used for brittle materials to measure their modulus of elasticity and flexural stress-strain response. For brittle materials, clamping can be a reason for premature cracking. Therefore, a non-clamping method such as three-point bending is suitable. The deflection at the center of the sample is used to measure the modulus of elasticity. Figure 3.36 shows the glass specimens used in DMA. Specimens have changing length from 30 to 50 mm, 12 mm width and 2 mm thickness.

The deflection at the center of the sample with a rectangular cross section is defined as

$$w_0 = \frac{PL^3}{48EI} \quad (3.1)$$

where w_0 is the maximum deflection, P is force, L is length and I is the moment of inertia.

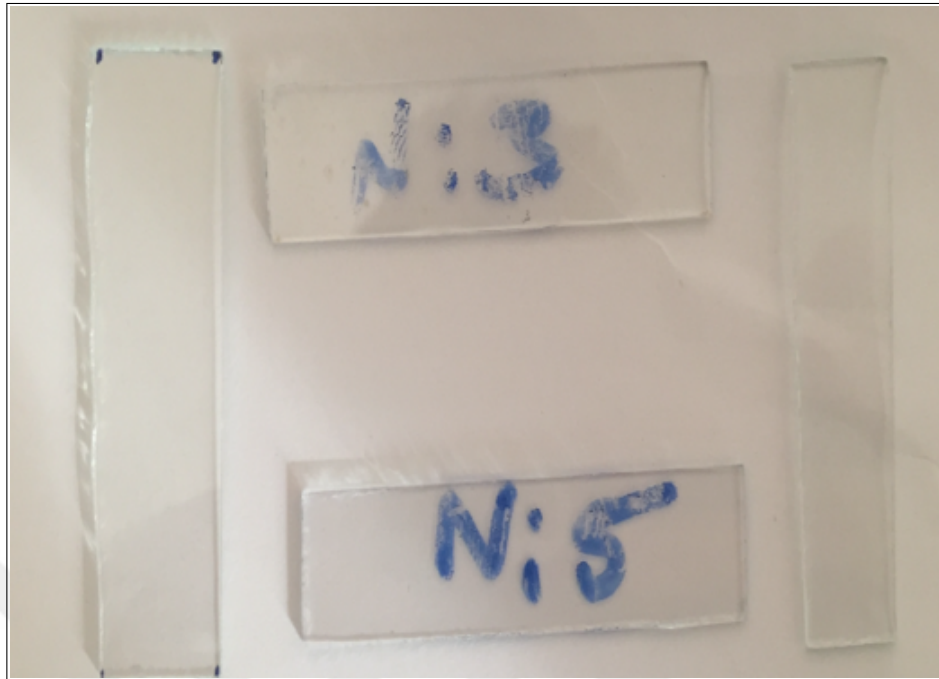


Figure 3.36. Glass specimens.

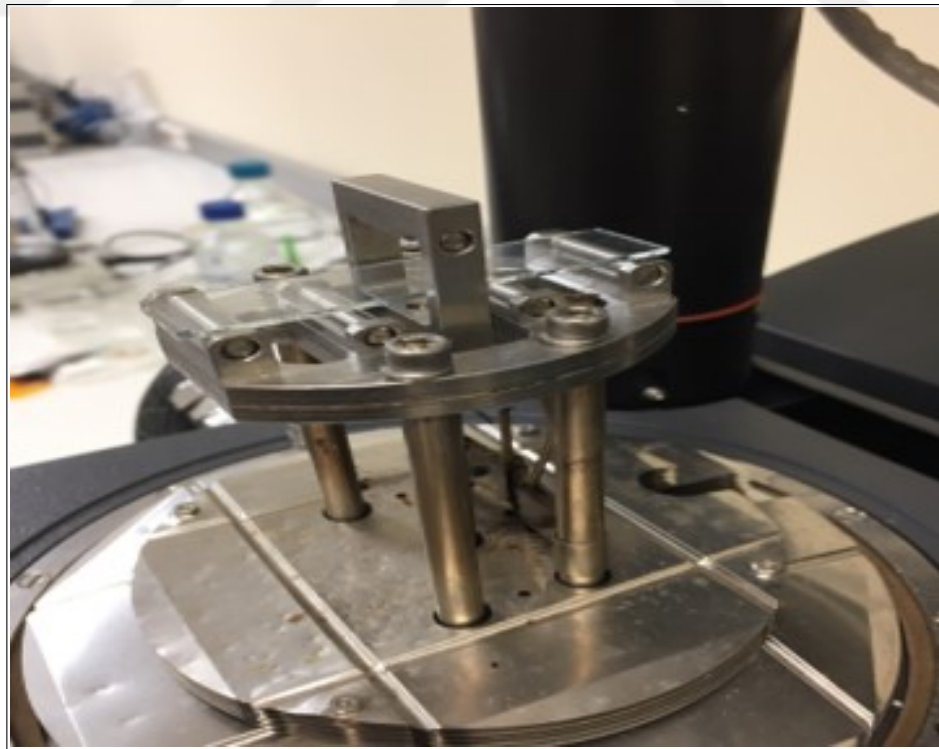


Figure 3.37. Glass specimen in three-point bending mode.

4. RESULTS

4.1. THERMAL DEFORMATIONS IN ENAMELLED STEEL SAMPLES

4.1.1. Coating Thickness and Thermal Deformation Measurements of the Sample

Coating thickness of samples are measured with Elcometer. The results given in micrometers are shown in Table 4.1. Also, thermal deformations are measured as mentioned in Section 3.3.

Arithmetic mean of the displacement values in Table 4.2 is 6.17 mm (in z-direction).

4.1.2. Validation of Analysis Methodology: Experimental and Numerical Results

To ensure the accuracy of a finite element model, validation with simple geometries is a logical method. For comparison, a plate composed of glass and steel layers is manufactured in Arcelik-Bolu Cooking Appliances factory in Bolu, Turkey. The manufacturing and deformation measurement procedures are mentioned in Section 3.3. The finite element model composed of separate heating and cooling stages are developed by using Altair Hypermesh (for preprocessing) and MSC Marc. The method involves transient structural analysis. Temperature dependent material models for glass and steel layers are used. The results are given in terms of displacement in z-direction.

The experimental and numerical results are given in Table 4.3. There are three methods which are:

- (i): Thermal expansion coefficient of glass in solid form is applied and constant throughout the analysis.
- (ii): Two different values of CTE (Solid and liquid) for glass which change at the T_g .
- (iii): Viscoelastic approach for glass where there are two CTE (Solid and liquid) and stress and structural relaxation parameters are present.

Table 4.1. Glass film thickness on specified points of the specimen (microns).

Sample	Point 1	Point 2	Point 3	Point 4	Point 5
1	94	80	81	87	114
2	138	139	138	128	168
3	143	108	117	132	157
4	89	73	88	101	121
5	132	103	131	132	145
6	148	112	107	143	140
7	125	67	79	116	112
8	111	57	74	92	101
9	139	106	124	125	158
10	125	134	155	122	168
11	96	83	76	98	130
12	164	110	106	124	150
13	159	139	143	145	183
14	81	73	77	92	135
15	145	128	114	153	155
16	112	81	75	112	124
17	154	137	136	140	118
18	143	122	165	137	184
19	135	124	130	141	173

4.2. THERMAL DEFORMATIONS IN ENAMELLED STEEL OVEN CAVITY

Thermal deformations on enamelled steel oven cavities are measured with CMM, as mentioned in Section 3.5. Numerical simulations of enamelling process of oven cavity are done with MSC. Marc. Finite element mesh is generated by Hypermesh and rest of the simulation is prepared and solved with MSC. Marc. The analysis procedure is the same as enamelling simulation of sample model and the procedure is explained in Section 3.6.2.

Table 4.2. Displacements of the middle area of samples.

Sample	Max. Displacement (mm)
1	6.2
2	5.6
3	6.1
4	5.9
5	6.2
6	6.2
7	5.7
8	6.3
9	6.5
10	6.5
11	5.8
12	6.0
13	6.0
14	6.0
15	7.3
16	5.2
17	5.2
18	7.6
19	6.9

4.2.1. Dimensional Measurement Results of Oven Cavity

Dimensional measurements of oven cavities are done before and after enamelling process. Tables 4.4 and 4.5 present the uncoated and coated oven cavities and their deviation from CAD model.

Table 4.3. Experimental and numerical results of plate sample.

	Displacement in z-direction(mm)
Experimental	6.17
One CTE	4.45
Two CTE	0.32
Viscoelastic	5.61

4.2.2. Numerical Simulation Results of Oven Cavity

At the end of the simulation procedure, the deformed mesh after enamelling process is obtained. The deformed finite element model is imported into Hypermesh and measured as nodal displacements. The measured regions are shown in Figure 3.17 and 3.18. The deviation between the experimental(CMM measurements from coated oven cavities) and numerical simulation results are compared by deviation between the results. The FEA results from point 1 to 15 are revised due to use of shell elements. The distance between shelves are measured from nodal results but the nodes/elements are placed on midsurface of the U-Chassis CAD model. Since the thickness of the U-Chassis part is 0.6 mm, 0.6 mm is subtracted from the nodal result. By this way, the nodal distances between left and right shelves can be compared with CMM results. The simulation was performed with two different material models for glass layer. First, glass with constant thermal expansion coefficient. Second, glass with viscoelastic behavior. The results were presented in Tables 4.6 and 4.7.

4.3. DMA RESULTS OF SLS SPECIMENS

DMA device can measure the storage modulus and $\tan \delta$ of the specimen with very small deflections. The deflection and the size of the specimen is given as an input to the DMA. Temperature range and increasing rate is also defined by a GUI.

Table 4.4. CMM results from uncoated oven cavities.

No	Direction	CMM (mm)	CAD (mm)	Deviation (mm)
1	z	465.3812	466	-0.6188
2	z	465.7773	466	-0.2227
3	z	466.9811	466	0.9811
4	z	465.4646	466	-0.5354
5	z	465.9215	466	-0.0785
6	z	466.6832	466	0.6832
7	z	465.5703	466	-0.4297
8	z	465.9811	466	-0.0189
9	z	466.6971	466	0.6971
10	z	465.3805	466	-0.6195
11	z	465.9457	466	-0.0543
12	z	466.8078	466	0.8078
13	z	465.091	466	-0.9090
14	z	465.4369	466	-0.5631
15	z	467.0529	466	1.0529
16	y	78.2154	78.6	-0.3846
17	y	78.9177	78.6	0.3177
18	x	-432.285	-431.2	-1.0850
19	x	-433.24	-431.2	-2.0400
20	x	-432.5515	-431.2	-1.3515
21	x	-432.6617	-431.2	-1.4617

Experiment is done with three different deflection values and seven different frequencies. Deflection values are 15, 20 and 30 μm . On Figure 4.1, storage modulus and $\tan \delta$ changing with increasing temperature can be seen. Frequency of deformation also effect the storage modulus results. The frequencies applied are 1, 3, 5 and 8 Hz. Figures 4.2 and 4.3 show how storage modulus changes with different frequency applied.

Table 4.5. CMM results from coated/enamelled oven cavities.

No	Direction	CMM (mm)	CAD (mm)	Deviation (mm)
1	z	466.1968	466	0.1968
2	z	467.0479	466	1.0479
3	z	468.0965	466	2.0965
4	z	466.3946	466	0.3946
5	z	467.5074	466	1.5074
6	z	468.1603	466	2.1603
7	z	466.5364	466	0.5364
8	z	467.8553	466	1.8553
9	z	468.4193	466	2.4193
10	z	465.9700	466	-0.0300
11	z	467.3563	466	1.3563
12	z	468.0990	466	2.0990
13	z	465.2697	466	-0.7303
14	z	465.9024	466	-0.0976
15	z	467.5818	466	1.5818
16	y	78.0080	78.6	-0.5920
17	y	78.8650	78.6	0.2650
18	x	-431.3529	-431.2	-0.1529
19	x	-432.4004	-431.2	-1.2004
20	x	-432.1947	-431.2	-0.9947
21	x	-432.3635	-431.2	-1.1635

Table 4.6. Numerical simulation results with constant CTE.

No	Direction	FEA (mm)	CMM (mm)	Deviation (mm)
1	z	465.919	466.197	0.278
2	z	465.984	467.048	1.064
3	z	466.004	468.097	2.093
4	z	465.768	466.395	0.627
5	z	465.874	467.507	1.633
6	z	465.979	468.160	2.181
7	z	465.708	466.536	0.828
8	z	465.820	467.855	2.035
9	z	465.969	468.419	2.450
10	z	465.678	465.970	0.292
11	z	465.827	467.356	1.529
12	z	465.980	468.099	2.119
13	z	465.787	465.270	-0.517
14	z	465.899	465.902	0.003
15	z	466.002	467.582	1.580
16	y	78.600	78.008	-0.592
17	y	78.732	78.865	0.133
18	x	431.119	431.353	0.234
19	x	431.146	432.400	1.254
20	x	431.300	432.195	0.895
21	x	431.298	432.364	1.065

Table 4.7. Numerical simulation results with viscoelastic behavior.

No	Direction	FEA (mm)	CMM (mm)	Deviation (mm)
1	z	465.894	466.197	0.303
2	z	465.667	467.048	1.381
3	z	466.050	468.097	2.047
4	z	465.698	466.395	0.697
5	z	465.873	467.507	1.634
6	z	466.033	468.160	2.127
7	z	465.622	466.536	0.914
8	z	465.811	467.855	2.044
9	z	466.027	468.419	2.392
10	z	465.580	465.970	0.390
11	z	465.809	467.356	1.547
12	z	466.045	468.099	2.054
13	z	465.558	465.270	-0.288
14	z	465.909	465.902	-0.007
15	z	466.061	467.582	1.521
16	y	78,887	78.008	-0.879
17	y	78.685	78.865	0.180
18	x	431.097	431.353	0.256
19	x	431.132	432.400	1.268
20	x	431.207	432.195	0.988
21	x	431.293	432.364	1.070

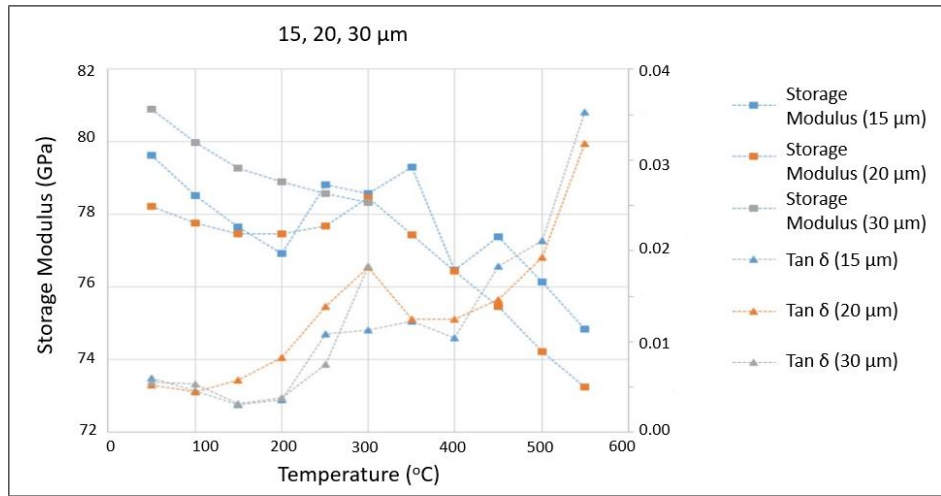


Figure 4.1. Storage modulus and Tan δ versus temperature.

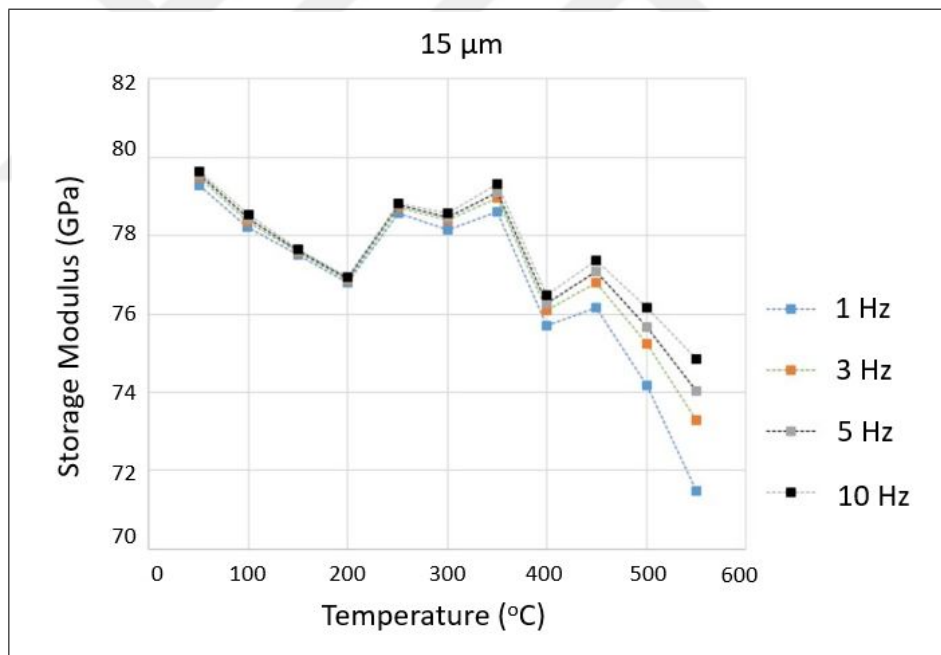


Figure 4.2. Storage modulus change for 15 μm maximum deflection.

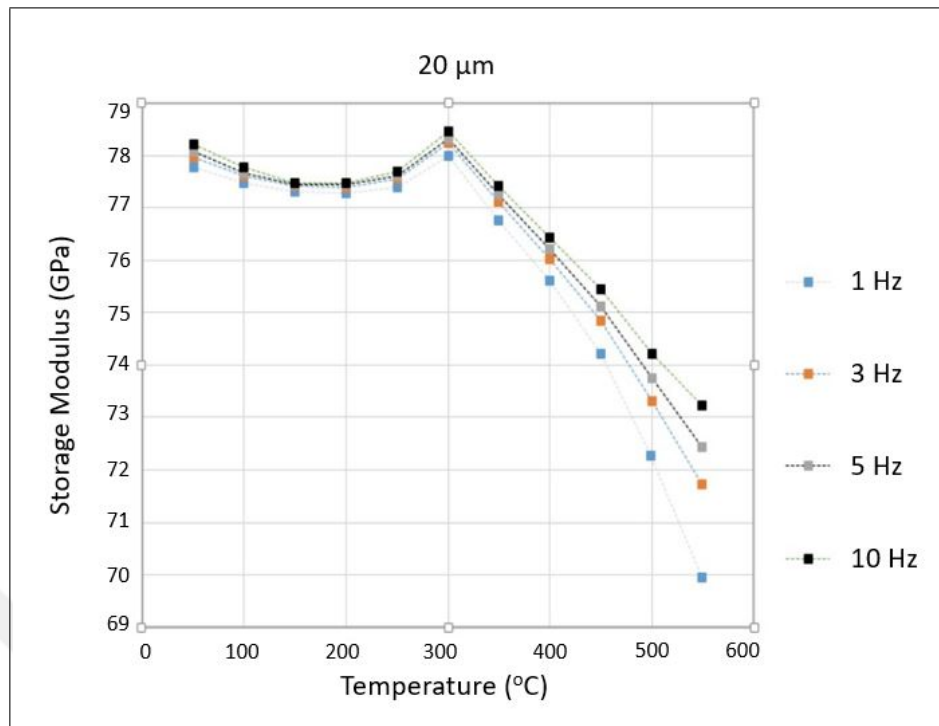


Figure 4.3. Storage modulus change for 20 μm maximum deflection.

5. DISCUSSION

Enamelled steel components were composed of steel and glass layers which have different mechanical and physical properties. Enamelling process involves heating and cooling stages. At first, glass frit (Glass powder) is coated on to sheet metal. Second, glass frit coated steel is heated up to 840°C and at this temperature, glass frit is fused and form a thin layer of glass. At this temperature, viscosity of glass is relatively low enough for molecular arrangements to occur fastly. This causes stress relaxation to occur very quickly, therefore, stress inside the glass layer do not increase. During cooling stage, between 650°C to 600°C, viscosity became high enough for stress development in glass layer. After this temperature, thermal deformation starts to occur. Deformed components. This deformation causes breakage in the glass layer during assembly. Also, thermal deformations cause quality problems. Design of enamelled steel products were done in order to minimize the excessive deformation of the component in manufacturing stage. Before manufacturing, these design must be tested to find out if it behaves as expected. Testing every design idea is not time and cost efficient. Using engineering simulation and performing virtual tests can hinder these time and cost losses. Finite Element Method is a widely used and well-developed engineering analysis tool and it can be used in enamelling process simulation. Developing a FEA methodology for enamelling simulation is essential for performing these virtual tests.

Enamelled steel samples were prepared in order to validate the finite element model which is then used to analyze a larger structure, oven cavity. Cooreman et al. [5] used a validation methodology which uses the Klotz test. In Klotz test, a U-Shaped sample was constrained from one end and tip displacement in the free-end is tracked by Linear Variable Displacement Transducer (LVDT). In this study, a rectangular sheet steel sample was coated with glass frit introduced into enamelling process. When compared with the Klotz test, the method used in this study is cheaper and more suitable for applying in factory conditions where the researcher can simply attach the sheet metal samples to the production line and get the prepared samples from the end of the line in a very short time (In our case, 2 hours for 19 samples). The measurement of the deflection of the samples were done manually

rather than by using CMM. The reason for this is the CMM machine uses magnets to stabilize the components. Since our samples are easy to deform with a small amount of force, this method is not recommended by the CMM specialists in Arcelik Bolu Plant. The manual measurement of the samples are simulated in nodal displacement measurement in Hypermesh. It was a very easy and time saving method for measurement of deformations.

Due to time dependent nature of the analysis, dynamic transient structural analysis method was used in MSC. Marc. At the start of this study, we have planned to perform the analysis in Altair Optistruct but then it was realized that using temperature dependent material models with composite shell mesh is not available at the moment. Because of this fact, finite element mesh prepared in Hypermesh is imported into MSC. Marc for further preprocessing and solving.

FE analysis of enamelled steel manufacturing process was studied in previous works of Van Abeele, Cooreman and Son et al [9][5][29]. Van Abeele states that the T_N (350°C) is the initial condition and the enamelled steel is cooled down to 20°C. Temperature dependent Young's modulus and thermal expansion coefficient is used as they stated. Since they worked in temperatures where glass layer is fully solid, there are only one thermal expansion coefficient which is not changing until the T_g . Cooreman et al. state that they have included stress and structural relaxation into FE analysis by introducing these formulations in a commercial FEA program with user subroutines. Son et al. accepted the low temperature CTE constant throughout the analysis.

In this study, previous methodology which do not take viscoelasticity into account were compared with the viscoelasticity included methodology. Three different material model approaches were used for glass layer. At first, thermal expansion coefficient of the glass is set as constant throughout the analysis. This method is used by Son et al. [29] in their work. Secondly, thermal expansion coefficient is changing at the T_g . This method is applied in order to take phase transformation at the T_g into account. Thirdly, viscoelastic behavior was included in glass material model. Although there are two thermal expansion coefficients stated, the deformation results are different than the second case. As it can be seen in Table 4.3, viscoelastic material model for glass gave the closest results to experimental

results. Although there are only one thermal expansion coefficient defined, the single CTE approach had given worse results than viscoelastic approach. This is because of the presence of stress relaxation and change of thermal strain by temperature which relates to Equation 2.60. By referring to these results, it is logical to use viscoelastic material model for thermal deformation analysis of enamel-steel systems. It must be admitted that in this study, viscoelastic parameters of soda-lime-silicate glass retrieved from the work of Carre and Daudeville [38]. Since our glass layer is a soda-lime-silicate based composition but there are coloring agents in order to meet visibility requirements. In this study, we could not carry out a study on characterization of glass in order to find and derive stress and structural relaxation parameters. It can be seen that, the results will be much closer if one use exact viscoelasticity parameters characterized with their own glass composition. In Table 5.1, the differences between the results were indicated as percentage. The experimental result was accepted as 100 per cent, numerical simulation results were evaluated according to experimental result.

Table 5.1. Deviation between experimental and numerical results.

	Deviation from Experimental Result(%)
Experimental	0
One CTE	-27.88
Two CTE	-94.81
Viscoelastic	-9.08

First (Constant CTE) and third (Viscoelastic) approaches to glass material behavior were used in FEA of enamelled steel oven cavity. The CMM measurement of coated oven cavities were compared with FEA results in Tables 4.6 and 4.7. Displacement between shelves were investigated. The deformation behavior in the U-Chassis shelf area is such that the distances between shelves are increasing from front to the rear areas of oven cavity. This was also a situation encountered in CMM results of actual oven cavities. The mismatch between the distances of rear areas between FEA and actual product can be seen. We assume that this can be due to several reasons.

- Welds between the parts were not introduced in the finite element model.
- The sheet metal parts were manufactured by deep drawing process. The residual stresses and strain hardening of the metal substrate was not included in this analysis.
- Viscoelastic behavior of SLS-glass was used. The glass used for enamelling process can be assumed as a derivative of SLS-glass according to Table 3.1. However, the glass transition temperature of the enamelling glass is lower than SLS-glass.
- Thermal expansion coefficient of the enamelling glass is higher than the SLS-glass because of the coloring agents included in enamelling glass composition.
- Cooling stage of the analysis is started from 600°C. It is assumed that above this temperature, glass layer can not develop any stress, therefore the structure do not warp. In reality, limit of stress-free state temperature can be above or below this temperature as mentioned in Cooreman's work [5].

In Table 5.2, simulation results of first and third approaches were compared. The deformation results were nearly the same with a little more deformation observed with viscoelastic approach.

Shell element moments and curvatures of oven cavity were calculated for first and third approaches. Since the stress in shell elements are calculated by moments and curvatures, it is logical to refer these outputs [40]. In Figure 5.1, shell element moments on oven cavity model is shown. The yellow circle on models represent the area that shell moment versus temperature curves were retrieved. The shell moment and curvature versus the temperature results are shown in Figure 5.1. It can be seen that the viscoelastic approach result in larger shell moments and curvatures. The yellow circles in Figure 5.1 represent the area that the equivalent of shell moment and curvature results taken in Figure 5.2.

In this study, although the results were not used in material models, DMA was used in order to characterize the stress and structural relaxation parameters of the glass. We have first started with SLS glass because of its accessibility. We have prepared samples for three-point bending mode. Since this mode was referred as the most suitable for glass and ceramics, because it does not apply tensile loads by constraining the sample, we have made the DMA analysis with this mode. The results from the DMA show that this method can be used for

Table 5.2. Numerical simulation results with viscoelastic behavior.

No	FEA(1st) (mm)	FEA(3rd) (mm)	CMM (mm)
1	465.919	465.894	466.197
2	465.984	465.667	467.048
3	466.004	466.05	468.097
4	465.768	465.698	466.395
5	465.874	465.873	467.507
6	465.979	466.033	468.160
7	465.708	465.622	466.536
8	465.820	465.811	467.855
9	465.969	466.027	468.419
10	465.678	465.58	465.970
11	465.827	465.809	467.356
12	465.980	466.045	468.099
13	465.787	465.558	465.270
14	465.899	465.909	465.902
15	466.002	466.061	467.582
16	78.600	78.887	78.008
17	78.732	78.685	78.865
18	431.119	431.097	431.353
19	431.146	431.132	432.400
20	431.300	431.207	432.195
21	431.298	431.293	432.364

determination of temperature dependent storage modulus of glass. Disc shaped SLS glass samples for compression mode are also prepared characterization of viscoelastic properties of the sample. This study could not be completed because the maximum force that the DMA device can apply is insufficient to create a measurable strain. This method can be used with DMA devices that can apply higher forces in compression mode.

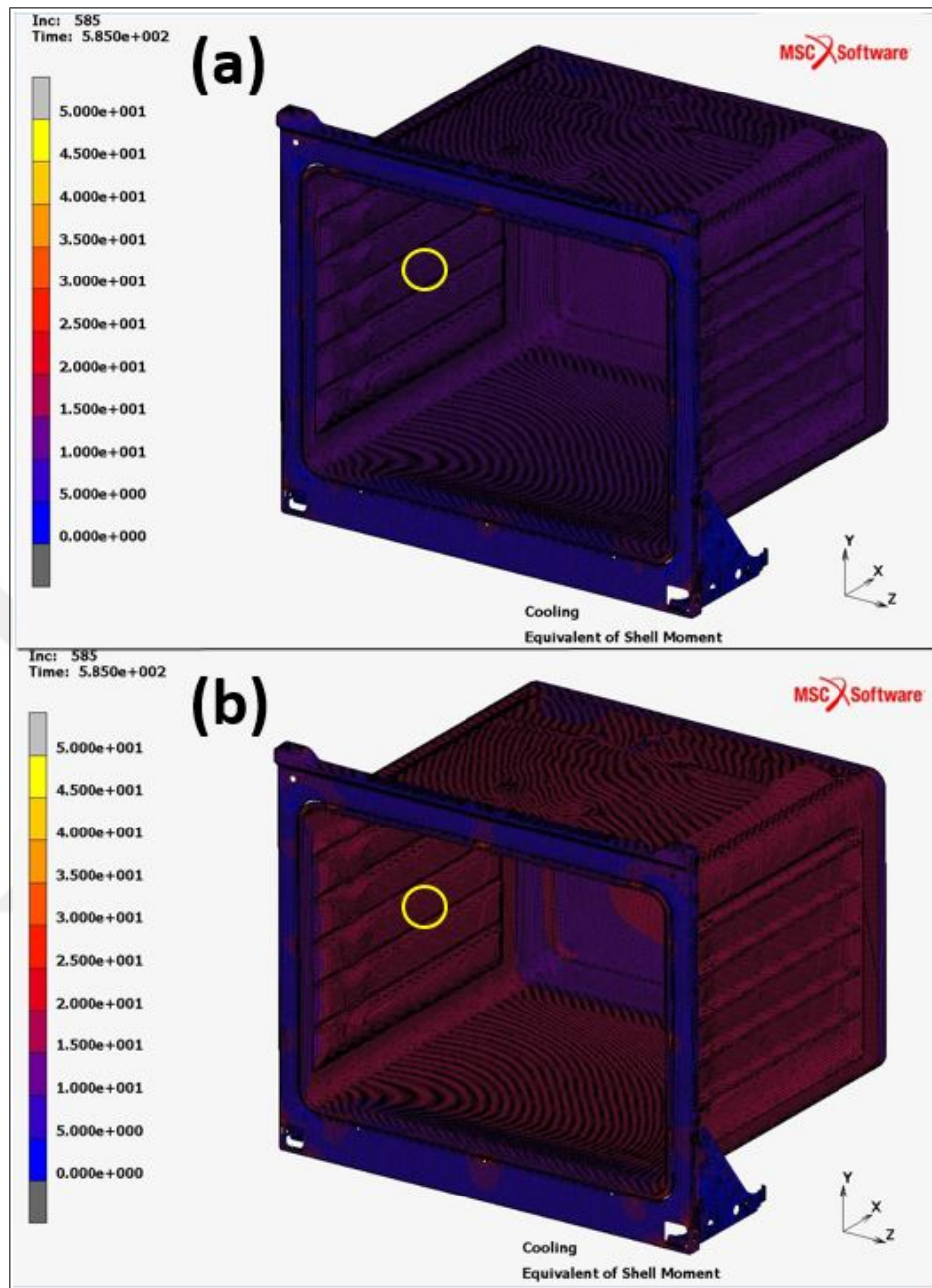


Figure 5.1. Shell moment variation for elastic and viscoelastic models.

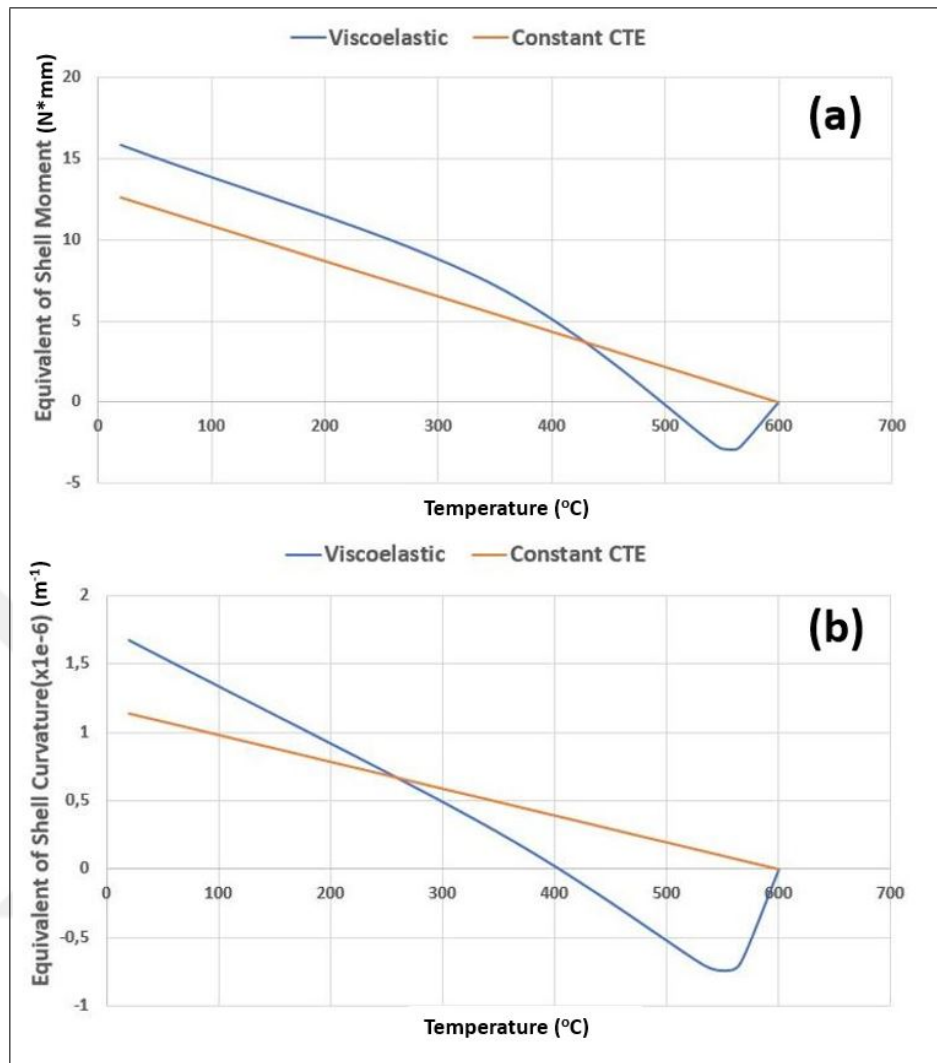


Figure 5.2. Equivalent of shell moment and curvature versus temperature.

6. CONCLUSION AND FURTHER WORK

In this study, a glass frit used in enamelled steel component production is characterized by using XRF and thermal dilatometry methods and effect of using viscoelasticity in analysis of thermal deformation of enamel-steel systems is investigated. Enamelled steel plate samples are produced directly in production facility of Arcelik were used in validation study of the finite element analysis methodology of analyzing enamel-steel systems under temperature loads. The viscoelastic approach is compared with elastic approach and superiority of the viscoelastic approach in thermal deformation analysis of glass-steel composite systems are shown. Furthermore, the viscoelastic approach is used in analysis of oven cavity, which is also composed of glass-steel layers. The oven cavity is measured with CMM while before and after enamelling. The differences between actual enamelled oven cavity and finite element analysis results are shown in Tables 4.6 and 4.7. It can be seen that the results and deformation behavior of the oven cavity can be predicted with the finite element analysis methodology presented in this study.

Dynamic Mechanical Analysis(DMA) is used in order to characterize the glass to obtain its temperature dependent storage modulus and stress relaxation parameters. The storage modulus of the glass can be predicted by this method. The stress relaxation parameters could be obtained by using compression mode of the DMA device but the maximum force that the DMA device can apply is insufficient to create a measurable strain. This characterization can be achieved with a DMA device that apply sufficient force.

Viscoelasticity of the glass layer is modelled with SLS glass viscoelasticity parameters. In order to increase the accuracy of the FE analysis, the glass used in enamelling process should be investigated in depth to obtain the viscoelasticity parameters.

REFERENCES

1. Demirhan E. Alüminyum Yüzey Üzerindeki Emaye Kaplamalara Titanyum Dioksit Katkısı ile Fotokatalitik Özellik Kazandırılması [M.Sc Thesis]. Istanbul: Istanbul Technical University; 2009.
2. Evcimen N. Emaye Üretiminde Kaplama ve Özelliklerin Araştırılması [M.Sc Thesis]. Istanbul: Yıldız Technical University; 2007.
3. Enamelled S. Arcelor Mittal Europe; 2015 [cited 2018 19 October]. Available from: <https://goo.gl/9ekpBX>
4. Shelby JE. *Introduction to glass science and technology*. 2nd Edition. Cambridge: The Royal Society of Chemistry; 2005.
5. Cooreman S, Gousselot P, Leveaux M, Antonissen PPJ. Understanding thermal warping and sagging in enamelled steel parts through an integrated FE simulation. *International Heat Treatment and Surface Engineering*. 2014;8(2):55-60.
6. Callister WD, Rethwisch DG. *Fundamentals of materials science and engineering, an integrated approach*. 4th Edition. USA: John Wiley and Sons; 2008.
7. Sezer AS. Emaye Kaplama Uygulamaları için Gerekli Çelik Sac Özellikleri ve Sacdan Kaynaklanan Emaye Hataları Tespiti [M.Sc Thesis]. Istanbul: Istanbul Technical University; 2009.
8. ASTM International. ASTM Standard No: A424-06. Standard Specification for Steel Sheet, for Porcelain Enameling. Pennsylvania: ASTM; 2006 [cited 2018 21 October]. Available from: www.astm.org.
9. Van den Abeele F, Hoferlin E, Duprez L, Gousselot P. Numerical simulation of thermal warping and buckling in enamelled steel parts. *XXI International Enamellers Congress*. Shangai-China; 2008.

10. Abawi AT. The Bending of Bonded Layers Due to Thermal Stress. California: Hughes Research Laboratories; 2004 [cited 2018 21 July]. Available from: <http://hlsresearch.com/personnel/abawi/papers/bend.pdf>.
11. Timoshenko S. Analysis of bi-metal thermostats. *Journal of Optical Society of America*. 1925;11(3):233-255.
12. TA Instruments. Dilatometry; 2013 [cited 2018 9 July]. Available from: <http://www.tainstruments.com/wp-content/uploads/BROCH-DIL-2013-EN.pdf>.
13. Bhadeshia HKDH. Thermal Analysis Techniques. Cambridge: University of Cambridge; 2002 [cited 2018 25 October]. Available from: www.msm.cam.ac.uk/phase-trans/2002/Thermal1.pdf.
14. Findley WN, Lai JS, Onaran K. *Creep and relaxation of nonlinear viscoelastic materials*. New York: Dover Publications; 1989.
15. Kadali HC. Experimental Characterization of Stress Relaxation in Glass [M.Sc. Thesis]. South Carolina: Clemson University; 2009.
16. Malkin AY, Isayev AI. *Rheology: concepts, methods and applications*. Toronto: ChemTec Publishing; 2006.
17. Menard KP. *Dynamic mechanical analysis: a practical introduction*. USA: CRC Press; 1999.
18. Bathe KJ. *Finite element procedures*. 2nd edition. Massachusetts: Prentice Hall; 2006.
19. Cook RD, Malkus DS, Plesha ME, Witt RJ. *Concepts and applications of finite element analysis*. 4th Edition. USA: John Wiley and Sons; 2002.
20. Dhondt G. CalculiX CrunchiX User's Manual Version 2.9. 2015 [cited 2018 5 October]. Available from: http://www.dhondt.de/ccx_2.9.pdf

21. Gohlke M. *Practical aspects of finite element simulation*. 3rd edition. Michigan: Altair Engineering; 2015.
22. Altair Engineering Inc. *Altair Optistruct tutorials and examples*. Troy: Altair Engineering Inc.; 2017.
23. Shieu FS, Lin KC, Wong JC. Microstructure and adherence of porcelain enamel to low carbon steel. *Ceramic International*. 1999;25(1):27-34.
24. Wang D. Effect of crystallization on the property of hard enamel coating on steel substrate. *Applied Surface Science*. 2009;255(8):4640-4645.
25. Rossi S, Scrinzi E. Evaluation of the abrasion resistance of enamel coatings. *Chemical Engineering and Processing*. 2013;68:74-80.
26. Scrinzi E, Rossi S. The aesthetic and functional properties of enamel coatings on steel. *Materials and Design*. 2010;31(9):4138-4146.
27. Holah JT, Thorpe RH. Cleanability in relation to bacterial retention on unused and abraded domestic sink materials. *Journal of Applied Bacteriology*. 1990;69(4):599-608.
28. Conde A, Damborenea J. Degradation of vitreous enamel coatings. *Reference Module in Materials Science and Materials Engineering*. 2016;3:2330-2336.
29. Son YK, Lee CJ, Lee JM, Kim BM. Deformation prediction of porcelain-enameled steels with strain history by press forming and high-temperature behavior of coating layer. *Transactions of the Nonferrous Metals Society of China*. 2012;22(3):838-844.
30. Thermal Analysis. TA Instruments; 2012 [Cited in 2018 24 September]. Available from: <http://www.tainstruments.com/pdf/brochure/2011%20TGA%20Brochure.pdf>.
31. Greaves GN, Greer AL, Lakes RS, Rouxel T. Poissons ratio and modern materials. *Nature Materials*. 2011;10:823-837.

32. MSC Software. Marc 2017.1 Volume A. Theory and User Information. USA: MSC Software Corporation; 2017 [cited 2018 24 October]. Available from: <https://simcompanion.mscsoftware.com/infocenter/index?page=content&id=DOC11403>
33. Roylance D. Engineering Viscoelasticity. USA: MIT; 2001 [cited 2018 15 March]. Available from: <http://web.mit.edu/course/3/3.11/www/modules/visco.pdf>
34. Narayanaswamy OS. Stress and structural relaxation in tempering glass. *Journal of American Ceramic Society*. 1978;61(3):146-152.
35. Narayanaswamy OS. A model of structural relaxation in glass. *Journal of American Ceramic Society*. 1971;54(10):491-498.
36. Gardon R. Thermal tempering of glass. *Glass Science and Technology*. 1980;5:145-216.
37. Gutierrez-Lemini D. *Engineering viscoelasticity*. New York:Springer; 2014.
38. Carre H, Daudeville L. Numerical simulation of soda-lime silicate glass tempering. *Journal de Physique IV Colloque*. 1996;1(6):175-185.
39. Daudeville L, Carre H. Thermal tempering simulation of glass plates: inner and edge residual stresses. *Journal of Thermal Stresses*. 1998;21(6):667-689.
40. Zienkiewicz OC, Taylor RL, Fox DD. *The finite element method for solid and structural mechanics*. 7th edition. UK: Butterworth-Heinemann; 2013.